Fast Pyrolysis Oil Stabilization:

An Integrated Catalytic and Membrane Approach for Improved Bio-oils

DOE Award No. DE-FG36-08GO18212

Final Report
February 1, 2009- August 31, 2011

Submitted by:
University of Massachusetts, Amherst
Amherst, MA 01003

Principal Investigator: George W. Huber

Prepared for:
United States Department of Energy

Executive Summary

This University of Massachusetts, Amherst project, "Fast Pyrolysis Oil Stabilization: An Integrated Catalytic and Membrane Approach for Improved Bio-oils" started on 1st February 2009 and finished on August 31st 2011. The project consisted of 7 tasks, which are described as follows:

Task 1.0: Char Removal by Membrane Separation Technology

Milestone 1 Removal of char fines down to 0.01 weight percent in entire bio-oil using membrane technology.

Milestone 2 Removal of char fines down to 0.01 weight percent in organic fraction of bio-oil using membrane technology.

The presence of char particles in the bio-oil causes problems in storage and end-use. Currently there is no well-established technology to remove char particles less than 10 micron in size. This study focused on the application of a liquid-phase microfiltration process to remove char particles from bio-oil down to slightly sub-micron levels. Tubular ceramic membranes of nominal pore sizes 0.5 and 0.8 µm were employed to carry out the microfiltration, which was conducted in the cross-flow mode at temperatures ranging from 38 to 45 ◦C and at three different trans-membrane pressures varying from 1 to 3 bars. Microscopic and ash content analysis of the feed and permeate streams were conducted to determine the efficacy of the process. The results demonstrated the removal of the major quantity of char particles with a significant reduction in overall ash content of the bio-oil. Water extraction and gas chromatography were employed to characterize the chemical composition of the bio-oil, and no significant change was observed due to the microfiltration process. Results of fouling analysis obtained from longer runs of bio-oil through the membranes are also presented in this study. The results clearly showed that the cake formation mechanism of fouling is predominant in this process. A membrane cleaning protocol for the fouled membrane was developed, comprising successive treatments with methanol, sodium hydroxide, and acetic acid.

Task 2.0 Acid Removal by Membrane Separation Technology

Milestone 3 Reduce total acid number (TAN) to less than 5 in the aqueous fraction of bio-oil using nanofiltration (NF) membranes.

Milestone 4 Reduce total acid number (TAN) to less than 5 in the total bio-oil using nanofiltration membranes.

The feasibility of removing small organic acids from the aqueous fraction of fast pyrolysis bio-oils using nanofiltration (NF) and reverse osmosis (RO) membranes was studied. Experiments were conducted with commercially available polymeric NF and RO membranes and aqueous solutions of increasing complexity, i.e. single solute solutions of acetic acid and glucose, binary solute solutions containing both acetic acid and glucose, and a model aqueous fraction of bio-oil (AFBO) containing acetic acid, formic acid, hydroxyacetone, furfural, guaiacol, catechol and glucose. Feed concentrations close to those in real AFBO were chosen. These concentrations, ranging as high as 34 wt %, were generally at least an order of magnitude higher than previously studied in the literature for related membrane separations. Retention factors above 90% for glucose and below 0% for acetic acid were observed at feed pressures near 40 bar for single and binary solutions, so that their separation in the model AFBO was expected to be feasible. However, all of the membranes were irreversibly damaged when experiments were conducted with the model AFBO due to the presence of guaiacol in the feed solution. Experiments with model AFBO excluding guaiacol were also conducted. NF membranes showed retention factors of glucose greater than 80% and of acetic acid less than -15% when operated at transmembrane pressures near 60 bar.

Task 3.0 Acid Removal by Catalytic Processing

Milestone 5 Decrease the TAN of the aqueous fraction of bio-oils to less than 5 by catalytic hydrogenation

Milestone 6 Decrease the TAN of the organic fraction of the bio-oil to less than 5 by catalytic hydrogenation.

It was found that the TAN reduction in bio-oil was very difficult using low temperature hydrogenation in flow and batch reactors. Acetic acid is very resilient to hydrogenation and we could only achieve about 16% conversion for acetic acid. Although it was observed that acetic acid was not responsible for instability of aqueous fraction of bio-oil during ageing studies (described in task 5). Since, acetic acid was found to be very resilient for low temperature hydrogenation, two-step hydrogenation with higher temperature of second step. Monometallic catalyst such as Pt/C and bimetallic catalyst namely PtRe/ceria-zirconia was used in the second step with Ru/C as catalyst in the first step. With higher hydrogenation temperature, carbon conversion to gas phase increased which offsets the increase in acetic acid conversion. The bimetallic catalyst PtRe/ceria-zirconia was found to be better of the two catalyst tested because of its ability to convert the acid functionality with low conversion to gas phase carbon. Hydrogenation of the whole bio-oil was carried out at 125°C, 1450 psi over Ru/C catalyst in a flow reactor. Again, negligible acetic acid conversion was obtained in low temperature hydrogenation. Hydrogenation experiments with whole bio-oil were difficult to perform because of difficulty to pumping the high viscosity oil and reactor clogging.

Task 4.0 Acid Removal using Ion Exchange Resins

Milestone 7 Decrease the TAN of the bio-oils to less than 5 using ion-exchange resins.

DOWEX M43 resin was used to carry out the neutralization of bio-oil using a packed bed column. The pH of the bio-oil increased from 2.43 to 3.7. The GC analysis of the samples showed that acetic acid was removed from the bio-oil during the neutralization and recovered in the methanol washing. But it was concluded that process would not be economical at large scale as it is extremely difficult to regenerate the resin once the bio-oil is passed over it.

Task 5.0 Characterization of Upgraded Bio-oils

Understanding the rheology and stability of biofuels has been identified as a major need in the large-scale production, storage and use. A challenging problem is the dramatic viscosity increase that can occur upon storage of pyrolysis oils. We investigated the viscosity, microstructure, and chemical composition of bio-oils prepared by a fast pyrolysis approach, upon aging these fuels at 90ºC for periods of several days. Our results suggest that the viscosity increase is not correlated with the acids or char present in the bio-oils. In addition, while there have been significant efforts on removing chars as a means of stabilizing biofuels, our results show that removal of neither large nor small char particles has any significant impact on the rate of viscosity increase. The viscosity increase is due to formation of high molecular weight polymeric species over time. Our work also suggests that hydrogenation of the samples is beneficial in eliminating the viscosity increase.

Task 6.0 Commercialization Assessment

Milestone 9 Complete designs for integrated bio-oil production systems incorporating the technologies developed through this project by UMass-Amherst.

Milestone 10 Within budget capabilities and as warranted by UMass-Amherst laboratory success, incorporate the technologies developed into an existing ROI plant and assess the performance of the integrated system.

Milestone 11 Conduct an economic analysis of the integrated system to determine business viability.

Renewable Oil International LLC (ROI) was responsible for Task 6.0, "Commercialization Assessment." As part of this effort ROI focused on methods to reduce char carryover in the vapor stream from the fast pyrolysis reactor and residence time of the vapor in the reactor. Chars in the vapor acts as a vapor cracking catalyst and chars carried over into the bio-oil accelerate bio-oil aging and exacerbate instability issues. Long vapor residence times allowed more time for secondary degradation reactions to occur which include conversion to carbon. Changes were made in the bio-oil recovery methodology and a reactor sweep gas used to reduce vapor residence time. Cyclones were placed in the vapor stream to reduce char particulate carryover. Microfiltration of the bio-oil was also researched to remove char particulate from the bio-oil. All methods reduced char content of the bio-oil. The capital cost for these improvements would be less than 2% of the total plant capital cost.

Task 7.0 Project Management and Reporting

Reports regarding the progress of the project were provided in accordance with the Federal Assistance Reporting Checklist. These include quarterly reports spreadsheet format, yearly project management forms, and a final report.

Tasks and Milestones

Task 1.0: Char Removal by Membrane Separation Technology

The objective of this task is to implement membrane technology that will allow us to remove the char particles from bio-oils down to a target of 0.01 weight percent. Since cyclone technology in the vapor phase can readily remove particles above 10 microns, we focused on membrane technology that will remove the char fines (0.1 to 10 microns) from the liquid phase product. The main challenges here will be (1) quantifying, understanding, and ameliorating membrane fouling and (2) dealing with the highly viscous liquid streams.

Milestone 1 Removal of char fines down to 0.01 weight percent in entire bio-oil using membrane technology.

Milestone 2 Removal of char fines down to 0.01 weight percent in organic fraction of bio-oil using membrane technology.

The presence of char particles in the bio-oil causes problems in storage and end-use. Currently there is no well-established technology to remove char particles less than 10 micron in size. This study focused on the application of a liquid-phase microfiltration process to remove char particles from bio-oil down to slightly sub-micron levels. Tubular ceramic membranes of nominal pore sizes 0.5 and 0.8 μm were employed to carry out the microfiltration, which was conducted in the cross-flow mode at temperatures ranging from 38 to 45 ∘C and at three different trans-membrane pressures varying from 1 to 3 bars. Microscopic and ash content analysis of the feed and permeate streams were conducted to determine the efficacy of the process. The results demonstrated the removal of the major quantity of char particles with a significant reduction in overall ash content of the bio-oil. Water extraction and gas chromatography were employed to characterize the chemical composition of the bio-oil, and no significant change was observed due to the microfiltration process. Results of fouling analysis obtained from longer runs of bio-oil through the membranes are also presented in this study. The results clearly showed that the cake formation mechanism of fouling is predominant in this process. A membrane cleaning protocol for the fouled membrane was developed, comprising successive treatments with methanol, sodium hydroxide, and acetic acid.

The main goal of this study was to apply microfiltration technology in removing char particles larger than 1 μm from the bio-oil. A microfiltration rig was built to house commercially available tubular ceramic membranes that were stable in a hot, pressurized bio-oil feed. Optical microscopy and ash analysis of the feed and permeate streams were used to determine the efficacy of the microfiltration. Water extraction and gas chromatography were employed to determine the effects of the microfiltration on the chemical composition of the bio-oil before and after microfiltration. Finally, flux data from longer bio-oil runs were analyzed to determine the predominant fouling mechanism.

1.1. Experimental

1.1.1. Materials

Membralox® TI-70 microfiltration membranes with nominal pore sizes of 0.5 and 0.8 μm were obtained from Pall Fluid Dynamics, Deland FL. These tubular membranes were 25 cm in length with an outer diameter of 10 mm and an inner diameter of 7 mm. Each membrane consists of a filtering layer which is about 10–15 μm thick. The filtering layer is supported by two layers; an underlayer with an approximate pore size of 10 μm and the macroporous support layer [1,2]. The total surface area available for filtration was 55cm^2. The microfiltration experiments were conducted by placing the membrane in a stainless steel housing (part # S700-00141) also obtained from Pall Fluid Dynamics. Rubber O-rings, metal and Teflon gaskets and stainless steel screws were used at both ends to secure the membrane inside

the holder. The bio-oil used for these experiments was provided by the US Department of Energy (DOE) and was manufactured by the National Renewable Energy Laboratory (NREL), Golden, Colorado. White oak pellets were used as biomass feedstock [3]. The bio-oil had a heating value of 17 MJ/kg with an oxygen content of about 28% [3]. The bio-oil was stored in a refrigerator at 4 ∘C immediately after its arrival in our laboratory. Portions were drawn off periodically for permeation or characterization experiments; samples of the feed, retentate, and permeate streams were refrigerated after each permeation experiment. The viscosity and water content of the bio-oil were measured within 30 days after its arrival in our laboratory.

The viscosity of the bio-oil was 0.1771 Pa s at 25 ∘C and 0.0638 Pa s at 40 ∘C, as measured with TA ARES G2 and TA AR 2000 Rheometers. Water content of the bio-oil was 28.1% as measured by a Mettler-Toledo Volumetric Karl–Fischer Titrator (model # V20). Methanol, sodium hydroxide and acetic acid all of purity >99% (from Fischer Scientific) were used for cleaning the membrane.

These chemicals were used without further purification according to the procedure described in Section 1.1.3. Baseline studies for the microfiltration process were carried out with pure water and suspensions of silica beads in water. Ultrapure water with resistivity in the range of 10–14MΩm obtained from a NANOpure Infinity UF system (model # d8981) was used in the experiments. Silica microspheres of nominal diameter 0.05 and 0.7 μm were obtained from Polysciences Inc. The coefficient of variation for these particles was typically in the range of 10–15%. The 0.7 μm beads were packaged in 10% (w/v) suspension in water while the 0.05 μm beads were a dispersion of 5% (w/v) amorphous silica particles in water with NaOH as stabilizer.

1.1.2. Permeation procedure

Figure 1.1 shows the schematic of the microfiltration permeation setup. The fluid was pumped into the tube side of the membrane using a positive displacement gear pump obtained from Cole Parmer. The pressure differential across the membrane was measured using a pressure gauge at the inlet side of the module. Since the outlet was at atmospheric pressure the gauge reading directly provided the pressure difference for the permeation experiment. Stainless steel tubing of 1/4 in. diameter was used at the inlet and the outlet tubing diameter was reduced to 1/8 in. A needle valve was used at the outlet to control the trans-membrane pressure. All experiments were conducted in the cross-flow mode to reduce fouling effects. The retentate flow was kept at nearly 90% of the total feed flow for both water and bio-oil permeation experiments.
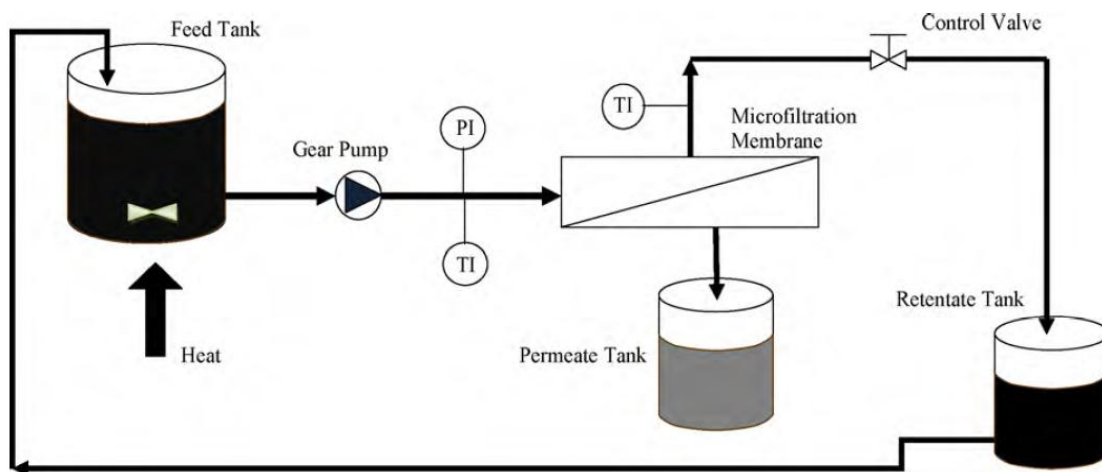

Figure 1.1 Schematic of the microfiltration process.

The retentate was collected and recycled back to the feed tank. The water permeation experiments were conducted at room temperature. However, due to the high viscosity of bio-oil, microfiltration of bio-oil was carried out at elevated temperatures near 40 ◦C; more precisely, temperature was maintained within in the range of 38–45 ◦C during the course of an experiment. For this purpose the bio-oil feed tank was placed on a heating mantle with a magnetic stirrer. The feed and retentate temperatures were monitored by using thermocouples placed at the two ends. To maintain the temperature across the module a heating tape covered with an insulation tape was wrapped around the tubing and the membrane housing. To determine the flux (volumetric flow rate per unit area) and permeance (flux per unit pressure), the flow rate of the permeate was measured by collecting samples of the liquid (water or bio-oil) for a time period ranging from 15 to 30 s. Volume of the samples collected varied between 15 and 30 ml for water and 1–5 ml for bio-oil. The primary focus was on the implementation of the microfiltration process to determine its efficacy in removing char particles from a fresh feed while minimizing fouling. Therefore the experiments were carried out in cross-flow mode with the retentate flow being approximately 95% of the feed stream, and the yield of permeate was small. The issues of yield, scale-up, and different flow configurations will be topics of future work.

1.1.3. Membrane cleaning procedure

Permeation experiments were conducted initially with water and then later with bio-oil. The membranes showed significant fouling tendency in both water and bio-oil permeation. The details are presented in Section 1.2. Cleaning procedures for membranes fouled with water and bio-oil were adapted from procedures as described by Al-Obeidani et al. and Blanpain-Avet et al. [4,5]. The membranes that were fouled after the water permeation experiments were cleaned by soaking for 6 h each in 0.5M NaOH and 0.5M acetic acid, respectively, at 70 ◦C. Membranes fouled after bio-oil experiments needed a much longer and more vigorous cleaning protocol than membranes fouled after the water permeation experiments. The membrane was first flushed with methanol solution for 5min and then backflushed again with methanol for another 5 min. After this, the membrane was soaked in methanol for 12 h inside the holder at a pressure of 0.5 bar. This was followed by soaking for 3 h each in 0.5M NaOH and 0.5M acetic acid, respectively, at 0.5 bar and 70 ◦C. Finally the membrane was flushed and back-flushed with methanol at room temperature. Methanol permeance was used as an indicator of the membrane revival after fouling. The native methanol permeance was 15,000 l h^{-1}m^{-2} bar^{-1} for 0.5µm and 21,000 l h^{-1}m^{-2} bar^{-1} for 0.8 µm membrane. Methanol permeance was restored to more than 90% of its original value after membrane cleaning using the above procedure.

1.1.4. Microfiltration characterization

Microscopic imaging was conducted to compare the feed and permeate streams in terms of the size and relative amount of char particles present. The microscopic images were taken using an Olympus DX 60 optical microscope with a Sony CCD video camera. To further quantify the microfiltration results, ash analysis was performed on the bio-oil feed and permeate streams. Procedure for determination of ash was slightly modified from the procedure outlined by Lu et al. [5]. Due to presence of high water content, bio-oil cannot be directly heated to temperatures higher than 150 ◦C as this causes bubbling and splashing of the bio-oil inside the furnace. First, water was evaporated from the bio-oil by heating it at 125 ◦C for 12 h. The temperature of the sample was then slowly raised to 250 ◦C. This temperature was maintained for nearly 2 h to completely char the bio-oil. Finally the charred sample was burned at 750 ◦C for 6 h to obtain the final ash. The effects of the microfiltration process on the chemical composition of the bio-oil were also probed. Water extraction was used to characterize the water-soluble fraction in the bio-oil, since the bio-oil readily phase separated upon addition of water. One part bio-oil was weighed in a centrifuge tube and four parts distilled water was added to it (typically 28 g distilled water was added to 7 g of bio-oil). The contents of the centrifuge tube were mixed vigorously by shaking so as to extract all the water-soluble compounds in aqueous fraction. The mixture was then separated in two layers in a centrifuge (Marathon 2100, Fisher Scientific) at 10,000rpm for 20 min. After centrifugation the top layer was

decanted and called the water-soluble fraction. The viscous bottom layer was called the water-insoluble fraction. The water-soluble layer was weighed to determine the amount of bio-oil that dissolved in water. It was assumed that no externally added water would go into the water insoluble fraction during the extraction process. Finally, gas chromatography (GC) was used to determine the weight percent of several key compounds. The bio-oil feed, retentate and permeate compositions were measured with Agilent Gas Chromatograph (Model 7890A). Samples for the GC analysis were prepared by making a 10 wt% solution of the total bio-oil in methanol. Flame Ionization Detector (FID) was used to conduct the analysis. Restek Rtx-VMS (Catalog No. 19915) column was used with a constant carrier gas flow rate of 1.24 ml/min. Helium was used as the carrier gas. Injector and detector were both held at 240 ∘C. The GC oven was programmed to hold at 40 ∘C for 5 min. The temperature was then ramped to 240 ∘C at 7.5 ∘C/min and finally held at 240 ∘C for 15 min.

1.2 Results and discussion

1.2.1. Water permeation

The water permeation experiments were carried out primarily to benchmark the microfiltration setup. The permeation experiments were run for approximately 6 h for each membrane. Water permeation experiments were conducted with both 0.5 and 0.8 μm pore size membranes. Theoretical values of the permeance for the two membranes were estimated using the Hagen–Poiseuille equation [6,7]:

$$P = \frac{J}{\Delta p} = \frac{\varepsilon r^2}{8\mu\tau\Delta x}$$

(1)

where P is the permeance, J is the flux ($lm^{-2}\,h^{-1}$), Δp is the transmembrane pressure, μ is the viscosity of water, ε and τ are the porosity and tortuosity of the membrane, respectively, Δx is the thickness of membrane, and r is the pore radius.

The viscosity of water at 20 ∘C is 1 cP. The porosity and tortuosity values for these membranes were taken as 0.4 and 3, respectively [2,8]. The thickness of the active filtering layer (Δx) is 15 μm [1,2]. Since we have little or no information about the thickness and structure of the underlayer and support layer, we neglected their contribution to the membrane resistance in our computation. The nominal pore diameters were used to estimate the value of radius of the pores. The theoretical value of permeance for the 0.5 μm membrane is 25,000 $l\,h^{-1}m^{-2}\,bar^{-1}$ and that for the 0.8 μm membrane is 64,000 $l\,h^{-1}m^{-2}\,bar^{-1}$. The experimental value for the initial permeance of the 0.5 μm membrane was 8,000 $l\,h^{-1}m^{-2}\,bar^{-1}$, and this decreased to 5,000 over the course of the experiment. The 0.8 μm membrane showed an initial permeance of 18,000 $l\,h^{-1}m^{-2}\,bar^{-1}$, and this decreased to 5,000 over the course of the experiment. The theoretical values are therefore higher by about a factor of three as compared to the initial values from the experiments. This might be attributed to the effects of the resistance of the underlayer and support layer [1], which could not be accounted for in the theoretical calculation, or possibly some adventitious adsorbed material that reduces the experimental flow.
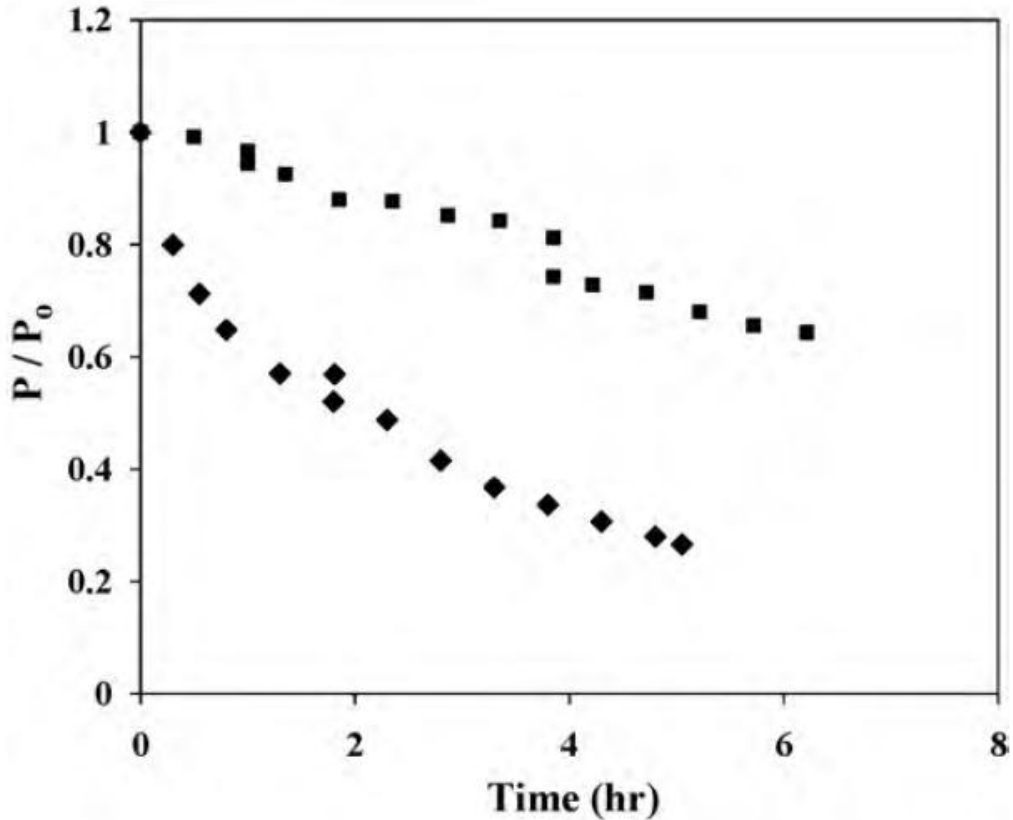
Figure1.2 Water permeance normalized by initial permeance with respect to time: ■ represents 0.5 μm and ◆ represents 0.8 μm membrane.

       Both membranes exhibited fouling with water over time. Fig. 1.2 shows the water permeance, normalized by the initial water permeance, as a function of time for the two membranes. The 0.8 μm membrane fouls at a significantly faster rate as compared to the 0.5 μm membrane. The spikes in data observed for the 0.5 μm membrane at nearly 4 h, and for the 0.8 μm membrane at 2 h, occurred due to stopping of the gear pump at these time intervals which resulted in the restarting of the whole microfiltration process. This type of fouling behavior in Membralox® membranes with water has also been previously reported in literature [1,2]. Elmaleh and Naceur [2] have reported about 85% drop in permeability for the 0.5 μm and approximately 90% drop in permeability for the 0.8 μm Membralox® membranes over a running time of 1 h. In comparison we observe a drop of nearly 40% for the 0.5 μm and 70% for the 0.8 μm membrane, and this drop in permeability occurs after 5–6 h of running water through the membranes. The greater and significantly more rapid drop in permeability observed by Elmaleh and Naceur may be attributed to the quality of water. The resistivity of water used by them was in the range of 0.5–1MΩm, which is nearly an order of magnitude lower than the resistivity of the water employed for our experiments. Elmaleh and Naceur have suggested the possible growth of micro-organisms in the size range of 1–10 μm within the membrane which causes the membranes to foul even with permeation of relatively pure water [2]. Prior to running the bio-oil experiments the 0.5 μm membrane was tested using silica beads of 0.7 and 0.05 μm diameter.

Absorbance UV spectroscopy was used to determine the rejection factors for the silica beads. For this purpose, calibration curves of UV absorbance versus weight percent of silica beads were generated by making standard solutions for both 0.7 and 0.05 μm beads. The rejection factor for the 0.7 μm beads was nearly 100% and the rejection factor for the 0.05 μm beads was around 60%. These results gave a good indication that the selected membranes would be suitable for removing the char particles in the size range from 0.1 to 10 μm. At the completion of the water permeation and silica rejection experiments, both membranes were cleaned according to the procedure described in Section 1.1.3. After cleaning, the water permeance was restored to nearly 100% of its original value.
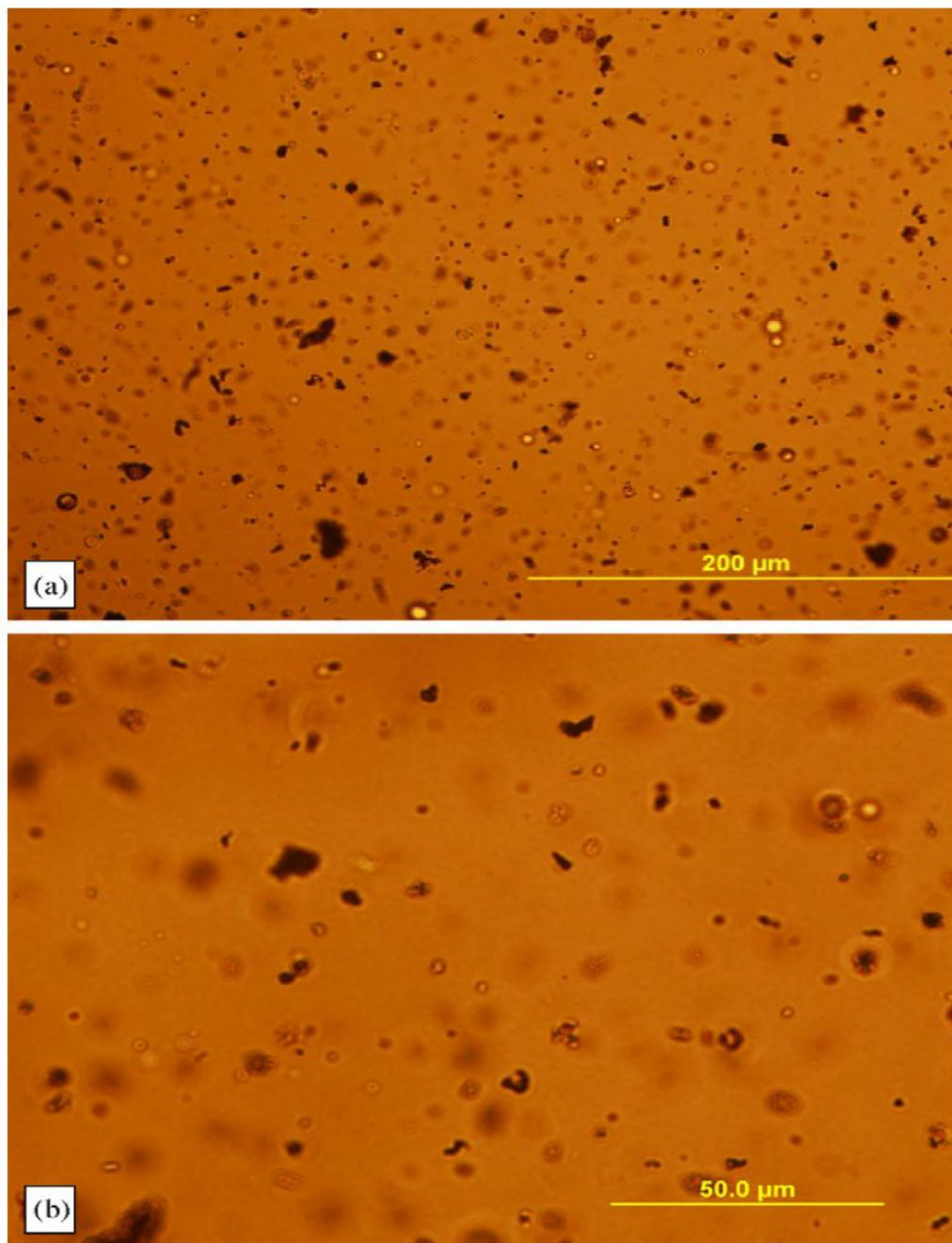
**Figure 1.3** Microscopic image of bio-oil feed at different magnification levels: a=20×and b=50×.

1.2.2. Bio-oil microfiltration

1.2.2.1. Microscopic and ash analysis

Figs. 1.3–1.5 show the microscopic images of bio-oil feed, 0.5 μm permeate and 0.8 μm permeate at magnification levels 20× and 50×. The microscopic analysis was conducted within 5 days of carrying out the microfiltration. The feed image shows the presence of a large number of char particles of varying sizes with some particles larger than 25 μm. Some of the particles appear to be agglomerates of smaller particles. Similar aggregation of char particles in the bio-oil have been previously reported by Tzanetakis et al. [9]. They found that char particles, being hydrophobic in nature, tend to bind to the organic phase in the bio-oil, which then agglomerate to form larger structures. The permeate images from the 0.5 μm membrane show that while the majority of the char particle have been removed by microfiltration we still observe some micron size particles especially at higher magnification. Since the tubular Membralox membrane have a pore size distribution, with some pores larger than the nominal pore size, the presence of a few particles in this size range is not surprising. The 0.8 μm membrane permeate shows similar microfiltration characteristics as observed in the 0.5 μm permeate. Based on microscopic images it is evident that the microfiltration using both pore size membranes has successfully removed the majority of the char particles, with only a small fraction of the smaller size char particles retained in the permeate. Ash characterization experiments were carried out within 7 days after the microfiltration. Fig.1.6 shows the ash weight percent of the feed and the filtered bio-oil. The feed has nearly 0.1 wt% ash. The weight percent of ash in bio-oil can be as high as 0.2 [10,11]; therefore, our bio-oil sample has a moderate level of ash content. The ash content after microfiltration is reduced by approximately 60%, to about 0.03 wt%. Both pore size membranes achieve similar levels of ash reduction after filtration. The residual bio-oil ash in permeate can be attributed to the small amount of micron level char particles observed in the microscopic images of the permeate streams and also perhaps to the presence of inorganic compounds directly in the liquid-phase that cannot be removed by a microfiltration process.
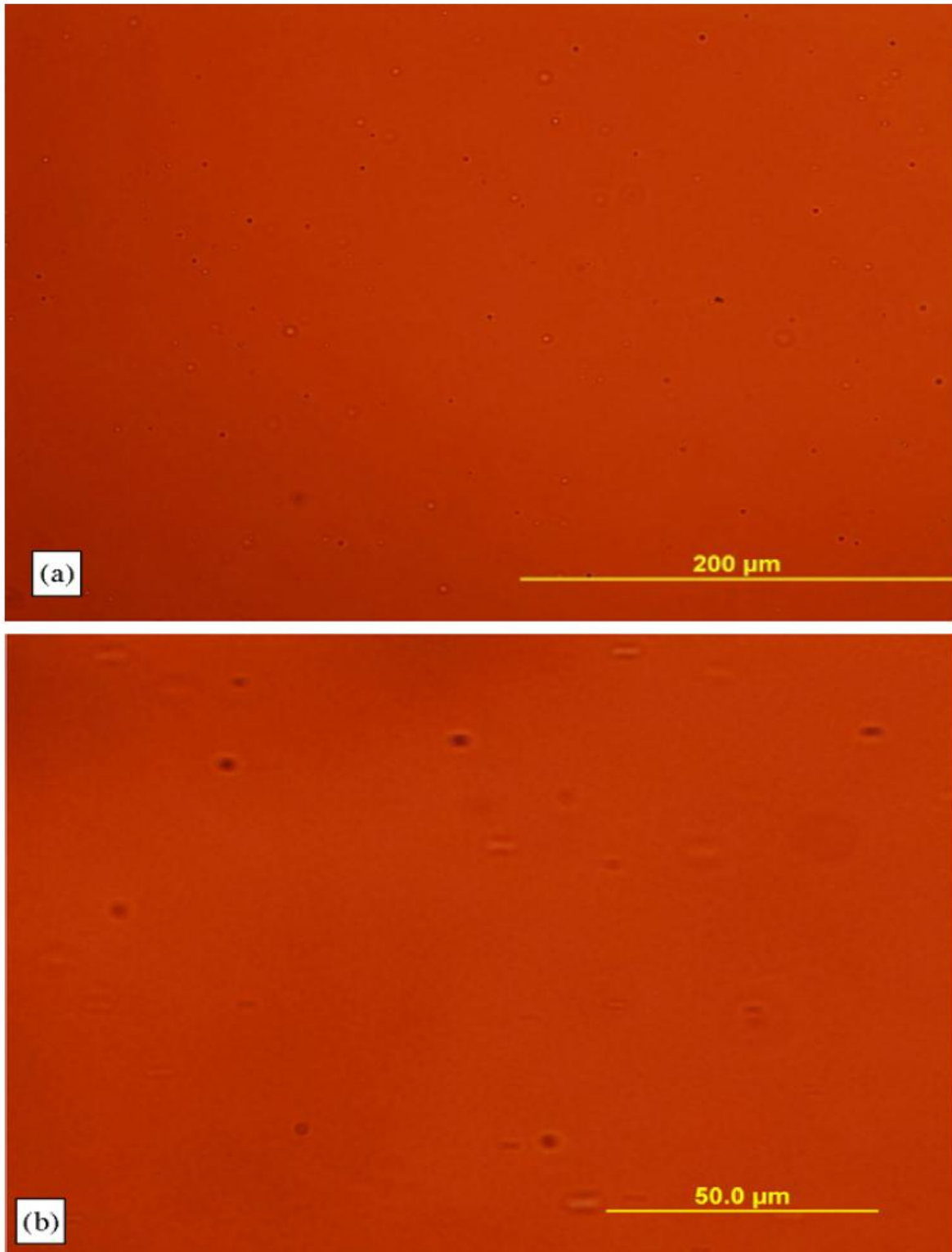
Figure 1.4 Microscopic image of 0.5 μm membrane permeate at different magnification levels: a=20× and b=50×.
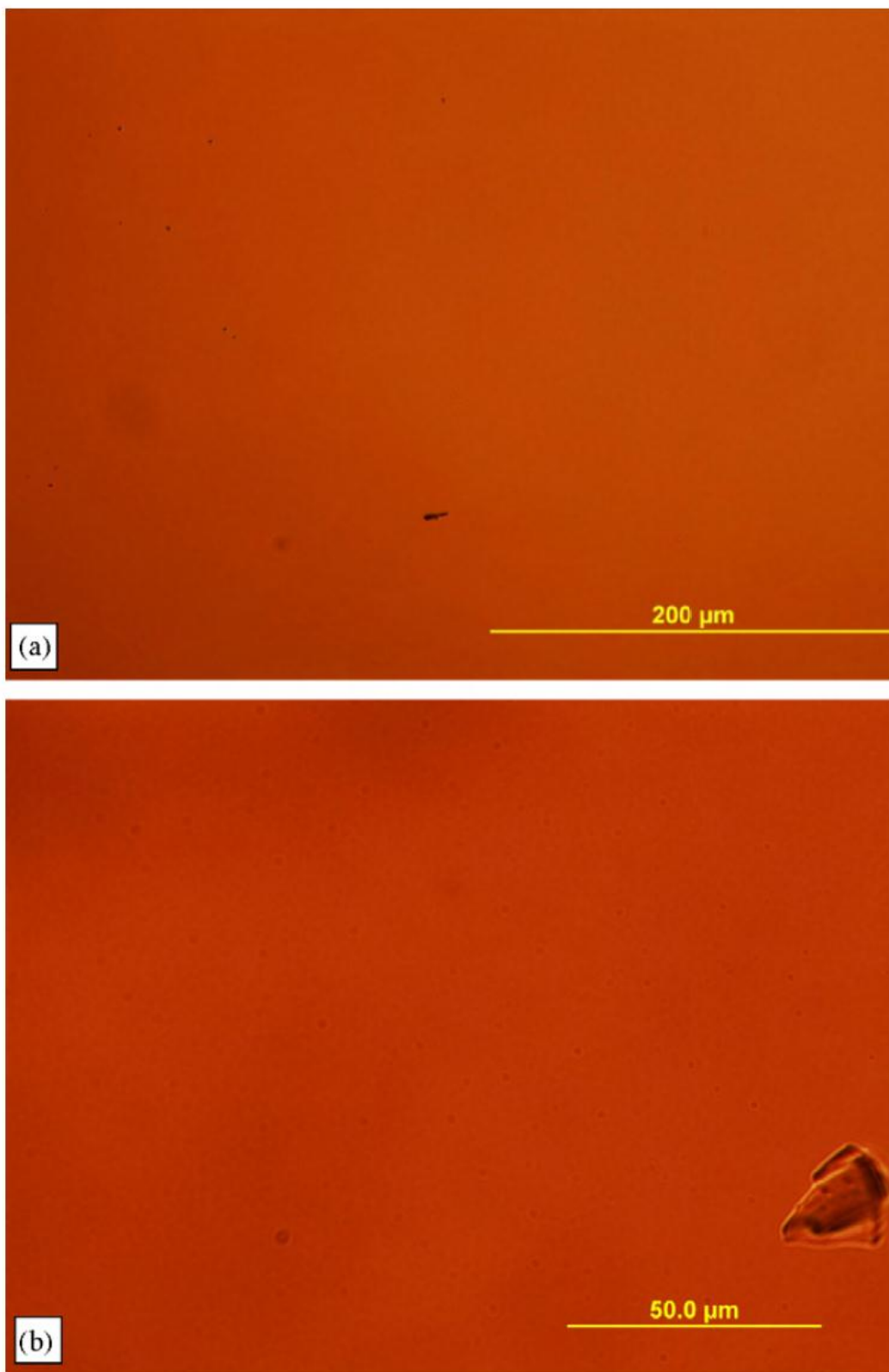
Figure 1.5 Microscopic image of 0.8 μm membrane permeate at different magnification levels: a=20×
and b=50×.

Six months after the microfiltration was carried out, samples of the feed and permeate streams were removed from refrigerated storage and subjected to the GC and water extraction experiments to probe for possible chemical differences. The time lapse is notable because bio-oil is known to undergo significant physico-chemical changes, commonly referred to as "aging", over time scales of months under ambient conditions. The GC data are given in Table 1.1. The weight percents are based on the total bio-oil. There is no significant difference in the concentration of the key components in the unfiltered and microfiltered bio-oil with the exception of hydroxyacetaldehyde, for which the concentration is more than two times higher in the filtered samples as compared to the feed. At this time we do not have an explanation for this exception. Microfiltration also does not seem to have any significant impact on the composition of bio-oil in terms of the water and water-soluble content as observed in Table 1.2. There is a slight decrease in the water-insoluble fraction, on the order of one or two percent, after filtration; this may be attributed to the removal of the solid chars which are themselves insoluble (char content is typically on the order of one percent by weight). It should be noted that the typical water-soluble content of fresh bio-oil is well above 50%, so the corresponding percentages in Table 1.2 are much lower than expected. This may be attributed to the aging process, which is known to increase the concentration of the water-insoluble fraction over time [12]. In one case, for the 0.8 μm membrane permeate, the water-soluble fraction was also measured very soon after the permeation experiment (6 months before the measurements used to generate the data reported in Table 1.2); the water-soluble fraction was 55% at that time, as compared to 27.2%. Although such time-dependent data are not available for the other samples, it is likely that similar aging phenomena occurred in all of them. Interestingly, the microfiltration process itself had little influence on the aging, with unfiltered feed and filtered permeate samples having similar water content and water-soluble fraction at the same point in time.

Table 1.1 Composition of bio-oil before and after microfiltration.

Compound	Weight percent		
	Unfiltered	0.8 μm permeate	0.5 μm permeate
Hydroxyacetaldehyde	3.16	8.21	7.70
Acetic acid	8.66	9.59	9.11
Hydroxyacetone	1.13	1.45	1.33
1-Hydroxybutanone	0.40	0.44	0.40
Furfural	0.47	0.47	0.42
2-Furanone	0.33	0.32	0.33
Levoglucosan	11.95	10.22	10.38

Table 1.2 Impact of microfiltration on the total water content and water soluble and insoluble content of bio-oil.

|	Unfiltered	0.5 μm permeate	0.8 μm permeate
Water	28.1	25.8	26.3
Water soluble	25.6	26.1	27.2
Water insoluble	74.4	73.9	72.8
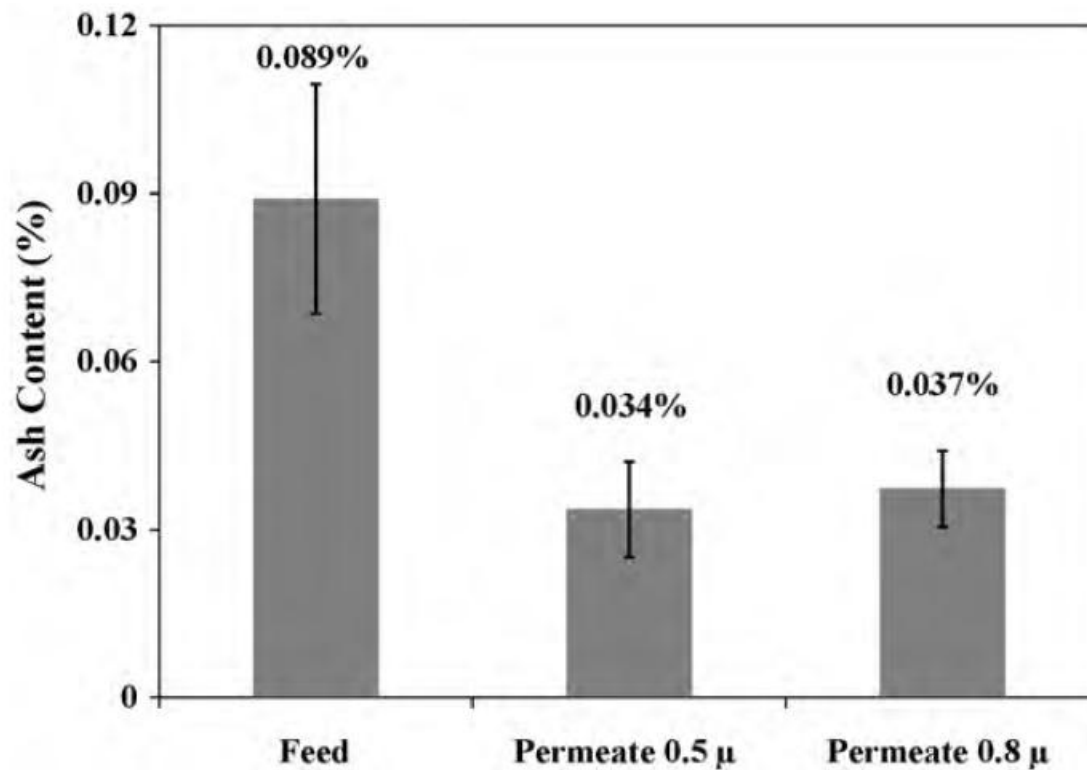
Figure1.6 Ash content of bio-oil feed, 0.5 and 0.8 μm permeate.

1.2.2.2. Fouling studies

In order to observe the fouling of the membrane and to analyze the fouling mechanism, the bio-oil sample was run for nearly 4 h at three different trans-membrane pressures ranging from 1 to 3 bar. The cross-flow velocity varied between 0.02 and 0.08ms^{-1} during the course of the experiments. Permeance readings were taken periodically with much shorter intervals at the beginning of the experiment as compared to the latter part of the run.

Fig. 1.7 shows the permeance of the bio-oil as a function of time through the 0.5 μm membrane. A sharp decrease in permeance is observed initially followed by a more gradual decline. The rate of decrease in permeance shows a positive correlation with the transmembrane pressure. Interestingly the trends for the permeance of bio-oil versus time through the 0.8 μm membrane are very similar to the 0.5 μm membrane as observed in Fig. 1.8. The permeance of the bio-oil through the two membranes was lower than water by nearly two orders of magnitude which is primarily attributed to the significantly higher viscosity of bio-oil as compared to water.
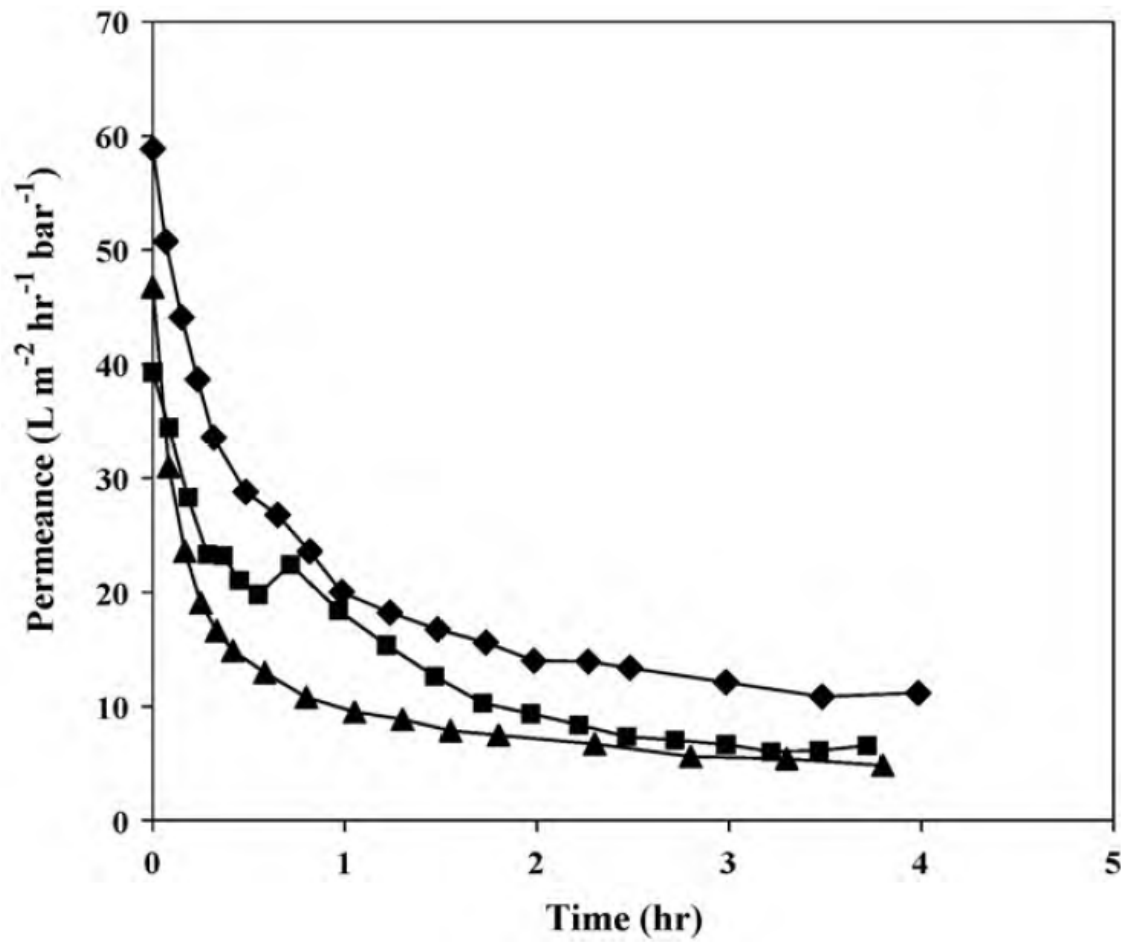
Figure1.7 Bio-oil permeance as a function of time for 0.5 μm membrane at three different trans-membrane pressures: ◆ represents data at ~1 bar, ■ represents data at ~2 bars and ▲ represents data at ~3 bars.
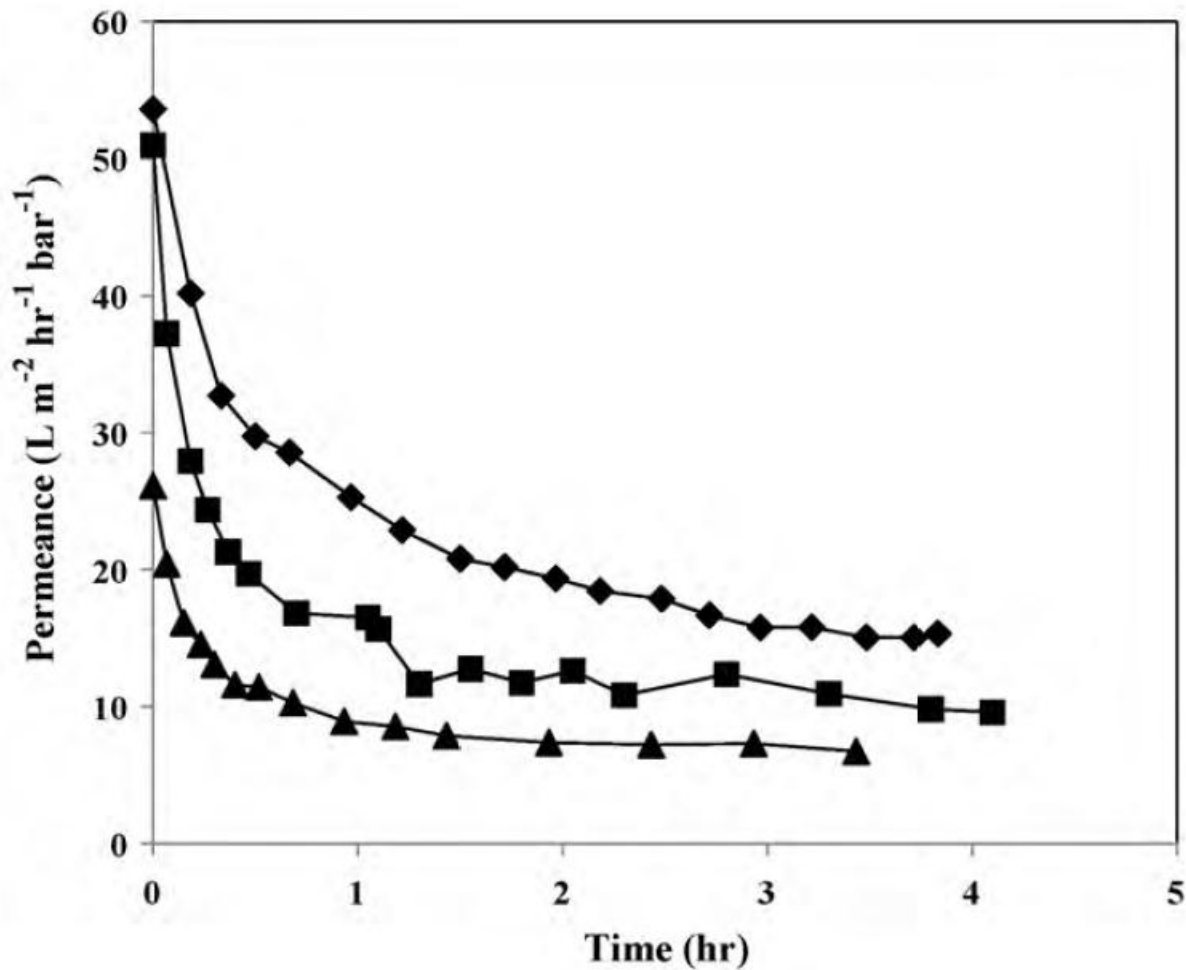
Figure 1.8 Bio-oil permeance as a function of time for 0.8 μm membrane at three different trans-membrane pressures: ◆ represents data at ~1 bar, ■ represents data at ~2 bars and ▲ represents data at ~3 bars.

Fouling in microfiltration can follow one of the four classical models, namely: (a) pore blockage, (b) intermediate pore blockage, (c) pore constriction and (d) cake filtration [13,14, 15,16]. The governing equation for all can be written in the form as established by Hermia [17]:

$$\frac{d^2t}{dV^2} = k\left(\frac{dt}{dV}\right)^n$$

(2)

where t is the filtration time, V is the cumulative filtrate volume, and k and n are two model parameters. The parameter n is a dimensionless number whose value depends on the fouling mechanism. For the cake filtration model n = 0, for pore constriction n = 3/2, for intermediate pore blockage n = 1 and for complete pore blockage n=2. The fouling mechanisms can be evaluated by analyzing the total resistance to flow with respect to time [18]. The total resistance to permeate flow can be written as:

$$R_{Total} = \frac{\Delta p}{\mu J}$$

(3)

where Δp is the trans-membrane pressure, μ is the fluid viscosity

and J is the permeate flux.

Tracey and Davis [18] have shown that a plot of RTotal as a function of time is concave up if $n > 1$ and is concave down if $n \leq 1$. Fig. 1.9 is a plot of RTotal as a function of time for the two membranes. Allowing for noise, the data for the 0.5 μm membrane appear to be always concave down, showing that the cake formation mechanism is predominant right from the start of the filtration process. For the 0.8 μm membrane at very short times (roughly the first 30 min) the data are seemingly concave up, but then the trend reverses to generally concave down. The 0.8 μm membrane data was therefore further analyzed to ascertain more details about the fouling mechanism. This analysis was carried out by using the linearized forms of Eq. (2) as given below in Eqs. (4)–(7) for the four fouling mechanisms [13]:
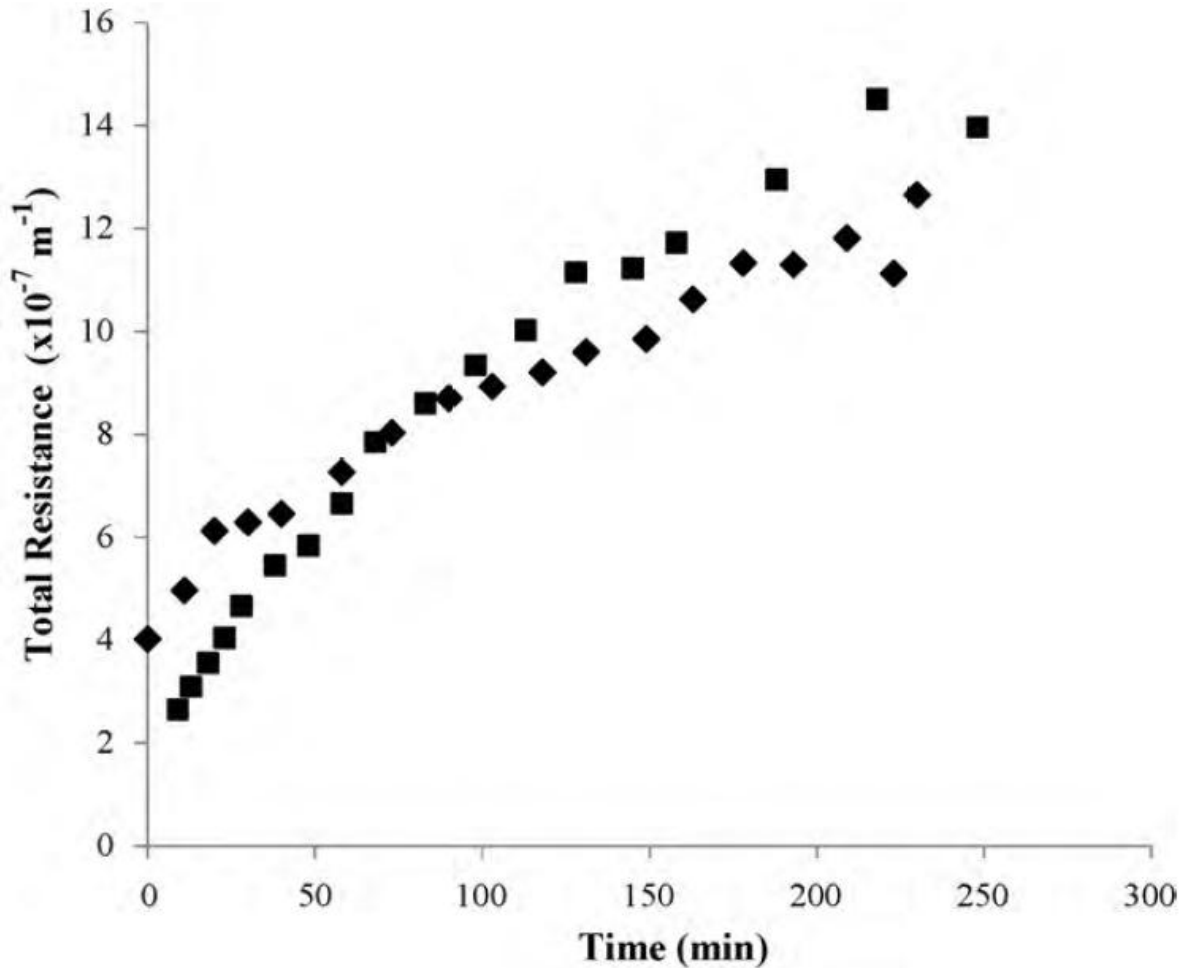
$$\frac{t}{V} = aV + b$$

(cake formation) (4)

$$\frac{t}{V} = at + b$$

(pore constriction) (5)

$$\frac{1}{Q} = at + b$$

(intermediate pore blockage) (6)

$$\ln(Q) = at + b$$

(pore blockage) (7)

where a and b are constants whose values depend on the fouling mechanism. Q is the volumetric flow rate in liters per min.

Figure 1.9 Total resistance with resistance to time: ■ represents 0.5 µm and ◆ represents 0.8 µm membrane.

Fig. 1.10 shows the analysis of the 0.8 µm membrane data for the entire run of the permeation experiment with respect to the different fouling mechanisms. The solid lines are the linearized models of Eqs. (4)–(7) fitted to the experimental results using standard least squares regression. The cake formation mechanism (Fig. 1.10a) shows the best fit to the experimental data over the entire run with a confidence level greater than 99%. However, the first few (short time, low V) data points do lie slightly below the overall best-fit line, admitting the possibility of another mechanism being operative at short times. The data show clear non-linearities when fitted to the other three models (Fig.1.10b–d) across the entire permeation run, showing that the other models are inadequate as expected based on the plot in Fig. 1.9. At very short times, however, any one of these models might be considered as nearly linear; fits to only the first three data points (not shown on the graphs) produce confidence levels in the range of 91–97%. The above analysis shows that, for the 0.5 µm membrane, the cake formation mechanism is predominant right at the onset of the filtration process. In the case of 0.8 µm membrane, the fouling may initially involve some contribution from pore blocking/constriction and intermediate pore blocking, however this shifts to the cake formation mechanism after no more than 30 min. This type of fouling behavior is quite typical when the size of the solute particles is significantly larger than the membrane pore size. As observed

earlier, the microscopic image of the feed shows a significant amount of char particles greater than 1 μm in size. Similar results were presented by Vela et al. [19] in the ultrafiltration of PEG through monotubular ceramic membranes.
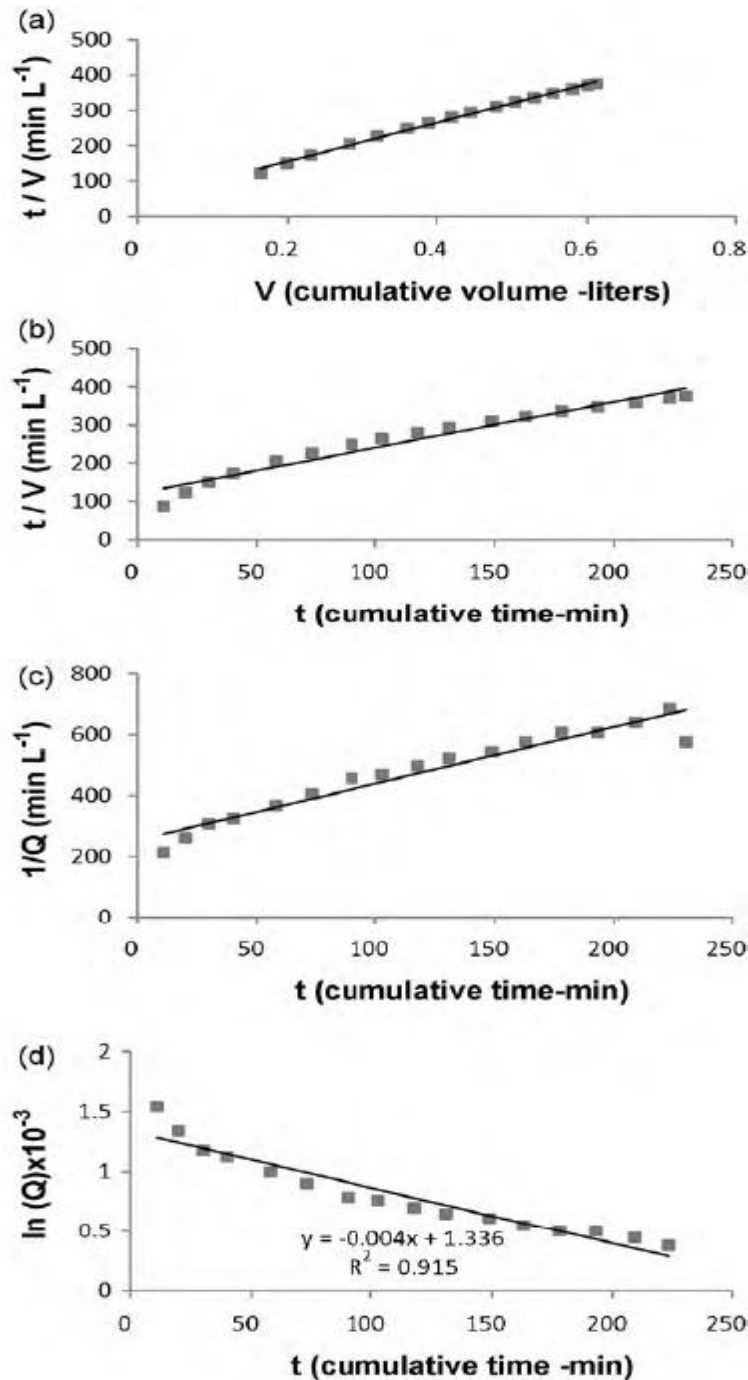
Figure 1.10 Fouling analysis for 0.8 μm membrane: ■ represents experimental data points at 1 bar trans-membrane pressure and solid line represents best fit to the fouling models: (a) represents cake formation, (b) pore constriction, (c) intermediate pore blockage and (d) complete pore blockage.

1.3 Conclusions

Char particles above 1µm in size were removed from fast pyrolysis bio-oil by microfiltration using ceramic membranes. The microscopic images and ash analysis confirm the removal of the majority of the optically visible char particles from the bio-oil with both the 0.5 and 0.8 µm membranes. Microfiltration had little impact on the concentration of the key components related to the energy content of bio-oil, which can be viewed as a positive finding. The microfiltration process and the removal of the char particles did not seem to have any effect the physico-chemical aging process of the bio-oil, although some theories have implicated char as an important contributor to the aging process. A detailed fouling analysis showed a clear predominance of the cake formation mechanism in the 0.5 and 0.8 µm membranes. For the 0.5 µm membrane this mechanism is predominant over the entire permeation run, however, in case of 0.8 µm membrane, there was some evidence that other fouling mechanisms such as pore constriction and pore blocking may contribute during the initial stages.

Currently there is no established process to remove char particles from bio-oil in the size range of 10 µm or less, and this study has shown that microfiltration is promising for this separation. One future goal is to develop this process for the pilot and industrial scale, in which will require more detailed investigation of the different factors affecting the fouling process including the crossflow velocity and the concentration of char particles present in the feed stream. Understanding the underlying mechanisms for char particle removal from bio-oil will allow more efficient membrane separation processes to be designed in the future.

1.4 Publications

Asad Javaid, Tatiana Ryan, Gayla Berg, Xiaoming Pan, Tushar Vispute, Surita R. Bhatia, George W. Huber, David M. Ford, Removal of char particles from fast pyrolysis bio-oil by microfiltration, Journal of Membrane Science 363 (2010) 120–127

1.5 References

[1] L.V. Cremades, et al., Comparative study of the performance of three cross-flow ceramic membranes for water treatment, Water SA 33 (2) (2007) 253–259.

[2] S. Elmaleh, W. Naceur, Transport of water through an inorganic composite membrane, J. Membr. Sci. 66 (2–3) (1992) 227–234.

[3] C. Feik, Pyrolysis oil analysis, Personal Communication, 2009.

[4] S.K.S. Al-Obeidani, et al., Chemical cleaning of oil contaminated polyethylene hollow fiber microfiltration membranes, J. Membr. Sci. 307 (2) (2008) 299–308.

[5] P. Blanpain-Avet, J.F. Migdal, T. Benezech, Chemical cleaning of a tubular ceramic microfiltration membrane fouled with a whey protein concentrate suspension—characterization of hydraulic and chemical cleanliness, J. Membr. Sci. 337 (1–2) (2009) 153–174.

[6] W.S.W. Ho, K.K. Sirkar, Membrane Handbook, Chapman&Hall,NewYork, 1992, xxi, 954 pp

[7] B. Van der Bruggen, et al., A review of pressure-driven membrane processes in wastewater treatment and drinking water production, Environ. Prog. 22 (1) (2003) 46–56.

[8] M.L. Mottern, et al., Permeation porometry: effect of probe diffusion in the condensate, J. Membr. Sci. 313 (1–2) (2008) 2–8.

[9] T. Tzanetakis, et al., Liquid fuel properties of a hardwood-derived bio-oil fraction, Energy Fuel 22 (4) (2008) 2725–2733.

[10] A.V. Bridgwater, G.V.C. Peacocke, Fast pyrolysis processes for biomass, Renew Sust. Energy Rev. 4 (1) (2000) 1–73.

[11] Q. Lu, W.Z. Li, X.F. Zhu, Overview of fuel properties of biomass fast pyrolysis oils, Energy Convers. Manage. 50 (5) (2009) 1376–1383.

[12] E. Fratini, et al., SANS analysis of the microstructural evolution during the aging of pyrolysis oils from biomass, Langmuir 22 (1) (2006) 306–312.

[13] R. van Reis, A. Zydney, Bioprocess membrane technology (vol 297, pg 16, 2007), J. Membr. Sci. 302 (1–2) (2007) 271.

[14] C.C. Ho, A.L. Zydney, A combined pore blockage and cake filtration model for protein fouling during microfiltration, J. Colloid Interf. Sci. 232 (2) (2000) 389–399.

[15] S. Mattaraj, C. Jarusutthirak, R. Jiraratananon, A combined osmotic pressure and cake filtration model for crossflow nanofiltration of natural organic matter, J. Membr. Sci. 322 (2) (2008) 475–483.

[16] F.L. Wang, V.V. Tarabara, Pore blocking mechanisms during early stages of membrane fouling by colloids, J. Colloid Interf. Sci. 328 (2) (2008) 464–469.

[17] J. Hermia, Constant pressure blocking filtration laws—application to power-law non-Newtonian fluids, Trans. IChem Eng. Lond. 60 (3) (1982) 183–187.

[18] E.M. Tracey, R.H. Davis, Protein fouling of track-etched polycarbonate microfiltration membranes, J. Colloid Interf. Sci. 167 (1) (1994) 104–116.

[19] M.C.V. Vela, et al., Analysis of membrane pore blocking models applied to the ultrafiltration of PEG, Sep. Purif. Technol. 62 (3) (2008) 489–498.

Tasks 2-4 all have the same objectives: to reduce the TAN number in the bio-oil. All of the options will be explored including membrane separation, catalytic processing and use of ion exchange resins.

Task 2.0 Acid Removal by Membrane Separation Technology

The objective Task 2 is to implement membrane technology that will allow us to reduce the total acid number (TAN) in bio-oil to less than 5, thus stabilizing it for long-term storage and further processing.

Milestone 3 Reduce total acid number (TAN) to less than 5 in the aqueous fraction of bio-oil using nanofiltration (NF) membranes.

Milestone 4 Reduce total acid number (TAN) to less than 5 in the total bio-oil using nanofiltration membranes.

The feasibility of removing small organic acids from the aqueous fraction of fast pyrolysis bio-oils using nanofiltration (NF) and reverse osmosis (RO) membranes was studied. Experiments were conducted with commercially available polymeric NF and RO membranes and aqueous solutions of increasing complexity, i.e. single solute solutions of acetic acid and glucose, binary solute solutions containing both acetic acid and glucose, and a model aqueous fraction of bio-oil (AFBO) containing acetic acid, formic acid, hydroxyacetone, furfural, guaiacol, catechol and glucose. Feed concentrations close to those in real AFBO were chosen. These concentrations, ranging as high as 34 wt %, were generally at least an order of magnitude higher than previously studied in the literature for related membrane separations. Retention factors above 90% for glucose and below 0% for acetic acid were observed at feed pressures near 40 bar for single and binary solutions, so that their separation in the model AFBO was expected to be feasible. However, all of the membranes were irreversibly damaged when experiments were conducted with the model AFBO due to the presence of guaiacol in the feed solution. Experiments with model AFBO excluding guaiacol were also conducted. NF membranes showed retention factors of glucose greater than 80% and of acetic acid less than -15% when operated at transmembrane pressures near 60 bar.

2.1 Experimental

2.1.1 Membranes and chemicals

NF and RO flat sheet membranes were purchased from Wilkem Scientific (Pawtucket, RI). The information provided by the manufacturers is summarized in Table 2.1. All the membranes were supplied in a dry form except for MPF 34, which were supplied in a wet form in a 0.7 % Roccal preserving solution (0.7% benzalkonium chloride + 0.25% sodium metabisulfite in water). Desal DK and RO AG membranes are thin film composites (TFC) that have a three-layered structure comprising active, intermediate and backing layers. The active (top) layer of Desal DK membrane is a polyamide, with polysulfone as backing layer. The intermediate layer is a proprietary polymer. The layers in RO AG membranes have a similar composition. MPF 34 also consists of three layers, with a backing made of a polypropylene – polyethylene blend. The intermediate and top polymeric layers are a proprietary polymer. RO CE membranes are asymmetric membranes, with a continuous variation in structure across the membrane thickness, made of cellulose acetate.

Table 2.1 Membrane parameters. All data are from the manufacturers, except for the permeability values in parentheses that were measured in this work

Membrane	Rejection	Polymer	Pure water permeability constant, A (L/m^2-hr-bar)	pH range @ 25 °C
GE Osmonics Desal DK	98 % $MgSO_4$	Aromatic polyamide	5.44(4.78)	2 – 11
Koch MPF 34	200 MWCO[a]	Proprietary	1.95(1.71)	0 – 14
GE Osmonics RO AG	99.5 % NaCl	Aromatic polyamide	2.85(2.87)	4 – 11
GE Osmonics RO CE	97% NaCl	Cellulose acetate	1.38(1.32)	2 – 8

D-glucose (anhydrous), acetic acid (glacial), phenol (laboratory grade), ethanol (200 proof), methanol (laboratory grade) were purchased from Fisher Scientific. Furfural (99 %), formic acid (98 %), catechol (99 %), guaiacol (99 %) were purchased from Acros and hydroxyacetone (technical) was purchased from TCI America. Aqueous solutions of model solutions were prepared using distilled water.

2.1.2 Permeation set-up

A Sepa® CF II Med/High foulant lab scale cross-flow membrane filtration unit from GE Osmonics was used to carry out the permeation experiments. Figure 2.1 shows the schematic diagram of the experimental equipment. The Sepa® CF II unit has three major components: cell body, cell holder, and hydraulic hand pump. Precut rectangular membranes (19 cm × 14 cm) with an effective area of 137 cm^2 were installed in the cell body. Feed spacer and permeate carrier were installed on the bottom and top of the membrane respectively. The unit was pressurized using the hydraulic hand pump to a pressure greater than the expected feed pressure; double O-rings in the cell body provide a leak-proof seal. The feed stream was pumped using an Eldex Optos reciprocating pump from a 1.5 L feed vessel to the inlet. Flow continued through a manifold into the membrane cavity and then flowed tangentially across the membrane surface. The transmembrane pressure was monitored by two digital pressure gauges located on the inlet and outlet of the cell. A back pressure valve was mounted on the retentate outlet to control the transmembrane pressure. The permeate pressure was always atmospheric. All the experiments were conducted at room temperature (21 ± 1 °C) at constant cross flow velocity of 0.026 m/s and at different transmembrane pressures ranging from 5 to 58 bar. A start-up period of at least 20 min allowed the system to reach steady state and then permeate samples were collected at each pressure and timed to calculate permeation flux. Both the permeate and the retentate were entirely recycled to feed vessel, except for a small sample of permeate (~ 2 mL) that was taken for chemical analysis at each flux measurement. Since the total volume of permeate (< 10 mL) taken for analysis during an experiment was very small compared to the feed volume (1.5 L), concentration changes in the feed during the experiments can be neglected. None of the membranes used in this work were subject to any kind of pretreatment (e.g. pressurizing membranes with pure water and/or immersing the membranes in different organic solvents) that is known to impact the flux and rejection [1]. Since the MPF 34 membranes were supplied in wet form, these membranes were washed with distilled water before using them in our experiments.
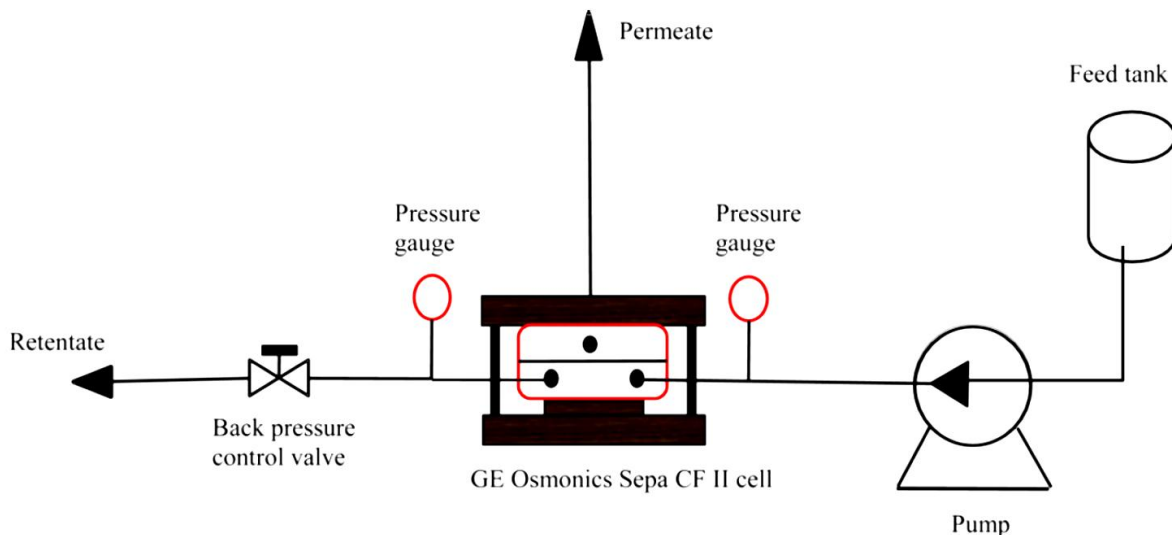
Figure 2.1 Schematic view of the membrane unit used.

2.1.3 Model aqueous solutions

Since the complete chemical analysis of AFBO is difficult, studies containing model compounds are helpful to understand the chemistry involved in hydrogenation and further processing of AFBO. Model compound studies also help in understanding the interaction between different components in the bio-oil. Based on the composition of bio-oil and literature data, Vispute and Huber [2] suggested a model solution to represent AFBO. Initial experiments were run with single and binary solute solutions of acetic acid and glucose to test the performance of the membranes. The model solutions used were: single solute solutions of 7 wt% acetic acid and 15 wt% glucose, binary solute solution of 7wt% acetic acid and 15wt% glucose and a model AFBO whose composition is given in Table 2.2. The pH of this model AFBO was close to 2, so that all of the solutes were expected to be in neutral form; therefore it is reasonable to expect that membrane charge did not play an important role in retention. We note that this model AFBO was actually more dilute than that suggested by Vispute and Huber [2]; this made the flux measurements convenient while still being realistic, since the amount of water required for extraction (and hence degree of dilution) will vary from one bio-oil to another.

Table 2.2 Composition of model aqueous fraction of bio-oil

Compound	Weight , %	Water solubility (g/100 ml)
Water	65	-----
Glucose	15	91
Acetic acid	7	100 (miscible)
Hydroxyacetone	4.65	100 (miscible)
Formic acid	2.3	100 (miscible)
Furfural	2.3	8.3
Guaiacol	2.3	2.9
Catechol	1.45	43

2.1.4 Chemical analyses

High performance liquid chromatography (HPLC) and gas chromatography (GC) were used for the analysis of feed and permeate samples. HPLC was equipped with Aminex HPX-87 H column and two detectors; refractive index (RI) and ultraviolet (UV) were used to analyze glucose and acetic acid, respectively. The mobile phase was 0.005 M H_2SO_4. For all other compounds, a RTx®-VMS capillary column was used in a Agilent Technologies 7980A chromatograph equipped with a flame ionization detector (FID). The carrier gas was helium and a single temperature programming profile was used. Feed samples were diluted by a factor of 10 to reduce the degradation of glucose in the detector. Optical microscopy was used to characterize the membrane surface. The observed retention, R_{obs}, of solute can be used to describe membrane performance and was calculated from Eq. (1), where C_p and C_f are the permeate and feed concentrations of solute, respectively.

$$R_{obs} = \left(1 - \frac{C_p}{C_f}\right) \times 100\% \tag{1}$$

2.2. Results and discussion

2.2.1 Pure water flux

Pure water flux data for all the four membranes used in our study are shown in Table 2.1 in terms of the water permeability constant, A, which was obtained from the slope of pressure- flux data as shown in Eq. (2). The osmotic pressure ($\Delta\pi$) is zero and $A = J/\Delta P$ for pure water. From Table 2.1, it is clear that the values measured in our lab (shown in parentheses) are consistent with the values provided by the manufacturers.

$$J = A\,(\Delta P - \Delta\pi) \tag{2}$$
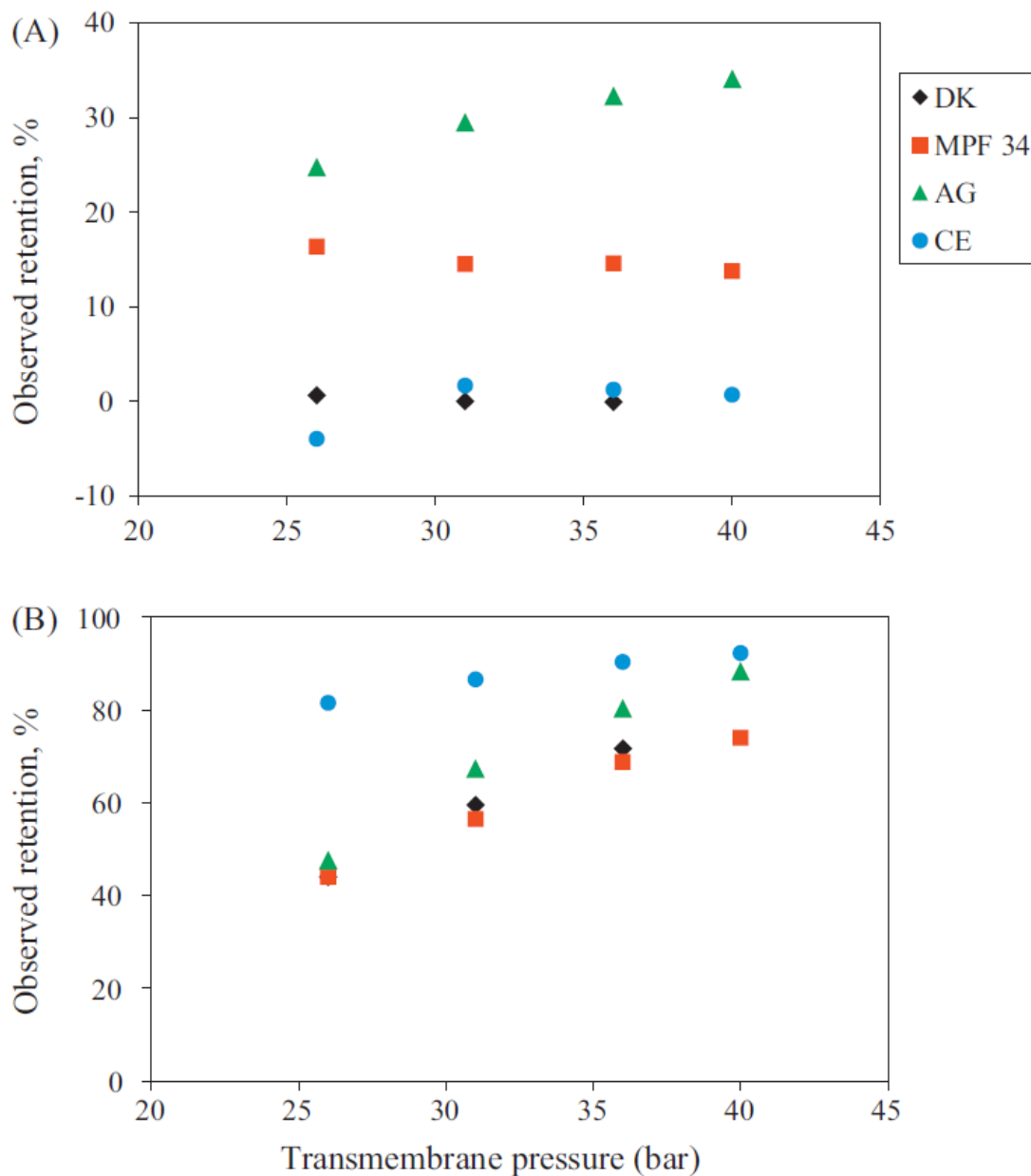
2.2.2 Single-solute solutions

Experiments were carried out with single solute solutions of acetic acid (7 wt %) and glucose (15 wt %) using all of the four membranes listed in Table 2.1. The effect of transmembrane pressure on flux and solute retention was explored. The variation of flux with transmembrane pressure is shown in Fig 2.2. In all experiments, the flux was nearly a linear function of transmembrane pressure and was lower than that of pure water. For example, with Desal DK membrane at 36 bar, the fluxes of 7 wt% acetic acid and 15 wt% glucose feed solutions were 85 and 5 L m^{-2} hr^{-1} respectively as compared to the pure water flux of 164 L m^{-2} hr^{-1}. For both single solute solutions, Desal DK and RO AG membrane have the highest and lowest fluxes, respectively.
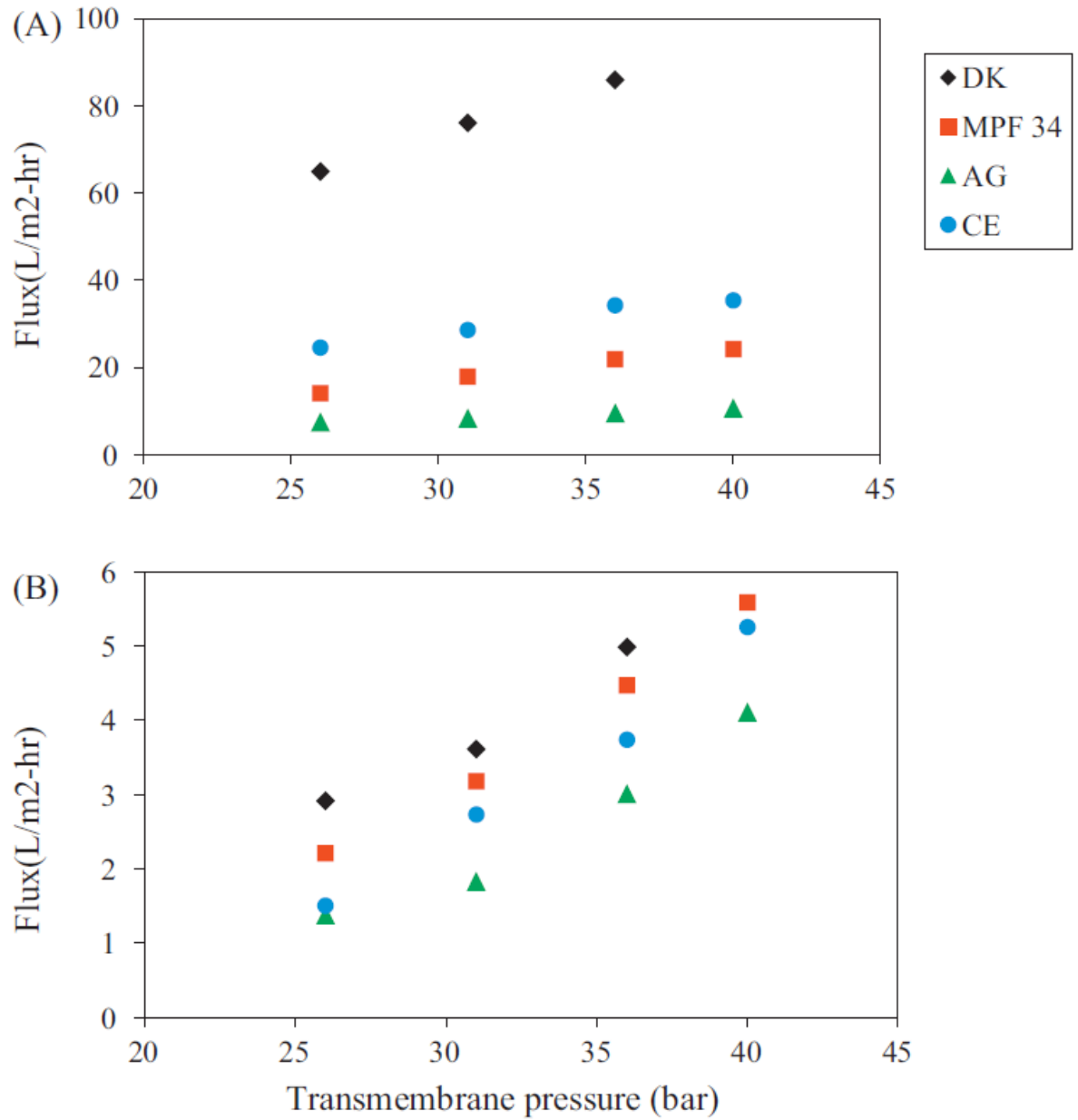
Figure 2.2 Influence of applied pressure on permeate flux: (A) 7 wt% acetic acid and (B) 15 wt% glucose solutions.

Figure 2.3 shows the effect of transmembrane pressure on acetic acid and glucose retentions. Glucose retentions up to 90% and acetic acid retentions down to - 4% were observed. For a particular membrane, glucose retention is always higher than that of acetic acid. Evidently, the higher glucose retention is due to the larger size of the glucose molecule, which is in accordance with the sieving effect [3, 4]. Negative retention (i.e., permeate enrichment) is unusual but it is not an entirely new phenomenon. Weng et al [5] observed negative retentions of acetic acid (varied between -2.3 % to 6.6%) with spiral wound Desal DK membrane module. Lonsdale et al. [6] also observed negative retention of phenol in

aqueous mixtures with cellulose acetate membranes. Possible explanations for negative retention are charge effects and intermolecular interactions between solvent and solute. In case of acetic acid, there is an inverse relation between flux and retention. The flux of acetic acid solution through the membranes decreased in the sequence DK > CE > MPF 34 > AG whereas the retention of acetic acid followed the reverse order (although DK and CE membranes showed essentially identical retentions). However, there is no such trend with glucose solution. In general, both flux and solute retention increased as the transmembrane pressure increased. This can be explained using solution – diffusion model for solvent and solute transport through the membrane [7]. According to this model, as pressure is increased the solvent (water) flux increases faster than solute flux and thus retention increases.


Figure 2.3 Observed retention as a function of transmembrane pressure: (A) 7 wt% acetic acid (B) 15 wt% glucose solutions.

2.2.3 Mixed-solute solutions

Figures 2.4 and 2.5 show, respectively, the acetic acid and glucose retentions obtained with all the membranes for one mixture composition (7 wt% acetic acid and 15 wt% glucose). The data for the single-solute solutions at the same concentrations are also shown for comparison. For acetic acid, the retentions in mixed-solute solutions are significantly lower than those in single-solute solutions. This is favorable for the separation process proposed here. A similar phenomenon was reported by Weng et al [5]. They investigated the separation of xylose and acetic acid by nanofiltration and observed that the acetic acid retention was significantly lower in the presence of xylose than that in single-solute solution. Laufenberg et al [8] studied retention characteristics of multicomponent organics by reverse osmosis. They observed that acetic acid retention could be lower or higher in the presence of other organic acids. In both the cases, it was concluded that the alteration in acetic acid retention may be attributed to intermolecular interactions between acetic acid and other components, although further studies are required to understand the link between the intermolecular interactions and the observed changes in retention. Other studies showed that in binary mixtures of salt and sugar, the salt retention was decreased as the sugar concentration increased [9]. This was explained as a result of viscosity increase in the concentration polarization layer due to high retention of sugar, which hampered the back diffusion of the salt. In contrast, Fig. 2.5 shows that the retention of glucose is not much affected by the presence of acetic acid, except for CE membrane for which the retention of glucose in mixed-solute solution is slightly lower than that in single-solute solutions. The observed flux is also slightly higher than that obtained with single-solute glucose solution (not shown). This implies that CE membranes might be swollen in the presence of acetic acid.
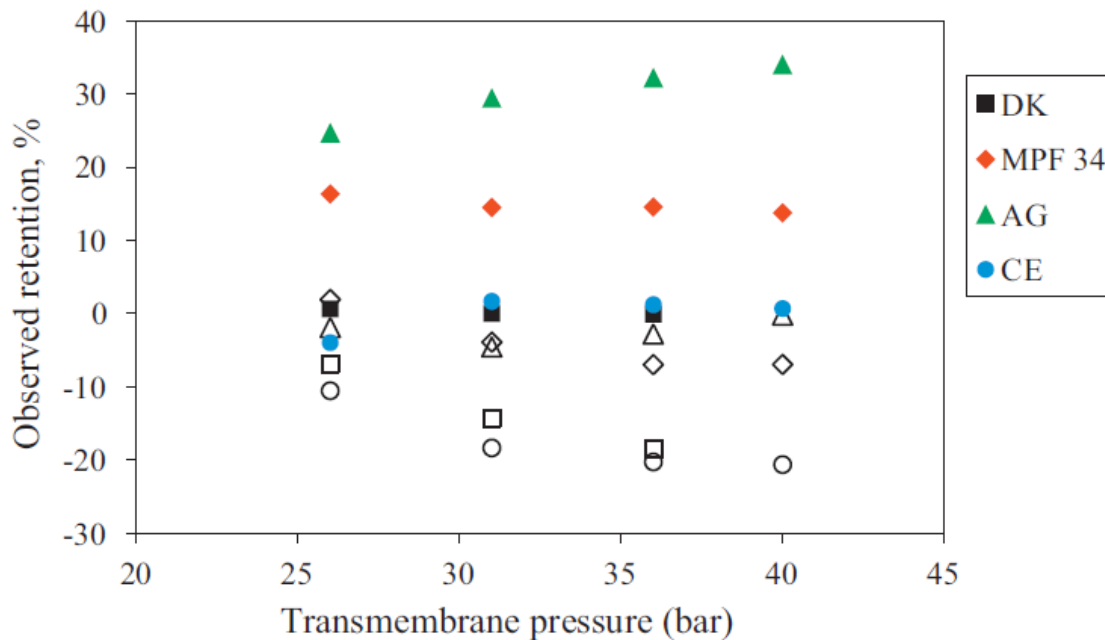

Figure 2.4 Acetic acid retention vs. transmembrane pressure for mixed-solute solution of 7 wt% acetic acid and 15wt % glucose, compared to 7 wt% acetic acid retention in single-solute solution. Closed and open symbols represent single and mixed solute retentions, respectively.
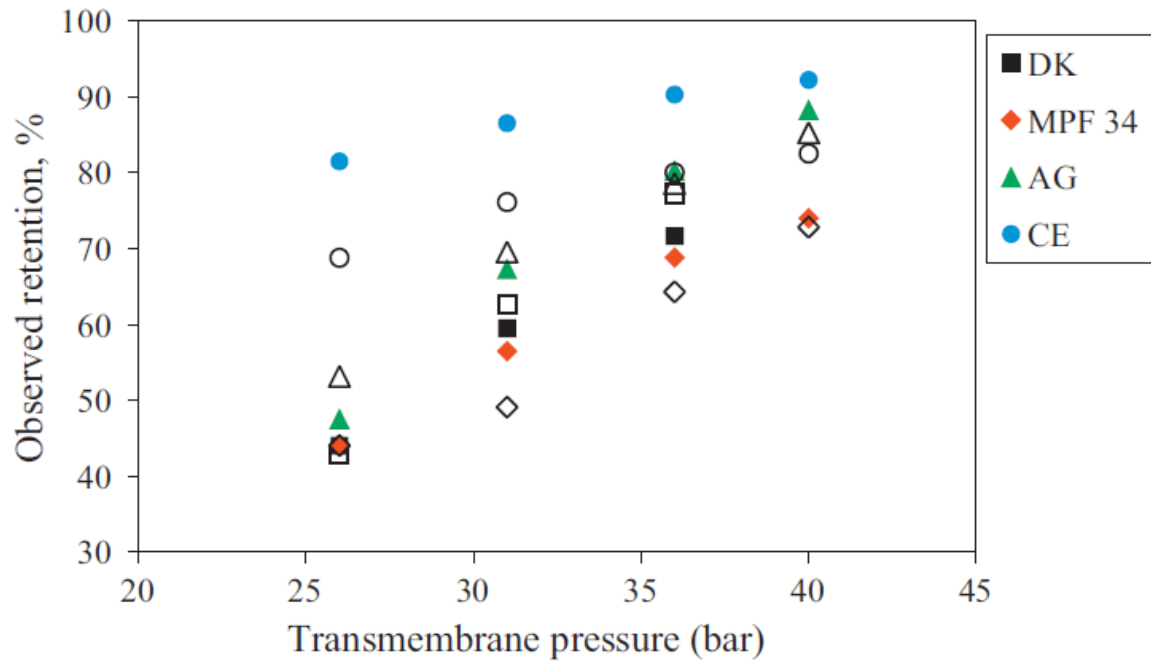
Figure 2.5 Glucose retention vs. transmembrane pressure for mixed-solute solution of 7 wt% acetic acid and 15wt % glucose, compared to 15 wt% glucose retention in single-solute solution. Closed and open symbols represent single and mixed solute retentions, respectively.

2.2.4 Membrane stability

Experiments were conducted with the model AFBO, as given in Table 2.2, using Desal DK membrane. A permeance that was unexpectedly high for this concentrated multicomponent mixture was observed, indicating that the model AFBO may have damaged the membrane. The membrane was tested again with pure water, and the flux was higher by a factor of 22 as compared to the data in Table 2.1, strongly indicating that irreversible damage had occurred. The results are summarized together with the permeances of single solute solutions of 7 wt% acetic acid and 15wt% glucose in Fig. 2.6. Most NF membranes are designed for treating aqueous systems that have low levels of contaminants. Past studies have shown that exposing such membranes to organic compounds at higher concentrations resulted in loss of structural integrity and separation performance [10,11]. The DK membranes were observed to curl after the permeation experiments with AFBO, which was not the case with binary solutions of glucose and acetic acid. These visual observations on the membranes also support the findings of Yang et al. [10], who observed curling of NF membranes when exposed to different organic solvents. Since the binary mixtures of glucose and acetic acid didn't cause any damage to these membranes, one or more of the new components of the multicomponent mixture likely were responsible.
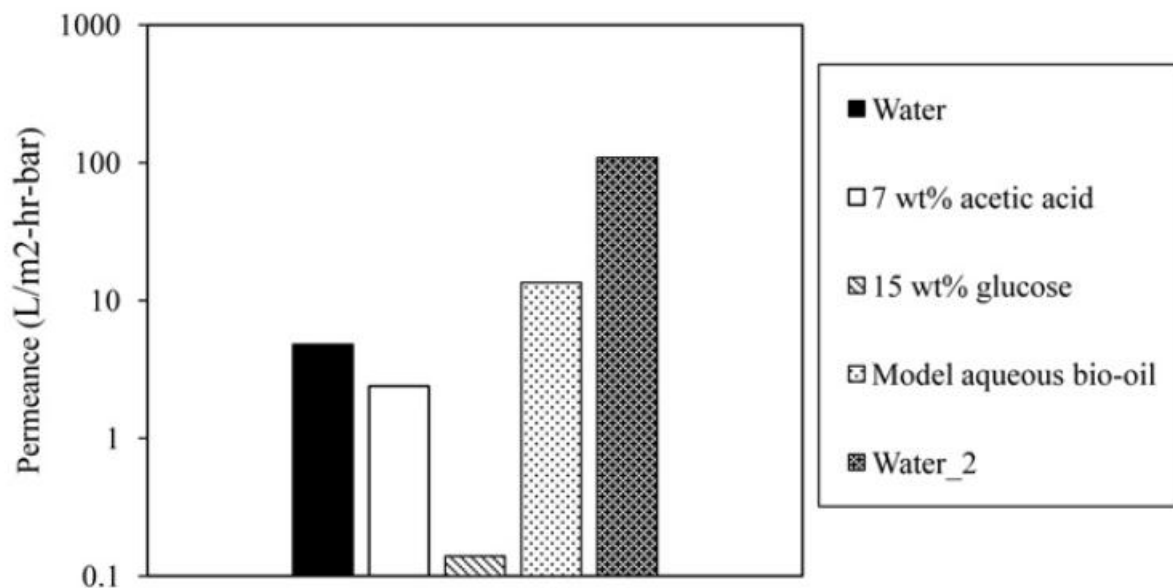
Figure 2.6 Stability test of Desal DK with different feed solutions. The permeance is Flux normalized by transmembrane pressure. Water_2 indicates a second pure water test following the model AFBO.

Permeation experiments were done with different feed solutions to further investigate the cause of damage. Initially, an aqueous solution of furfural was filtered through the membrane. After that catechol, hydroxyacetone, and guaiacol were added step by step. The individual component concentrations were maintained close to those in model AFBO. At each step, the membranes were exposed to feed solution for 30 min and the permeances were measured. The results are shown in Fig. 2.7. The permeance declined with addition of new components until guaiacol was introduced into the feed solution. Then the permeance went up dramatically, as it did in the case of model AFBO.
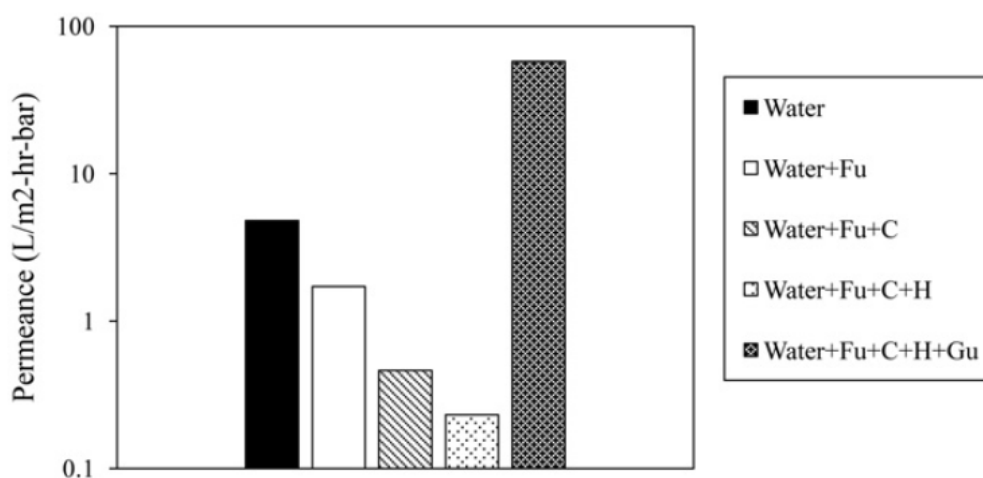

Figure 2.7 Variation in permeance with change in feed components: furfural (Fu), Catechol (C), hydroxyacetone (H), guaiacol (Gu).

Although polyamide membranes are known to be sensitive to chlorine via ring chlorination [12], to our knowledge there exist no literature reports on their sensitivity to phenolic compounds. Polyamide reverse-osmosis membranes were used by Sagehashi et al. [13] to separate phenols and furfural from pyrolysis derived aqueous streams. Van der Bruggen et al. [3] studied separation performance of different NF membranes made up of polyamide and polysulfone with a wide variety of organic compounds including phenolics. No membrane damage was reported in either of these studies. However, the concentration of phenolics used in their experiments was an order of magnitude lower than that in our experiments. The effect of solute concentration on membrane compatibility was examined by performing filtration experiments with solutions of guaiacol and phenol at different concentrations using Desal DK and MPF 34 membranes. At each concentration, the feed solutions were filtered for 30 min and the concentration was increased step by step. The results are summarized in Fig. 2.8. Both membranes showed similar qualitative behavior with guaiacol and phenol. Permeance initially decreased as the concentration of the phenolic compounds in the feed solution was increased, up to a "critical concentration" at which it started to increase. The critical concentrations at which the membranes started to show signs of damage were different for guaiacol (~1.5 wt%) and phenol (~5 wt%). Above the critical concentration, the active (top) layer of treated membranes developed visible pinches while the bottom layer seemed unaffected. Optical microscopy was carried out to characterize both virgin and guaiacol-treated Desal DK membranes. The images are shown in Fig. 2. 9. The images show that the active surface was not uniformly dissolved in guaiacol but was damaged at certain spots. On the other hand, the bottom layer was not affected. Experiments using RO_AG and RO_CE membranes were also conducted with 1.5 wt% of guaiacol solution. The RO_AG membranes developed a very high permeance similar to that of Desal DK and MPF 34 membranes. In contrast, the flux through the RO_CE membrane was seen to drop until it was no longer measurable, suggesting that the mechanism of damage may be different for this membrane.
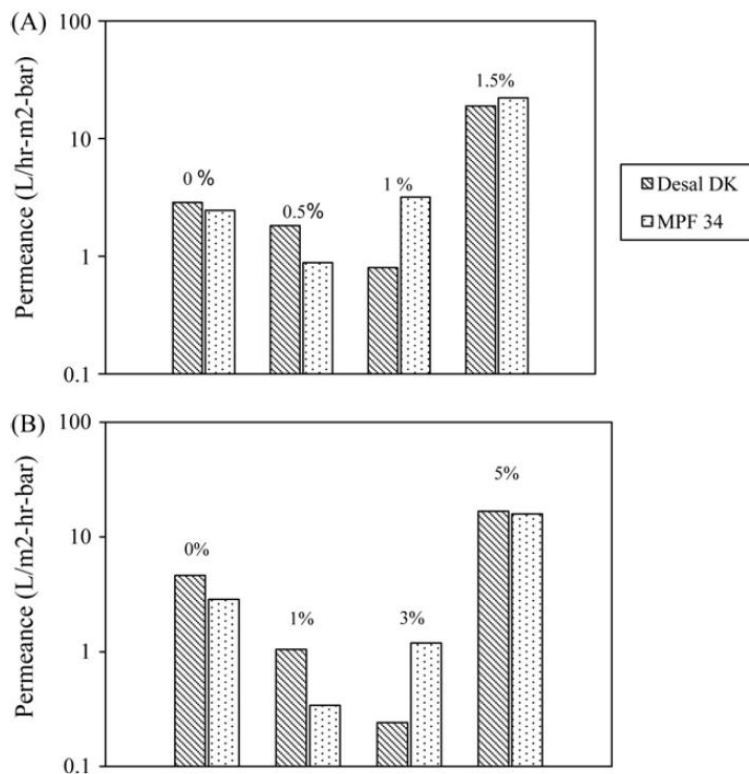
Figure 2.8 Contents in feed solutions for Desal DK and MPF 34: (A) Guaiacol and (B) Phenol.
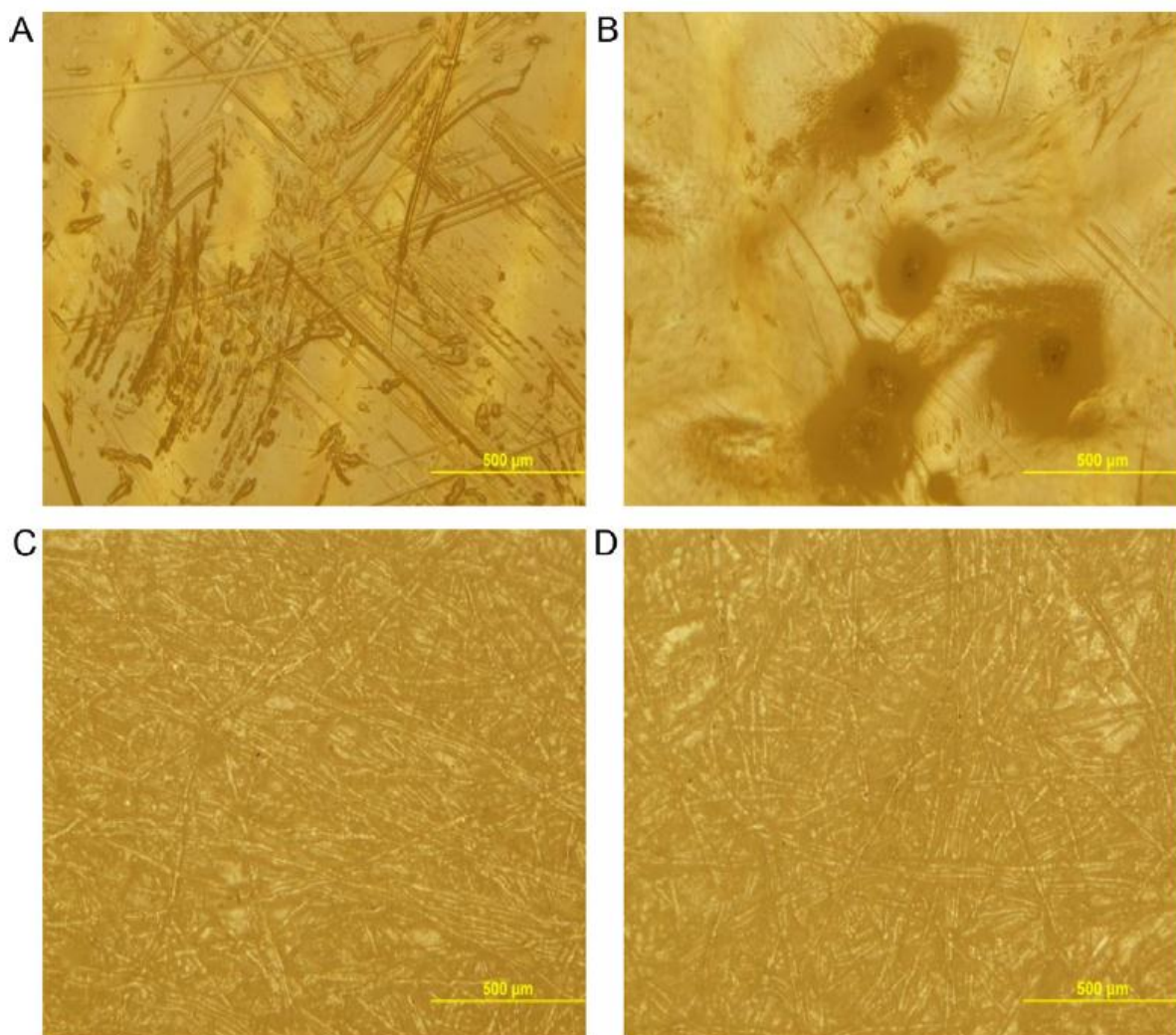
Figure 2.9 Optical microscopic images. (A) Top layer and (B) Bottom layer of virgin membrane. (C) Top layer and (D) Bottom layer of guaiacol treated membrane.

Experiments with aliphatic alcohols, methanol and ethanol, were also conducted. Both the membranes, Desal DK and MPF 34, were very stable up to alcohol concentrations as high as 18 wt%. Compared to aliphatic alcohols (pKa ~ 15), phenolics (pKa~10) have a greater tendency to deprotonate, resulting in highly water-soluble phenoxide ions, *e.g.* $C_6H_5O^-$. (One explanation for the greater acidity of phenolics is the delocalization of negative charge over the aromatic ring.) These phenoxide anions might react with an amide group on the membrane and convert it to a corresponding ester, providing a possible explanation for the observation that membrane damage occurred with phenolics but not with aliphatic alcohols. However, comparing the two phenolics, membrane damage occurred at a lower solute concentration with guaiacol as compared to phenol, though the pKa values of both are almost equal. At this point further investigation is needed to explain the chemical mechanism behind the damage.

2.2.5 Modified model aqueous fraction of bio-oil

Due to membrane damage by guaiacol, experiments with model AFBO excluding guaiacol were conducted using all four types of membranes at a transmembrane pressure of 40 bar. Both the RO

membranes failed to yield meaningful results. With the RO_CE membrane there was no measurable flow. The active layer of RO_AG membranes turned pink after treating with model AFBO and glucose retention was very low (~ 20%). The permeate solution was believed to be contaminated due to the chemical changes that took place in the active layer; therefore the data for RO_AG is not presented here. Data at 40 bar were obtained with the two NF membranes, Desal DK and MPF 34, and was averaged over two membrane samples in each case. Solute retentions are summarized in Table2.3 (Columns 2 and 4). Formic acid and catechol had very low signals in the feed and permeate and were almost undetected by GC, so they are not shown in the table. Glucose retention is positive and all other solutes have negative retentions. However the glucose retention is lower than that in single and binary solutions. This result is consistent with the findings of Goulas et al. [14] who found that in mixtures of oligosaccharides, individual sugar retentions decreased as the total sugar concentration increased. Another possible explanation is that there might be positive coupling between glucose and other components present in the model AFBO that in turn reduced the glucose retention.

Table 2.3 Retention of components present in model aqueous fraction of bio- oil, without guaiacol. Formic acid and catechol were undetectable. The total flux is also shown.

		Retention, %		
		Desal DK		MPF 34
		40 bar	58 bar	40 bar
Compound	Flux (L m^{-2} hr^{-1})	2.71	4.165	0.584
Glucose		**47.4**	**83.1**	**54.7**
Acetic acid		-14	-16.7	-7.7
Hydroxyacetone		-9	-15.9	-1.35
Furfural		-12	-35.6	-14.4

Since the glucose retentions achieved at 40 bar with model AFBO were moderate, experiments were performed with the Desal DK membrane at a higher pressure, 58 bar. The results are also shown in Table 2.3 (Column 3). Glucose retention is increased from 47% to 83% as the transmembrane pressure increased from 40 to 58 bar. Furthermore, the retentions of all other compounds became more negative. These results indicate that the separation of acids and other low molecular weight organic compounds from glucose is operationally feasible at high transmembrane pressures.

2.2.6 Effect of concentration on flux

The effect of total feed concentration on flux is shown in Fig. 2.10. Our results indicate that higher the concentration of the feed solution the lower the flux. These results are consistent with the findings of Sjöman et al [15]. With Desal DK membranes they found an order of magnitude decrease in flux as the concentration of the feed (binary mixture of xylose and glucose in the mass ratio 1:1) increased from 10 wt% to 30 wt%. Yang et al [10] observed similar behavior with aqueous solutions of dyes. At a pressure of 30 bar, the water fluxes at dye concentrations of 35 and 10000 mg/L were 24 and 18 L m^{-2} h^{-1}, respectively. Due to high feed concentrations and low cross flow velocities used in our work, concentration polarization cannot be neglected. Accordingly, flux would decrease due to the increased resistance near the membrane surface. Also when a solute is added to the pure water, the driving force for water flux decreases as can be seen from Eq. 2; the effective transmembrane pressure that drives the feed is equal to the applied hydraulic pressure minus osmotic pressure difference. Other possible explanations include increase in viscosity, adsorption, or blocking of the membrane pores.
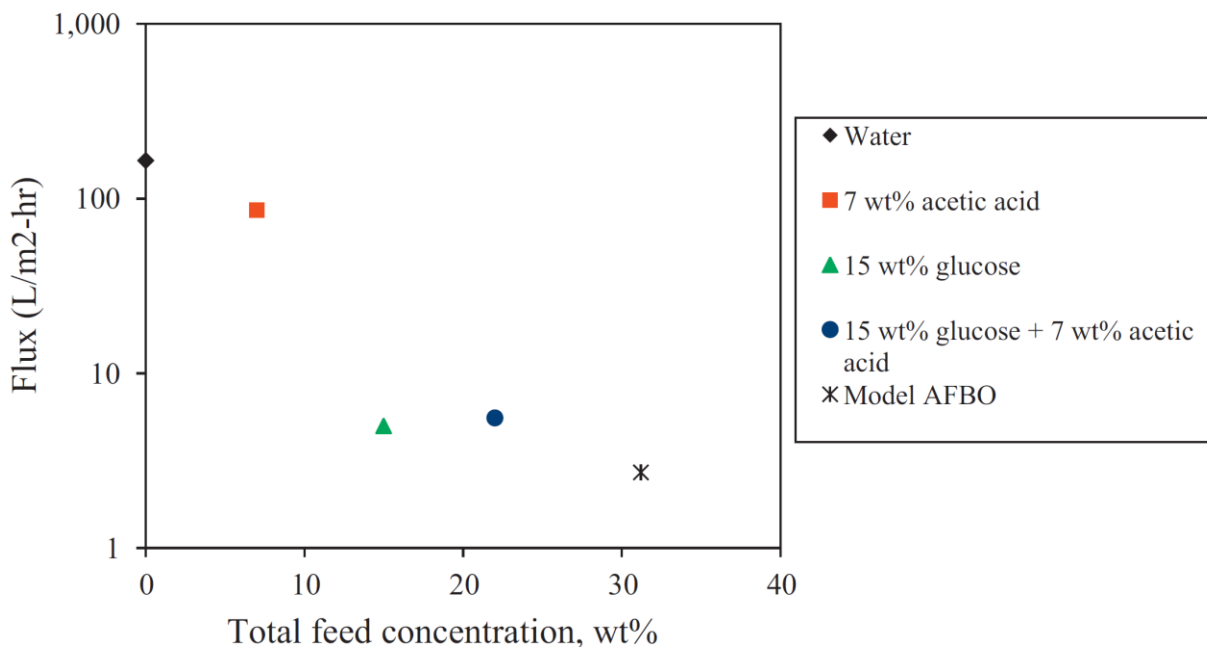
Figure 2.10 Effect of total feed concentration on flux (measurements were made at constant pressure, 36 bar).

2.3 Conclusions

Commercially available NF and RO membranes were used to study the possibility of separating carboxylic acids from sugars in AFBO. Experiments with single and binary aqueous solutions of acetic acid and glucose showed that retention factors of glucose above 90% and negative retention factors of acetic acid could be achieved at moderate (~ 40 bar) feed pressures. Fluxes were linearly dependent on transmembrane pressure and decreased with increasing solute concentration. The binary experiments showed that glucose retention is largely unaffected by the presence of acetic acid (except for the RO CE membrane) but acetic acid retention decreases significantly in the presence of glucose. Experiments with the model AFBO resulted in irreversible damage to the membranes. Subsequent experiments identified guaiacol as the detrimental compound and further demonstrated that phenol causes a similar effect. Experiments with guaiacol-free model AFBO showed that high retentions (> 80%) of glucose are possible with NF membranes at higher feed pressures (~ 60 bar). In summary, the separation of acids and other low molecular weight compounds from sugars in AFBO using NF/RO membranes appears to be feasible, with two important caveats. First, a practical membrane process would require a different, resistant polymer formulation or a pretreatment to remove phenolics. Second, relatively high transmembrane pressures are needed to achieve sufficient retention of glucose and overall flux.

2.4 Publications

Achyuta Teella, George W. Huber, David M. Ford Separation of acetic acid from the aqueous fraction of fast pyrolysis bio-oils using nanofiltration and reverse osmosis membranes Journal of Membrane Science 378 (2011) 495– 502

2.5 References

[1] M. Mänttäri, A. Pihlajamäki, E. Kaipainen, M. Nyström, Effect of temperature and membrane pretreatment by pressure on the filtration properties of nanofiltration membranes, Desalination, 145 (2002) 81-86.

[2] T.P. Vispute, G.W. Huber, Production of hydrogen, alkanes and polyols by aqueous phase processing of wood-derived pyrolysis oils, Green Chemistry, 11 (2009) 1433-1445.

[3] B. Van der Bruggen, J. Schaep, D. Wilms, C. Vandecasteele, Influence of molecular size, polarity and charge on the retention of organic molecules by nanofiltration, Journal of Membrane Science, 156 (1999) 29-41.

[4] P.-Y. Pontalier, A. Ismail, M. Ghoul, Mechanisms for the selective rejection of solutes in nanofiltration membranes, Separation and Purification Technology, 12 (1997) 175-181.

[5] Y.H. Weng, H.J. Wei, T.Y. Tsai, W.H. Chen, T.Y. Wei, W.S. Hwang, C.P. Wang, C.P. Huang, Separation of acetic acid from xylose by nanofiltration, Separation and Purification Technology, 67 (2009) 95-102.

[6] H.K. Lonsdale, U. Merten, T. Tagami, Phenol transport in cellulose acetate membranes, J. Appl. Polym. Sci., 11 (1967) 1807-1820.

[7] R.W. Baker, Membrane Technology and Applications, John Wiley & Sons, Ltd, West Sussex, England, 2004.

[8] G. Laufenberg, S. Hausmanns, B. Kunz, The influence of intermolecular interactions on the selectivity of several organic acids in aqueous multicomponent systems during reverse osmosis, J. Membr. Sci., 110 (1996) 59-68.

[9] E. Vellenga, G. Trägårdh, Nanofiltration of combined salt and sugar solutions: coupling between retentions, Desalination, 120 (1998) 211-220.

[10] X.J. Yang, A.G. Livingston, L.F. Santos, Experimental observations of nanofiltration with organic solvents, J. Membr. Sci., 190 (2001) 45-55.

[11] Y. Zhao, Q. Yuan, Effect of membrane pretreatment on performance of solvent resistant nanofiltration membranes in methanol solutions, J. Membr. Sci., 280 (2006) 195-201.

[12] S. Avlonitis, W.T. Hanbury, T. Hodgkeiss, Chlorine degradation of aromatic polyamides, Desalination, 85 (1992) 321-334.

[13] M. Sagehashi, T. Nomura, H. Shishido, A. Sakoda, Separation of phenols and furfural by pervaporation and reverse osmosis membranes from biomass-superheated steam pyrolysis-derived aqueous solution, Bioresour. Technol., 98 (2007) 2018-2026.

[14] A.K. Goulas, P.G. Kapasakalidis, H.R. Sinclair, R.A. Rastall, A.S. Grandison, Purification of oligosaccharides by nanofiltration, J. Membr. Sci., 129 (2002) 312-335.

[15] E. Sjöman, M. Mänttäri, M. Nyström, H. Koivikko, H. Heikkilä, Separation of xylose from glucose by nanofiltration from concentrated monosaccharide solutions, Journal of Membrane Science, 292 (2007) 106-115.

Task 3.0 Acid Removal by Catalytic Processing

Acid removal from bio-oil can also be achieved by catalytic hydrogenation. Acids can undergo hydrogenation in presence of catalyst to produce corresponding aldehydes and on further hydrogenation, corresponding alcohols. Employing this method to remove acids from whole bio-oil is hindered by the bio-oil instability at high temperatures. Nevertheless aqueous fraction of bio-oil can be subjected to mild catalytic hydrotreating to convert the acids to alcohols. The objective of this task was to develop continuous flow catalytic processes for hydrogenation of the acids in the aqueous and organic fraction. We have previously shown that we can hydrogenate the acids in the aqueous fraction of the bio-oil, however further development is necessary to bring this to a commercial level.

Milestone 5   Decrease the TAN of the aqueous fraction of bio-oils to less than 5 by catalytic hydrogenation

Milestone 6   Decrease the TAN of the organic fraction of the bio-oil to less than 5 by catalytic hydrogenation.

3.1 Experimental

3.1.1 Materials

Three kinds of bio-oil were used for this study. The 1st kind bio-oil used in these studies was obtained from the Renewable Oil International (ROI) LLC and was made from oak wood using ROI's fast pyrolysis process[1,2]. ROI uses a proprietary Auger reactor to make the bio-oils in high yield. The bio-oil was stored in the refrigerator to minimize ageing. The 2nd kind of bio-oil used in our studies is Pine Wood Bio-oil (PWBO). It was obtained from Mississippi State University. The 3rd kind of bio-oil used in our studies was supplied by the US Department of Energy and was manufactured by National Renewable Energy Laboratory, Golden, Colorado using the Thermochemical Process Development Unit from white oak pellets. It is called DOE-BO in this report.

3.1.2 Elemental analysis, viscometry and catalyst characterization

Elemental analysis (C, H and O) of the bio-oil and its various fractions was done at Schwarzkopf Microanalytical Laboratory, Woodside, NY. All the viscosity measurements were done at 25 °C. Catalysts were characterized by hydrogen chemisorption in a Quantachrome Autosorb 1C. About 0.1 gm catalyst was loaded in a chemisorption cell and reduced. Reduction temperature regime was: room temperature to 260 °C at 30 °C h^{-1} and hold at 260 °C for 2 h. The isotherms were then taken at 30 °C and 267, 533, 800, 1067 and 1333 N m^{-2}. The chemisorption cell was then evacuated for 30 minutes. Isotherms were again taken at 30 °C and 267, 533, 800, 1067 and 1333 N m^{-2} to calculate the extent of physisorption. The amount of chemisorbed hydrogen was calculated from the difference between the two isotherms. The liquid samples were analyzed for the carbon content by a Shimadzu 5000A Total Organic Carbon (TOC) analyzer. The aqueous samples were further diluted by distilled water to the concentration below 1000 ppm carbon for the TOC analysis. The TOC samples were fortified with 0.5 N HCl (1.2 gm for 38.8 gm diluted sample) to remove the dissolved CO_2. The TOC analyzer was standardized by sorbitol solutions of known concentrations.

3.1.2 Bio-oil extraction and pre-treatment

The bio-oil was mixed with distilled water to separate into two phases: an aqueous rich phase (WSBO: water soluble fraction of bio-oil) and an organic rich phase (WIBO: water insoluble bio-oil

fraction). The mixture was then centrifuged in a Marathon 2100 centrifuge (Fisher Scientific) at 10,000 rpm for 30 minutes to ensure the phase separation. The two phases, aqueous (top) and non-aqueous (bottom), were then separated by decanting. The weight of the aqueous faction was measured to determine the amount of bio-oil that dissolved in water. For the experimental purpose 28 gm of bio-oil was added to 112 gm of water and mixed well. The aqueous and non-aqueous phases were separated by centrifugation followed by decanting. The resulting aqueous solution is about 13.4 wt% water soluble bio-oil in water, which is about 5 wt% carbon in water. This aqueous solution was used in the batch hydrogenation experiments. The product of batch hydrogenation was further diluted to about 2 wt% carbon in water.

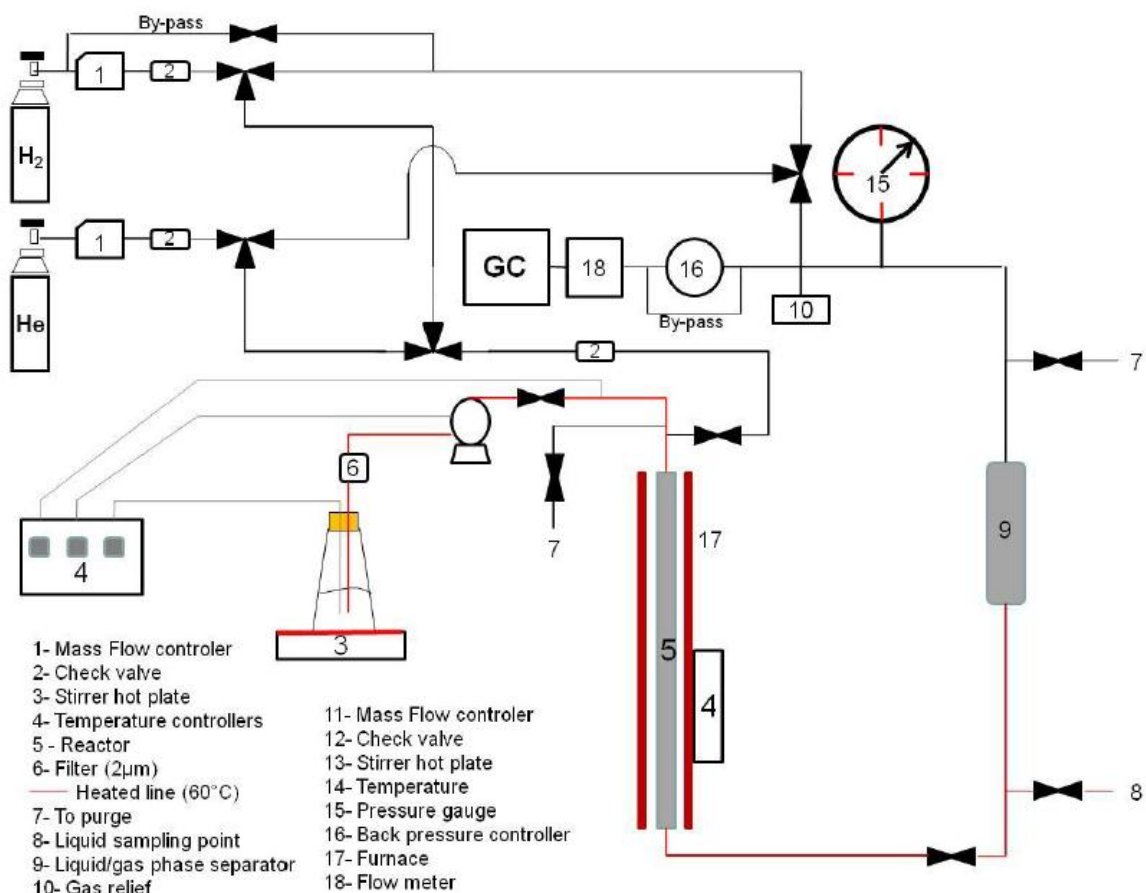### 3.1.3 Low Temperature Hydrogenation (LTH) of the Aqueous Fraction of Bio-oil

3.1.3.1 Batch Reactor

The low temperature hydrogenation was carried out in batch as well as flow reactor. In the case of batch reactor, about 80 ml of the aqueous fraction of the bio-oil (with about 5 wt% carbon) was loaded in the reactor along with 3-4 gm (50 wt% moisture content) of 5 wt% Ru / activated C catalyst (Strem Chemicals, Product No. 44-4059). The reactor was then purged at least 4-5 times with helium gas to get rid of the air present in the reaction vessel. The reactor was then purged with hydrogen at least 4-5 times to replace all the helium with hydrogen. The reactor pressure was set to 700 psi by adding hydrogen and the heating and stirring were started. Once the temperature reached the desired value, the reactor pressure was increased to 1000 psi total by adding more hydrogen. Additional hydrogen was added to the reactor during the course of reaction to compensate for the hydrogen consumption. The total pressure was maintained at 1000 psi. Amount of hydrogen consumed during the reaction was calculated from the decrease in pressure. Liquid samples were withdrawn during the run from the liquid sampling tube. The liquid samples were filtered before analysis to remove the catalyst particles. Typical operating temperature and pressure were 175 °C and 1000 psi respectively. The product and feed compositions were measured with a Shimadzu Gas Chromatograph (GC) (model 2010) and a High Performance Liquid Chromatograph (HPLC). Flame ionization detector (FID) was used on the GC to quantify all the reactants and products except sugars, sugar alcohol and levoglucosan. The reactants and products were also verified by GCMS. Restek Rtx-VMS (Catalog No. 19915) column was used with constant column linear velocity of 31.3 cm s^{-1}. Ultra high purity helium was used as the carrier gas. Injector and detector were both held at 240 °C. The GC oven was programmed with following temperature regime: Hold at 35°C for 5 min, ramp to 240 °C at 10 °C min^{-1} and hold at 240 °C for 5 min. On HPLC, RI detector (held at 30 °C) was used to quantify sugars, sugar alcohol and levoglucosan in the feed and product of batch hydrogenation. Bio-Rad's Aminex HPX-87H column (Catalog No. 125-0140) was used with distilled water as the mobile phase with the flow rate of 0.5 to 1 ml min^{-1}. The column oven temperature was held constant at 30°C.

3.1.3.2 Flow Reactor

A gas and liquid down-flow reactor was built to study the hydrogenation of the bio-oil. Typically a ¼" diameter and 1 foot long stainless steel tube was loaded with the 5 wt% Ru/C catalyst. Both the sides were plugged with glass wool to ensure that catalyst bed stays at its place. No voids were left in the reactor tube to avoid any homogeneous reactions. An empty reactor tube was used to study the homogeneous reactions. An High Performance Liquid Chromatography (HPLC) pump (Eldex Lab Model 1SM) was used 13 to pump the aqueous fraction of the bio-oil. A mass flow controller was used to maintain the flow rate of hydrogen at 150 ml min^{-1}. The catalyst was reduced *in-situ* in flowing hydrogen prior to the reaction with following temperature regime: Room temperature to 260 °C at 30 °C h^{-1} and then hold at 260 °C for 2 h. The Ru/C catalyst came in the wet form, and was dried at 100 °C for 4 hour in an oven before loading in the reactor. The liquid and gas phase products flow to a gas-liquid (G-L)

separator. The gaseous products continue to flow to a back pressure regulator which is used to maintain the pressure of the entire reaction system. The gaseous products are collected in a gas bag and analyzed by Gas Chromatograph-Flame Ionization Detector (GC-FID) and GC-Thermal Conductivity Detector (GC-TCD). The G-L separator is drained periodically and the liquid sample is analyzed offline by TOC analysis and by GC-FID, and HPLC. The schematic of the reactor is shown in Figure 3.1. The steady state is achieved in the reactor within 4-6 h and at least 3 samples were collected to ensure that the steady state is achieved. The feed line can be heated to up to 60 °C if required.

1- Mass Flow controler
2- Check valve
3- Stirrer hot plate
4- Temperature controllers
5 - Reactor
6- Filter (2μm)
—— Heated line (60°C)
7- To purge
8- Liquid sampling point
9- Liquid/gas phase separator
10- Gas relief
11- Mass Flow controler
12- Check valve
13- Stirrer hot plate
14- Temperature
15- Pressure gauge
16- Back pressure controller
17- Furnace
18- Flow meter

Figure 3.1 Schematic of the single stage flow reactor system used for the hydrogenation

3.2 Results

3.2.1 Characterization of Bio-oil

Various characterization techniques were used to characterize the bio-oil. Physical characterization was done by the viscosity and solubility measurements. GC-MS was used to identify the components. GC-MS, GC-FID and HPLC were used for the quantification of the components.

Two phases form, when our bio-oil is mixed with water at a water to bio-oil weight ratio of greater than 1 to 4. For the bio-oil in this study, about 60 to 65 wt% of the bio-oil is soluble in water irrespective of the amount of water added. The two phases can be separated by centrifuging and then decanting. Water is inert for hydrogenation. Furthermore, a significant fraction of the bio-oil is water

soluble, making water an ideal solvent for hydroprocessing of bio-oil. About 62 wt% of the original bio-oil is in the aqueous phase. This also includes water that was present in the bio-oil. In terms of energy, about 57% of the energy in bio-oil is extracted in the aqueous phase.

The water insoluble bio-oil (WIBO) was mixed with methanol and analyzed by GC-MS. It mainly consists of guaiacol and its substituted forms which are known to be coming from the lignin part of the wood. The WSBO was analyzed with GC-MS, GC-FID, HPLC and TOC as shown in Table 3.1. The major components of the aqueous fraction are acetic acid, hydroxyacetone, hydroxyacetaldehyde, levoglucosan, furfural, 2-furanone and sugars. We were only able to identify 60% of the carbon in the aqueous fraction of the bio-oil with our methods used in this study. This did however help us in understanding some of the bio-oil conversion reactions. The rest of the carbon was probably present in the form of compounds like formic acid, various furans, and higher molecular weight sugars (i.e. cellobioses and trioses). The column used in HPLC can separate sugar, sugar alcohols and anhydro sugars. But it cannot separate various sugars from each other. A broad peak was observed for sugars in HPLC. Various sugars may be present including glucsoe, xylose, fructose, mannose and galactose. Piskorz *et al.* have identified hydroxyacetaldehyde up to 10 wt% in the bio-oil [3]. We found that only 1.5% of the carbon in WSBO was from hydroxyacetaldehyde. Formic acid could not be observed in our solution due to the large amounts of water we used and hence is not quantified here. High molecular weight degradation products of pentoses, hexoses are also present in the bio-oil [4] and were not detected by our analytical methods. Cellobiosan is known to be present in the bio-oil in a significant amount [5,6].Luo *et al.* have identified phenolic compounds (phenol and its alkyl derivatives) up to 20 wt% in the bio-oil made from *P. indicus* [7]. Phenol and its alkyl derivatives were also not detected in significant amounts in the bio-oil we used for this study.

Table 3.1 Identification of major components of aqueous fraction of bio-oil. The aqueous fraction of bio-oil was made by mixing 80 gm of water with 9 gm of bio-oil.

Quantification Method	Species	Concentration (mmole Carbon L^{-1})	% of Total Carbon
GC-FID	Hydroxyacetone	135.5	6.5
GC-FID	Hydroxyacetaldehyde	28.1	1.4
GC-FID	Guaiacols and derivatives	30.8	1.5
HPLC	Sugars	377.4	18.2
HPLC	Levoglucosan	390.6	18.8
GC-FID	Acetic acid	182.2	8.8
GC-MS	Furfural and 2-Furanone	100.0	4.8
	Total carbon content identified by GC & HPLC	1244.6	60.0
	Total carbon content measured by TOC	2075.9	100

The water insoluble bio-oil is highly viscous sticky brown liquid with the viscosity of more than 50000 cP. Its viscosity also decreases exponentially upon addition of methanol. The phenolic compounds originating from lignin are present in the bio-oil as both monomeric and oligomeric compounds [4]. These phenolic compounds are present in significantly higher concentrations in the WIBO than in the WSBO. These high molecular weight oligomers (molecular weight up to 5000) can form network due to intermolecular interactions resulting in high viscosity of the bio-oil. A rheological study of bio-oil obtained from the soft wood bark residue indicates the existence of self-aggregating intermolecular

interactions forming long-range network structures [8]. These interactions will be stronger in the water insoluble bio-oil due to its concentrated nature, explaining the very high viscosity observed for it. Addition of methanol to bio-oil or WIBO results in disrupting of the intermolecular network due to solvation significantly reducing the viscosity.

3.2.2 Low Temperature Hydrogenation of the Aqueous Fraction of Bio-oil in a batch reactor

The aqueous fraction of bio-oil contains thermally unstable compounds (*e.g.* glucose, levoglucosan) that decompose when heated to high temperature. If they are not converted to thermally stable compounds then they can cause deactivation of the catalyst by coke formation. The thermally unstable compounds can be converted to thermally stable compounds by a low temperature aqueous phase hydrogenation. In the low temperature hydrogenation, compounds such as hydroxyacetaldehyde, hydroxyacetone, and furfural are converted to corresponding alcohols such as ethylene glycol, propylene glycol and tetrahydrofurfuryl alcohol respectively. The challenge with the low temperature aqueous phase hydrogenation step is to selectively hydrogenate targeted C-O bonds and not break C-C or C-O bonds. Cleavage of C-C and C-O bonds results in formation of lighter products including undesired methane. The aqueous phase hydrogenation reactions in this study were all performed in a batch reactor.

Batch hydrogenation of the aqueous fraction of bio-oil was done in the temperature range of 125-175 °C with a 5 wt% Ru/Carbon catalyst. The hydrogen uptake of this catalyst was 33.2 μmol H/gm dry catalyst, which corresponds to surface to bulk Ru ratio of 6.7%. Table 3.2 depicts the data gathered for batch hydrogenation where temperature is increased in steps from 125 °C to 150 °C to 175 °C. Ethylene glycol, propylene glycol, butanediols, tetrahydrofurfuryl alcohol, Ƴ-butyrolactone and 1,2-cyclohexanediol all reach their respective maximum concentrations within 2.5 h at 125 °C. All the hydroxyacetone is also consumed during this same period. Acetic acid do not react at the reaction conditions used.

Sugars and levoglucosan do not undergo complete conversion at 125 °C. Levoglucosan has a very slow rate of hydrogenation at 125 °C. Initially levoglucosan concentration decreases rapidly from 390.6 mmol-C L^{-1} to about 275 mmol-C L^{-1} at 125°C. However, it then stays the same for 3 h. The levoglucosan concentration does decrease when the temperature is increased further. This implies that the high reaction temperature is required for the hydrogenation of levoglucosan. Levoglucosan is converted to sorbitol in two steps, hydrolysis of levoglucosan to glucose [6], followed by hydrogenation of glucose to sorbitol. The first reaction is an acid catalyzed reaction, whereas the second reaction is catalyzed by a hydrogenation catalyst, in this case Ru/C. In the absence of any externally added acid in the reaction mixture, it is possible that the first reaction is catalyzed by acids that are present in the aqueous fraction of bio-oil. Disappearance of the sugars follow a similar but less obvious trend as levoglucosan. At 125 °C, sugars (377 mmol-C L^{-1} to 175 mmol-C L^{-1}) disappear twice as fast as levoglucosan (390 mmol C L^{-1} to 275 mmol-C L^{-1}) does in 3.5 hours. This implies that the first step (levoglucosan to glucose) is the slower one and hence the rate limiting step in the conversion of levoglucosan to sorbitol. Increasing the acidity of the feed could therefore help expedite the conversion of levoglucosan to sorbitol [6].

A low hydrogenation temperature is preferred to minimize carbon loss from liquid in the form of methane. About 25% carbon is converted to methane at 175 °C, whereas at 125 °C, only about 10% carbon is converted to methane. However, sugars and levoglucosan are not completely converted to corresponding alcohols at 125 °C for shorter reaction time (<3.5 h). Thus, there requires some

optimization of reaction temperature and time. At high temperature, shorter reaction times (just sufficient to convert all the reactants to desired products), should be used to keep carbon loss to methane low. At low temperature, longer reaction time may be required to convert the reactants to respective alcohols. Hydrogen is consumed during the hydrogenation step (see Table 3.2).

Hydrogen consumption is about 0.034 gm/gm WSBO at 125 °C and doubles for every 25 °C rise in the temperature. Hydrogen consumption at the end of the run was found to be 0.12 gm/gm WSBO. Hydrogen consumption should be minimized by using as low temperature as possible. At low temperature unwanted reactions, such as saturation of aromatic rings, which consume a considerable amount of hydrogen, are suppressed. The hydrogen consumption at low temperature (125 °C) is comparable to that reported by Baker and Elliott for the two stage hydroprocessing process, where 0.034 gm H_2 is consumed per gm of bio-oil [9].

Table 3.2 Hydrogenation of the aqueous fraction of pine wood bio-oil with initial carbon concentration of 24900 mg L^{-1} (by TOC), Catalyst: 3 gm of 5 wt% Ru/C (wet basis), total P: 68.9 bar.

	Temperature/°C	25	125	125	125	125	150	150	150	175	175	175
	Minutes	*0*	*30*	*60*	*150*	*210*	*270*	*320*	*360*	*400*	*455*	*545*
Method		Concentration/mmol-C L^{-1}										
GC-FID	Hydroxyacetone	135.5	55.7	24.5	0.0	0.0	0.0	0.0	0.0	0.0	0.0	0.0
GC-FID	Hydroxyacetaldehyde	28.1	0.0	0.0	0.0	0.0	0.0	0.0	0.0	0.0	0.0	0.0
GC-FID	Ethylene glycol	0.0	90.6	172.3	212.2	216.9	198.9	191.6	204.6	222.6	210.9	197.3
GC-FID	Propylene glycol	0.0	25.4	113.1	159.0	164.1	154.9	163.0	172.5	186.6	182.7	171.0
GC-FID	Butanediols^a	0.0	13.3	36.6	52.7	55.5	51.8	59.1	63.0	64.3	61.1	57.9
GC-FID	THFA^b	0.0	9.9	12.5	15.7	14.9	13.5	11.4	13.3	12.0	15.0	18.0
GC-FID	γ-Butyrolactone	0.0	24.7	31.7	30.4	29.4	30.5	30.3	30.7	30.8	29.8	26.9
GC-FID	Guaiacols^c	30.8	28.8	0.0	0.0	0.0	0.0	0.0	0.0	0.0	0.0	0.0
HPLC	Sugars	377.4	242.5	232.6	N.A.	174.7	140.4	125.9	117.7	80.4	67.3	47.5
HPLC	Sorbitol	0.0	0.0	0.0	N.A.	56.6	89.8	117.1	141.2	186.7	204.7	213.8
HPLC	Levoglucosan	390.6	274.8	271.4	N.A.	276.7	235.8	216.0	212.9	150.7	132.0	123.6
GC-FID	Acetic acid	182.2	126.1	192.6	170.9	167.1	186.0	196.3	201.1	206.8	210.2	202.6
	Total mmol-C L^{-1}	1144.5	891.8	1087.2	N. A.	1155.9	1101.7	1110.8	1157	1141.0	1114	1058.6
	% C identified in liquid	55.2	50.5	59.8	N. A.	63.8	59.6	61.8	61.7	64.6	63.8	63.0
	% C in liquid by TOC	100.0	85.1	87.6	86.1	87.3	89.2	86.7	N.A.	85.1	84.2	81.0
	H$_2$ Consumption (g/g WSBO)	0	0.007	0.016	0.024	0.034	0.038	0.048	0.061	0.070	0.091	0.120

^{a} 1,2 and 1,4-butanediol. ^{b} Tetrahydrofurfuryl alcohol. ^{c} Contains guaiacol and methyl guaiacol, N.A. = not analyzed.

A concentrated (39.6 wt%) aqueous fraction of the PWBO was also hydrogenated in the Parr batch reactor. This hydrogenated aqueous fraction was subjected to the accelerated stability test and the results were compared with that for non-hydrogenated aqueous fraction. These resulted are discussed under Task 5.

3.2.3 Hydrogenation of pinewood bio-oil down flow continuous reactor:

Since, in the batch reactor hydrogenation, we were not able to convert the acetic acid, low temperature hydrogenation was also carried out in a down flow reactor at different temperatures and pressures. The Low Temperature Hydrogenation (LTH) step stabilizes the bio-oil by hydrogenating the carbonyl groups in it. During the LTH, a fraction of carbon in WSBO is lost to the gas phase, predominantly in the form of methane. It is thus imperative to use lowest possible temperature so as to minimize the carbon loss to gas phase. We studied the effect of temperature in the range of 75-175 °C on

the conversion of various components of the aqueous fraction of PWBO. The data obtained are depicted in Table 3.3. These experiments were done with void space (about 50%) in the reactor as this data is collected before studying the extent of homogeneous reactions in LTH of WS-PWBO. At 75 °C, only 2-furanone, furfural and 5-HMF show a significant activity towards hydrogenation. Only 4% conversion of total reactants is observed at 75 °C. At 100 °C, hydroxyacetaldehyde and 3-methyl-1,2-cyclopentadione start disappearing. Hydroxyacetone, phenol, guaiacol, catechol, levoglucosan, and sugars start reacting at 125 °C. About 90% conversion is observed for all the major reactants at 150 °C except acetic acid and phenol. Acetic acid is resilient to hydrogenation at temperatures below 175 °C. At 175 °C, reactor plugging was observed. The reactants and products concentration in feed and products of this experiment are shown in Table 3-4.

Table 3.3 Reactant conversion for hydrogenation of WS-PWBO

Compound	Conversion (%)				
	75 °C	100 °C	125 °C	150 °C	175 °C
Hydroxyacetaldehyde	0	38	93	100	100
Acetic Acid	0	0	16	13	10
Hydroxyacetone	0	0	58	96	100
2(5H)-Furanone	89	88	72	74	97
Phenol	2	1	37	39	33
3-Methyl-1,2-Cyclopentadione	14	46	100	100	100
Guaiacol	6	3	11	100	N/A
Catechol	4	12	56	87	95
Furfural	71	73	89	100	100
5-HMF	59	73	89	100	100
Levoglucosan	3	8	53	100	100
Sugars	11	14	70	97	99
Total Reactants	4	16	57	89	90

Low temperature hydrogenation step converts all the thermally unstable bio-oil functionalities to corresponding alcohols. At 75 °C, only Furfural, 5-HMF and 2(5H)-Furanone show significant conversion. As we increase the temperature conversion for all the reactants increase. At 150 °C we achieve about 90% conversion for total reactants. Once again, Acetic acid is very resilient to hydrogenation and we could only achieve about 16% conversion for acetic acid. The product distribution for the above experiment is shown in Table 3.3. We were able to increase the pH of the aqueous fraction form 2.5 to about 3.2 by the hydrogenation at 125 °C.

Table 3-4 Reactant and product concentration for low temperature hydrogenation of WS-PWBO at different temperatures

Compound	Product Concentration (mmol-C L^{-1})					
	Temperature (°C)					
	Feed	75	100	125	150	175
Reactants						
Hydroxyacetaldehyde	376.2	386.2	233.2	24.9	0.0	0.0
Acetic acid	191.9	205.2	203.9	161.9	166.6	172.1
Hydroxyacetone	160.9	196.4	203.8	67.4	5.8	0.0
2-Furanone	34.1	3.7	4.1	11.6	8.9	1.1
Phenol	2.2	2.2	2.2	1.4	1.4	1.5
3-Methyl-1,2-Cyclopentadione	43.4	37.2	23.3	0.0	0.0	0.0
Guaiacol	9.4	8.8	9.1	8.3	0.0	4.0
Catechol	247.1	237.4	218.2	108.1	33.1	13.5
Furfural	17.78	5.2	4.9	0.0	0.0	0.0
5-Hydroxymethylfurfural	57.4	23.6	15.6	6.4	0.0	0.0
Levoglucosan	602.4	582.5	553.2	280.8	0.0	0.0
Sugars	171.9	153.8	148.7	163.3	4.8	0.9
Products						
Methanol	15.1	34.0	40.6	23.1	22.1	16.0
Ethanol	0.0	3.1	3.6	8.9	10.1	10.8
1-Propanol	0.0	3.9	2.2	4.0	6.8	8.7
1-Butanol	0.0	0.0	0.0	2.6	3.2	4.3
1-Pentanol	0.0	0.0	0.0	0.0	0.0	2.7
Ethylene glycol	0.0	139.8	287.0	275.5	185.6	128.9
Cyclopentanol	0.0	0.0	0.0	2.0	5.6	7.7
Propylene glycol	0.0	4.4	6.1	96.5	153.8	139.5
Cyclohexanol	0.0	0.0	0.0	3.5	37.3	38.1
1,2-Butanediol	0.0	0.0	0.0	23.1	49.2	30.0
Tetrahydrofurfuryl alcohol	0.0	10.0	11.2	10.8	18.0	23.6
1,4-Butanediol	0.0	2.8	11.5	33.6	27.8	17.7
γ-Butyrolactone	0.0	54.2	57.3	55.0	72.7	60.5
γ-Valerolactone	0.0	0.0	0.0	4.1	7.0	8.7
Glycerol	0.0	13.4	16.7	10.0	11.6	5.4
1,2-Cyclohexanediol	0.0	0.0	0.0	2.6	32.0	33.0
Hydroxymethyl-γ-butyrolactone	0.0	22.1	22.7	29.2	27.7	17.0
Sorbitol	0.0	48.8	37.7	36.0	67.2	12.1
Total C identified	1929.7	2178.6	2116.7	1453.9	958.2	757.7
Carbon content by TOC	2633.3	2519.6	2539.0	2451.5	1971.2	1680.9
%C lost to gas phase	-	4	4	7	25	36

The major products from the LTH of WS-PWBO are ethylene glycol, propylene glycol, butanediols and γ-butyrolactone as shown in Table 3.4. The products concentration maximizes at 125 °C. More propylene glycol is observed at 150 °C but the ethylene glycol starts undergoing secondary reactions at that temperature. A large amount of carbon (25.2%) is lost to gas phase (mostly methane and ethane) at 150 °C. For the process to be economically attractive this carbon loss needs to be minimized. The carbon loss to gaseous compounds is moderate (7%) at 125 °C with all the bio-oil components showing reasonable hydrogenation activity. Ethylene glycol concentration is also a maximum at 125 °C. Due to all these reasons we chose 125 °C as the optimum temperature for any further LTH experiments. The experiments depicted in Tables 3.3 and 3.4 are carried out at comparatively high space velocity of 3 h-1. In the next section we show that almost 100% conversion of all the reactants except acetic acid is achievable at 125 °C with lower space velocities. Also the catalyst was very stable with no signs of deactivation or coking. We studied the catalyst stability for 5 wt% Ru/C catalyst with WS-PWBO feed at WHSV of 1.5 h-1 for 78 hours. No catalyst activity loss was observed over the studied time period.

We have also studied the effect of space velocity on the extent of hydrogenation. We could hydrogenate 85% of the quantifiable reactants at the lower WHSV of 0.65 h^{-1}.Conversion was higher than 90% for all of the reactants except acetic acid. Only 13% conversion was observed for acetic acid.

Table 3.5 Effect of space velocity on conversion of reactants in LTH of WS-PWBO

Compound	Conversion (%)			
	WHSV: 0.75 h$^-$	1.5 h^{-1}	3.0 h^{-1}	6.0 h^{-1}
Hydroxyacetaldehyde	100.0	100.0	100.0	96.8
Acetic acid	12.6	9.8	16.8	13.3
Hydroxyacetone	100.0	100.0	100.0	92.8
2-Furanone	25.9	27.8	42.6	57.4
Phenol	100.0	100.0	100.0	92.4
3-Methyl-1,2-cyclopentadione	100.0	100.0	100.0	96.0
Guaiacol	100.0	100.0	100.0	100.0
Catechol	100.0	100.0	100.0	68.6
Furfural	100.0	100.0	100.0	100.0
5-Hydroxymethylfurfural	100.0	100.0	100.0	100.0
Levoglucosan	91.2	76.7	47.6	32.1
Sugars	89.3	54.5	65.3	0.7
Total	85.0	78.1	70.7	56.6

Catalyst: 5wt% Ru/C, T: 125 °C, P: 750 psi, H2 flow rate: 150 ml min-1, feed: ~13wt% WS-PWBO solution in water

The hydrogenation results show that we can hydrogenate more than 85% of the bio-oil functionalities to corresponding alcohols. We were not able to hydrogenate acetic acid on Ru/C at temperature less than 125 °C. Although this low temperature hydrogenation did stabilize water soluble

bio-oil as seen from accelerated stability testing, implying that acid do not play role in the instability of hydrogenated aqueous fraction of the bio-oil.

3.2.4 Homogeneous reactions during hydrogenation

We also carried out a blank run where we hydrogenate the aqueous fraction without any catalyst. This helped up understand some of the homogeneous reactions taking place. The results are shown in Figure 3.2.
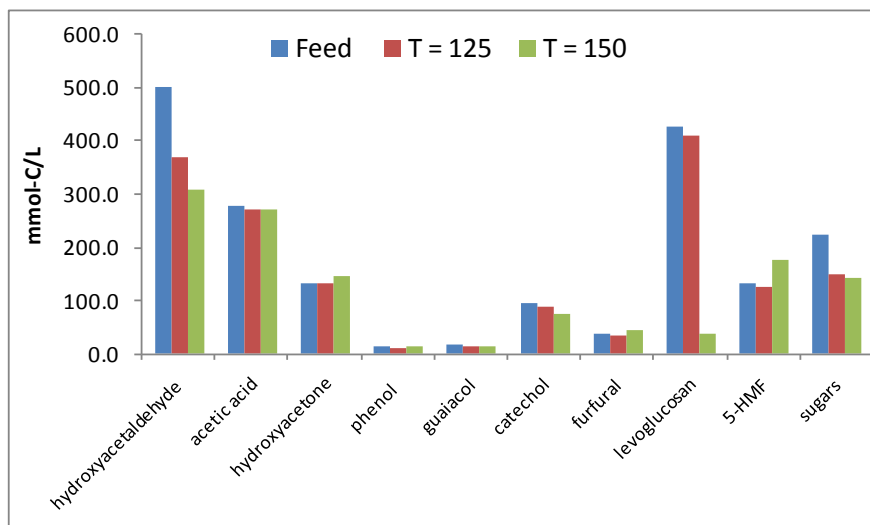
Figure 3.2 Reactant distribution after blank hydrogenation

Even at the low temperature of 125 °C, we see the presence of homogeneous reactions. Homogeneous reactions are especially important for hydroxyacetaldehyde and sugars at 125 °. At higher temperature of 150 °C, extensive homogeneous reactions happen. Levoglucosan is almost completely consumed at 150 °C. The reactor plugged at 150 °C without the presence of catalyst due to coking reactions of levoglucosan and sugar. About 1% and 28% carbon in the feed goes to gas phase products at 125 °C and 150 °C respectively. This data helped us to know the temperature above which to expect the coke formation. Also we eliminated all the voids from our reactor tube to make sure that extent of homogeneous reactions is minimized.

3.2.5 Two-step hydrogenation of oak wood bio-oil

We added a second high temperature step in series after the first low temperature step to hydrogenate all the acetic acid present in the bio-oil. The block diagram of the process is shown below,
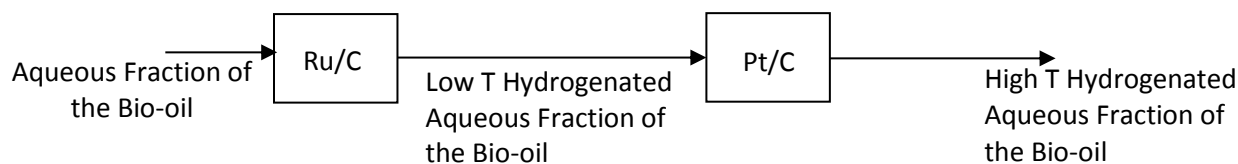
Figure 3.3 Block diagram for two step hydrogenation of aqueous phase of bio-oil

We used Ru/C catalyst in the first step for all the runs. For the 2nd stage we have tested Ru/C and Pt/C catalysts. Pt/C catalyst was found to be better with respect to carbon loss to gas phase than Ru/C catalyst. With Ru/C as 2nd stage catalyst we could convert all the bio-oil functionalities except acetic acid to corresponding alcohols in yields above 95% at temperatures above 200 °C at relatively high space velocity of 3 h^{-1}. Acetic acid conversion at 200 and 220 °C was about 7%. The conversion increased to 75% at 250 °C. However at 250 °C, 62% carbon was lost to the gas phase. The decrease in acetic acid concentration over Ru/C was due to its conversion to CO and CH$_4$.

To reduce the carbon loss to gas phase, we replaced the second stage Ru/C with Pt/C catalyst. At 220 °C, we could convert all the bio-oil functionalities to corresponding alcohols except acetic acid. The conversion of acid with temperature and carbon loss to gas phase is tabulated below,

Table 3.6 2-stage Hydrogenation of aqueous fraction of bio-oil

2nd Stage Temperature (°C)	Acetic Acid Conversion (%)	Carbon Loss to Gas Phase (%)
220	8	9.7
250	28	15.0
275	61	35.8

1st stage: Ru/C, 125 °C, 1450 psi, WHSV: 3 h^{-1}; 2nd stage: Pt/C, 1450 psi, WHSV: 3 h^{-1}

We are able to convert 61% acetic acid while lowering the carbon loss to gas phase to 36% on Pt/C as compared 62% on Ru/C catalyst.

3.2.6 Two-step hydrogenation of oak wood bio-oil with bimetallic catalyst

We did more detailed characterization of the hydrogenation product from water soluble DOE bio-oil over Ru/C and PtRe catalyst. We were able to completely remove the acetic acid from the aqueous fraction of DOE bio-oil by 2-stage hydrogenation over Ru/C catalyst (125 °C) followed by on PtRe on ceria-zirconia catalyst (250 °C). This catalyst performs better as compared to monometallic Pt/C catalyst which can only reduce about 65% acetic acid. But the carbon loss to the gas phase products (mainly methane) for both these catalyst is more than 35% which can render the process uneconomical. We suspect that this high carbon loss to gas phase is due to the high acetic acid content in the DOE bio-oil. The carbon loss to gas phase with pine wood bio-oil aqueous fraction which had 4 times less acetic acid than the aqueous phase of DOE bio-oil was only 15% with Pt/C catalyst 250 °C. The future work hence should be focused on producing bio-oils with low acetic acid content, which can be hydrogenated by our process over PtRe/ceria-zirconia catalyst.

With PtRe/ceria-zirconia catalyst, the product selectivity is significantly different than that for the monometallic Pt catalyst. The major products are ethanol (703.0 mmol-C L-1), 1-propanol (205.7 mmol-C L-1), methanol (99.3 mmol-C 120 L-1), cyclohexanol (82.9 mmol-C L-1), and 1-butanol (59.9 mmol-C L-1). The PtRe bimetallic catalyst produced large amount of monohydric alcohols due to its ability to selectively activate the C-O bonds in compounds such as ethylene glycol and propylene glycol. No ethylene glycol was observed in the products and a very little propylene glycol was observed. The carbon loss to the gas phase for PtRe catalyst was 39.4%. The bimetallic catalyst hence can be a very good choice if you want to selectively produce gasoline cut 1 compounds (C2 to C4 monohydric alcohols) from the aqueous fraction of bio-oil. It also completely reduces the acetic acid and propanoic acid, hence simplifying the further processing of hydrogenated water soluble bio-oil.

Table 3.7 Feed and product composition for 2-stage hydrogenation of WS-DOE-BO. Feed: ~13 wt% WS-DOE-BO solution in water. P: 1450 psi, WHSV: 3 h^{-1}

Compound	Feed	Concentration (mmol-C L^{-1})	
		Ru/C, 125 °C - Pt/C, 250 °C	Ru/C, 125 °C – PtRe on Ceria-Zirconia, 250 °C
Reactants			
Methanol	28.2	111.7	99.3
1-Propanol	8.0	78.8	205.7
Hydroxyacetaldehyde	326.0	0.0	0.0
Acetic Acid	723.2	273.1	0.0
Hydroxyacetone	123.6	0.0	0.0
Propanoic acid	39.0	16.1	0.0
Hexanoic acid	0.0	0.0	0.0
1-Hydroxy-2-butanone	39.8	0.0	0.0
Furfural	15.9	0.0	0.0
2-Cyclopenten-1-one	22.2	0.0	0.0
γ-Butyrolactone	14.7	17.0	15.2
2(5H)-Furanone	28.2	0.0	0.0
Phenol	0.4	0.0	0.0
3-Methyl-1,2-cyclopentadione	21.7	0.0	0.0
5-Hydroxymethyl-furfural	28.1	0.0	0.0
Levoglucosan	988.1	0.0	0.0
Sugars	207.4	0.0	0.0
Sorbitol	0.0	0.0	0.0
Products			
Ethanol	0	249.6	703.9
2-Propanol	0	8.8	50.7
2-Butanol	0	5.6	27.1
1-Butanol	0	23.4	59.9
2-Pentanol	0	3.9	11.4
1-Pentanol	0	0.0	9.8
Ethylene glycol	0	210.3	0
Cyclopentanol	0	22.8	44.3
Propylene glycol	0	161.3	14.7
3-Methylcyclopentanol	0	30.7	20.8
2,3-Butanediol	0	19.6	20.8
Cyclohexanol	0	50.3	82.9
1,2-Butanediol	0	48.3	9.0
Tetrahydrofurfuryl alcohol	0	82.3	12.9
1,4-Butanediol	0	16.0	9.9
γ-Butyrolactone	0	17.0	15.2
1,2-Cyclohexanediol	0	49.9	41.9

3.2.7 Hydrogenation of whole bio-oil

The aqueous fraction contains only about half the energy of the bio-oil. The organic fraction of the bio-oil mainly contains lignin derived oligomers with ether linkages. It would be preferable to hydrotreat the entire bio-oil instead of just the aqueous fraction. Hence we subjected the DOE bio-oil to low temperature hydroprocessing over 5 wt% Ru/C catalyst at 1450 psi and temperatures in the range of 75 °C to 125 °C. The microfiltered (0.8 μm membrane) DOE bio-oil was used as feed. None of the bio-oil components showed significant reactivity up to the temperature up to 100 °C. The data for DOE-BO hydrogenation over Ru/C catalyst at 125 °C, 1450 psi at the space velocity of 1.6 hour^{-1} is tabulated in Table 3.8. As seen in this table, different conversions are obtained for different feed components but no corresponding hydrogenation products were detected except for a small amount of sorbitol. Hence the disappearance in the reactants is most likely due to the homogeneous reactions that occur when bio-oil is heated to the hydrogenation reaction temperature. The same reactants that can be successfully hydrogenated when present in the aqueous fraction cannot be hydrogenated when present in the whole bio-oil. This indicates that the lignin-derived oligomers in the bio-oil might be permanently occupying and essentially deactivating the active catalytic sites.

Table 3.8 Composition of DOE-BO feed low temperature hydrogenated DOE-BO. Hydrogenation carried out over 5 wt% Ru/C catalyst, 125 °C, 1450 psi, 1.6 hour^{-1}

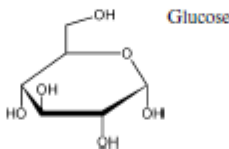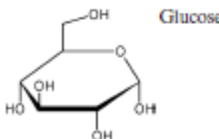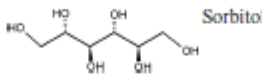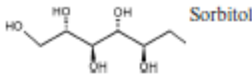| Compound	mmol carbon min^{-1}		% Conversion
	DOE-BO Feed	Hydrogenated DOE-BO	
Methanol	3.50×10^{-3}	3.47×10^{-3}	-
Methyl acetate	1.66×10^{-3}	3.17×10^{-3}	-
Hydroxyacetaldehyde	0.116	0	100
Acetic acid	0.109	0.127	0
Hydroxyacetone	2.11×10^{-2}	2.75×10^{-2}	0
Furfural	8.14×10^{-3}	5.60×10^{-3}	31.2
2-Furanone	6.50×10^{-3}	5.07×10^{-3}	31.4
3-Methyl-1,2-cyclopentadione	5.65×10^{-3}	0	100
Phenol	1.38×10^{-3}	4.45×10^{-3}	0
1-Hydroxy-2-butanone	6.72×10^{-3}	0	100
2-Cyclopenten-1-one	4.01×10^{-3}	0	100
γ-Butyrolactone	2.91×10^{-3}	5.07×10^{-3}	0
5-Hydroxymethylfurfural	8.33×10^{-3}	0	100
Levoglucosan	0.113	9.49×10^{-2}	16.4
Sugars	2.27×10^{-2}	1.73×10^{-2}	24.0
Sorbitol	0	2.20×10^{-3}	-
Total carbon identified	0.432	0.262	
Total carbon as determined by elemental analysis	1.294	1.269	
%C to gas phase products	-	1.9	
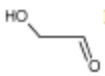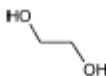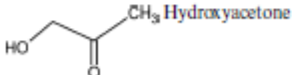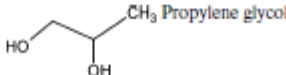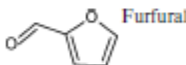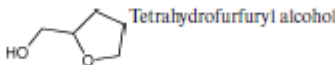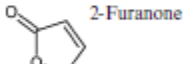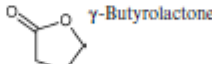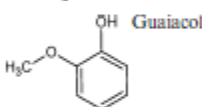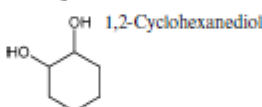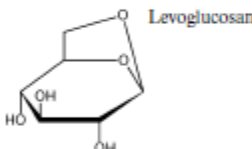
During hydrogenation of the entire bio-oil, we faced two major problems namely: difficulty to pump and reactor clogging.

3.3 Conclusions:

3.3.1 Low Temperature Hydrogenation of the Aqueous Fraction of Bio-oil

Low temperature hydrogenation makes the aqueous fraction of bio-oil amenable to further processing. Ruthenium on activated carbon was selected as this catalyst is known to exhibit high activity and stability for similar hydrogenation reactions in the aqueous phase [10-12]. The temperature and reaction time both influence the products that are formed. Optimization of the reaction temperature and time is required. Strong acid (*e.g.* H_2SO_4, HCl) can be added to the reaction mixture to increase the rate of acid catalyzed hydrolysis of levoglucosan to glucose. Helle *et al.* showed that increasing the concentration sulfuric acid increases the rate of hydrolysis of levoglucosan in water at 110 °C [6].

Table 3.9 Reactions in hydrogenation of water soluble fraction of bio-oil

Reactant	Product	Type of reaction
Hydroxyacetaldehyde	Ethylene glycol	Hydrogenation
Hydroxyacetone	Propylene glycol	Hydrogenation
Furfural	Tetrahydrofurfuryl alcohol	Hydrogenation
2-Furanone	γ-Butyrolactone	Hydrogenation
Guaiacol	1,2-Cyclohexanediol	Hydrogenation
Levoglucosan	Glucose	Hydrolysis
Glucose	Sorbitol	Hydrogenation
Sorbitol	Ethylene glycol, propylene glycol and 1,4-butanediol	Hydrogenolysis

Based on GC-MS and HPLC analysis of the feed and product of the hydrogenation reaction, the major reactions occurring during this step are identified and are depicted in Table 3.9. The last reaction in Table 3.9 is the hydrogenolysis reaction, wherein α, ω-diols are produced from the sugar alcohols such as sorbitol in the presence of hydrogen. Ruthenium metal can catalyze the hydrogenolysis reactions [13-15]. Ruthenium can also catalyze the C-C bond breaking reactions. The relative rates of hydrolysis of C-O

bonds and cleavage of C-C bonds decide the final product distribution. Apart from the reaction mentioned in Table 3.9, decarbonylation and methanation reactions also happen during this step. Another process option is to extract the polyols from the hydrogenated aqueous-fraction of the bio-oil. The three major products after hydrogenation are ethylene glycol, propylene glycol and 1,4-butanediol. We produce 0.102 gm ethylene glycol/gm WSBO, 0.064 gm propylene glycol/gm WSBO and 0.021 gm 1,4-butanediol/gm WSBO. The polyols can be separated from the aqueous fraction either by distillation or nanofiltration. The concentration of the aqueous phase will decide the distillation efficiency. Nanofiltration is an attractive option where molecules can be separated based on size and functionality. The smaller polyols (C2 to C4) can be separated from the hydrogenated aqueous fraction, and be used for the production of hydrogen. Whereas the larger polyols (sugar alcohols) can be used to produce alkanes.

It was found that the TAN reduction in bio-oil was very difficult using low temperature hydrogenation. Acetic acid is very resilient to hydrogenation and we could only achieve about 16% conversion for acetic acid. Although it was observed that acetic acid was not responsible for instability of aqueous fraction of bio-oil during ageing studies (described in task 5).

3.3.2 Two-step hydrogenation of aqueous fraction of bio-oil

Since, acetic acid was found to be very resilient for low temperature hydrogenation, two-step hydrogenation with higher temperature of second step. Monometallic catalyst such as Pt/C and bimetallic catalyst namely PtRe/ceria-zirconia was used in the second step with Ru/C as catalyst in the first step. With higher hydrogenation temperature, carbon conversion to gas phase increased which offsets the increase in acetic acid conversion. The bimetallic catalyst PtRe/ceria-zirconia was found to be better of the two catalyst tested because of its ability to convert the acid functionality with low conversion to gas phase carbon.

3.3.3 Hydrogenation of whole bio-oil

Hydrogenation of the whole bio-oil was carried out at 125°C, 1450 psi over Ru/C catalyst in a flow reactor. Again, negligible acetic acid conversion was obtained in low temperature hydrogenation. Hydrogenation experiments with whole bio-oil were difficult to perform because of difficulty to pumping the high viscosity oil and reactor clogging.

3.4 References

[1]   P. Badger, *Method or System for Accomplishing Flash or Fast Pyrolysis with Carbonaceous Materials,* US Pat., Application No. 11/480 914.
[2]   P. Badger and P. Fransham, *Improved Methods of Accomplishing Flash or Fast Pyrolysis with Carbonaceous Materials,* US Pat., Application No. 11/480 915.
[3]   J. Piskorz, D. S. Scott and D. Radlien, in *Pyrolysis Oils from Biomass: Producing Analyzing and Upgrading,* ed. E. J. Soltes and T. A. Milne, American Chemical Society, Washington DC, 1988, pp. 167-178.
[4]   D. Mohan, C. U. Pittman and P. H. Steele, *Energy Fuels,* 2006, 20, 848 - 889.
[5]   K. Sipila, E. Kuoppala, L. Fagernas and A. Oasmaa, *Biomass Bioenergy,* 1998, 14, 103-113.
[6]   S. Helle, N. M. Bennett, K. Lau, J. H. Matsui and S. J. B. Duff, *Carbohydr. Res.,* 2007, 342, 2365-2370.

[7]   Z. Y. Luo, S. R. Wang, Y. F. Liao, J. S. Zhou, Y. L. Gu and K. F. Cen, *Biomass Bioenergy,* 2004, 26, 455-462.

[8]   M. Garcia-Perez, A. Chaala, H. Pakdel, D. Kretschmer, D. Rodrigue and C. Roy, *Energy Fuels,* 2006, 20, 364-375.

[9]   E. G. Baker and D. Elliott, in *Thermochemical Biomass Conversion,* ed. A. V. Bridgwater and J. L. Kuester, Elsevier Science Publishers Ltd, Barking, England, 1988, pp. 883-895.

[10]   J. Wisniak and R. Simon, *Ind. Eng. Chem. Prod. Res. Dev.,* 1979, 18, 50-57.

[11]   P. Gallezot, N. Nicolaus, G. Flèche, P. Fuertes and A. Perrard, *J. Catal.,* 1998, 180, 51-55.

[12]   Z. Zhang, J. E. Jackson and D. J. Miller, *Appl. Catal., A,* 2001, 219, 89-98.

[13]   I. T. Clark, *Ind. Eng. Chem.,* 1958, **50**, 1125-1126.

[14]   D. K. Sohounloue, C. Montassier and J. Barbier, React. Kinet. Catal. Lett., 1983, 22, 391-397.

[15]   M. Schlaf, Dalton Trans., 2006, 4645-4653.

Task 4.0 Acid Removal using Ion Exchange Resins

Ion exchange resins are a very good candidate to remove organic acids in a solution. Whole bio-oil or only the aqueous fraction of the bio-oil can be contacted with ion exchange resins. Resins retain the acids on them hence reducing the TAN of the bio-oil. The spent resins can be easily regenerated by contacting them with basic solution and can be used again. Acid salts can also be removed using this approach with the help of appropriate resin. Some preliminary results depicting the usefulness of this approach are discussed.

Milestone 7 Decrease the TAN of the bio-oils to less than 5 using ion-exchange resins.

Ion exchange resins were to be used for the removal of acids from bio-oil and its various fractions. The same continuous flow system that was designed for Task 5 is to be used for this Task.

4.1 Materials and Experimental

DOWEX M43 resin was used to carry out the neutralization of bio-oil using a packed bed column. The resin was initially dried at 100 ˚C for 3 hours. Stainless tube of ½ inch diameter and 2 feet length was packed with 25-30 gm of the dried resin. An Isco pump was used to pump the filtered bio-oil (0.8 micron permeate) through this packed bed with down flow configuration. The flow of the bio oil was maintained at 0.25 ml/min.

4.2 Results

The pressure drop across the bed was as high as 113 psi. The pH of the bio-oil increased from 2.43 to 3.7. Even higher pH can be obtained by passing bio-oil. The resin was washed with methanol till clear methanol with neutral pH was obtained from the other end of the column. Then resin was then regenerated by passing 400 ml of 3 wt% NaOH in methanol at the flow rate of 1 ml/min. The column was washed again with methanol and water to remove the traces of NaOH in the column. After the regeneration, bio-oil was again passed through the resin bed. The pH of the sample increased from 2.4 to 4.9. The GC analysis of the samples showed that acetic acid was removed from the bio-oil during the neutralization and recovered in the methanol washing.

4.3 Conclusion

No further work is done for this task as we think process would not be economical at large scale as it is extremely difficult to regenerate the resin once the bio-oil is passed over it.

Task 5.0 Characterization of Upgraded Bio-oils

The purpose of this task is to characterize the upgraded bio-oil. We used the following tests on the upgraded bio-oil: microscopy, NMR, HPLC, GCMS, TAN, viscosity measurements, and accelerated stability tests.

Understanding the rheology and stability of biofuels has been identified as a major need in the large-scale production, storage and use. A challenging problem is the dramatic viscosity increase that can occur upon storage of pyrolysis oils. We investigated the viscosity, microstructure, and chemical composition of bio-oils prepared by a fast pyrolysis approach, upon aging these fuels at 90ºC for periods of several days. Our results suggest that the viscosity increase is not correlated with the acids or char present in the bio-oils. In addition, while there have been significant efforts on removing chars as a means of stabilizing biofuels, our results show that removal of neither large nor small char particles has any significant impact on the rate of viscosity increase. The viscosity increase is due to formation of high molecular weight polymeric species over time. Our work also suggests that hydrogenation of the samples is beneficial in eliminating the viscosity increase.

The instability of bio-oil is known to be caused by several polymerization reactions [1-5]. One of the appearances of instability is the significant increase of viscosity with increasing storage time. So we use the standard accelerated stability test method from Department of Energy to evaluate the stability of bio-oil. The increase rate of viscosity was the criterion. Acids and chars may be working as catalysts and the unstable chemical components may be working as reactants in the polymerizations [1-5]. So we tried to remove acids and chars, hydrogenated the unstable chemicals, compared the viscosity increase rates and determined the major reasons of instability, and then tried to find some approaches to inhibit the polymerization reactions.

5.1 Materials and Experiments

5.1.1 Materials

Bio-oil. Crude Pine wood bio-oil (PWBO) is from Mississippi State University.

5.1.2 Experiments

5.1.2.1 Accelerated stability test

The samples are sealed very well with Teflon and incubated in oven at 90ºC for some time(8 hours, 24 hours, 2 days, etc.), and then cooled down to room temperature for rheological measurement.

5.1.2.2 Viscosity measurement

After startup of the rheometer, the bio-oil samples were loaded at room temperature to the geometry. For viscous bio-oil sample, 40mm parallel plates of rheometer ARES G2 in Engineering Lab II were applied and the viscosity was measured at 40ºC with solvent trap. For diluted sample, concentric cylinder of rheometer AR2000 in Polymer Science Department building was applied and the viscosity was measured at room temperature to reduce the solvent loss. All the measurement followed the standard procedure, equilibrium for 10 minutes at desired temperature and then steady state flow test at shear rate from 0.001 1/s to 10 1/s.

5.1.2.3 Filtration

The bio-oil samples were filtered by syringe filter. The pore sizes of filter mentioned in this work were 5 μm and 0.45 μm in filtration section and hydrogenation section respectively.

5.1.2.4 Neutralization

Alkali metal base, dehydrated Na_2CO_3, was used to neutralize the acidic bio-oil. The amount is a little over the TAN (total acid number).

5.1.2.5 Preparation of water soluble bio-oil (WSBO)

The pine wood bio-oil (PWBO) was mixed with distilled water to separate into two phases: an aqueous rich phase (WSBO: water soluble fraction of bio-oil) and an organic rich phase (WIBO: water insoluble bio-oil fraction). The mixture was then centrifuged in a Marathon 2100 centrifuge (Fisher Scientific) at 10,000 rpm for 20 minutes to ensure the phase separation. The two phases, aqueous (top) and non-aqueous (bottom), were then separated by decanting. The weight of the aqueous fraction was measured to determine the amount of bio-oil that dissolved in water. For the experimental purpose 100 gm of bio-oil was added to 80 gm of water and mixed well. The aqueous and non-aqueous phases were separated by centrifugation followed by decanting. The resulting aqueous solution is about 39.6 wt% water soluble bio-oil (WSBO) in water. About 52.5 wt% of the PWBO was found to be water soluble.

5.1.2.6 Hydrogenation of water soluble fraction of bio-oil

Hydrogenation of the aqueous fraction of the bio-oil was carried out in a 170 ml Parr batch reactor at 125 °C and 1000 psi. About 90 gm of the aqueous fraction of the bio-oil (39.6 wt% WSBO) was loaded in the reactor along with 1.5 gm (wet basis, 50 wt% moisture content) of 5 wt% Ru / activated C catalyst (Strem Chemicals, Product No. 44-4059). The reactor was then purged at least 4-5 times with helium gas to get rid of the air present in the reaction vessel. The reactor was then purged with hydrogen at least 4-5 times to replace all the helium with hydrogen. The reactor pressure was set to 700 psi by adding hydrogen and the heating and stirring were started. Once the temperature reached 125 °C, the reactor pressure was increased to 1000 psi total by adding more hydrogen. Additional hydrogen was added to the reactor during the course of reaction to compensate for the hydrogen consumption. The total pressure was maintained at 1000 psi. The reaction was continued for 135 minutes. The product is filtered at end using a 0.45 μm filter to remove the catalyst particle. This product was then subjected to the accelerated stability test.

5.1.2.7 Visual observation with optical microscopy

Samples were loaded to glass slide and observed using Olympus DX60 in Polymer Science Department. The micrographs were taken by Sony CCD color video camera.

5.2 Results and Discussion

5.2.1 Effects of filtration

Figure 5.1 and 5.2 gave us a basic idea and reference of viscosity increase in original PWBO without any treatment. The viscosity behaviors of treated PWBO with filtration and neutralization were

compared with untreated PWBO. The efficiency of hydrogenation treatment is investigated with aqueous fraction of PWBO.
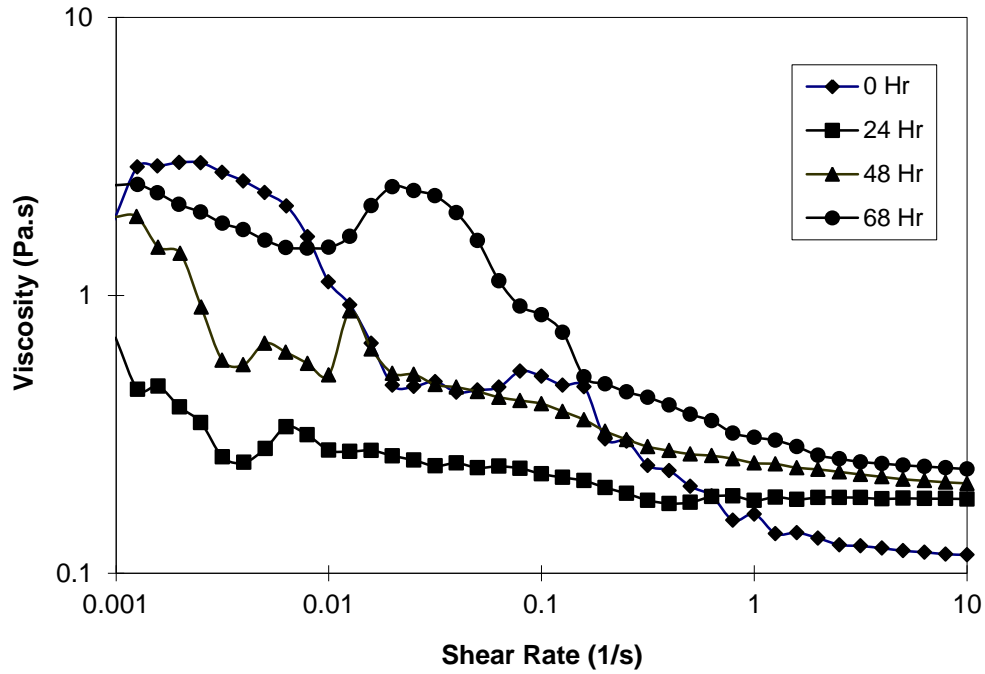
**Figure 5.1** Viscosity of untreated bio-oil (PWBO) versus shear rate..
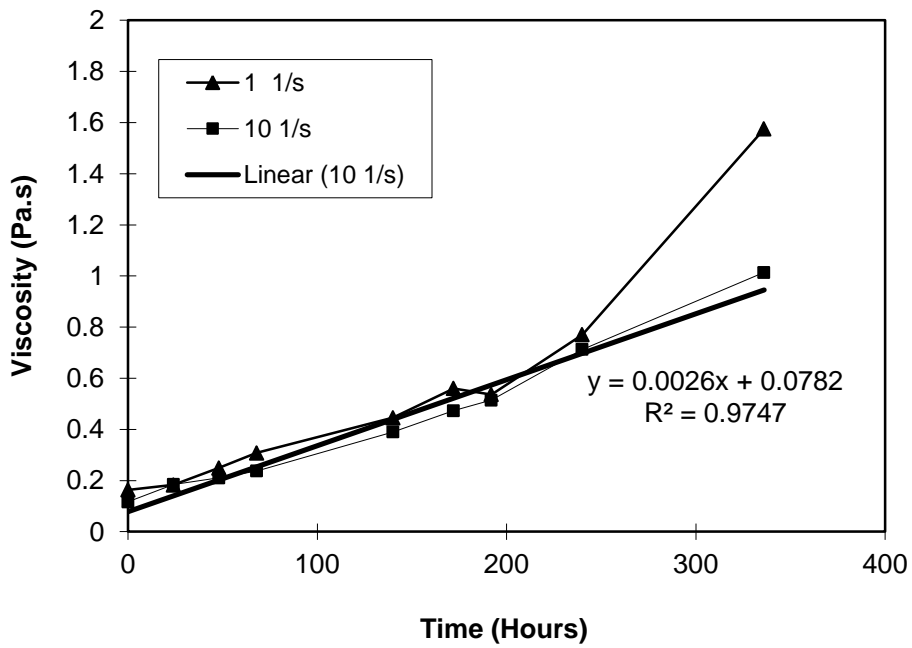
Figure 5.2 Viscosity of untreated bio-oil (PWBO) versus incubation time at 90ºC. The linear line is the trendline of viscosity at shear rate 10 1/s. Samples were incubated at 90ºC, viscosity was measured at

Figure 5.3 shows the filtration with 5µm syringe filter has some influence in the microstructure. The viscosity lines of filtered PWBO have less fluctuation than untreated PWBO at low shear rate, where the shear stress is close to inertia force and sensitive to the homogeneity, such as particle density, particle size and particle shape. However, the viscosity increase rate didn't have significant change from the comparison between Figure 5.2 and 5.4. The efficiency of filtration from visual observation could be evaluated in Figure 5.5 and 5.6. Figure 5.6 shows the 5 µm filter didn't remove the chars completely, there are small particles remaining in filtered PWBO. If we assume 5 µm syringe filter removed a lot of chars, this result may suggest the chars may be not a critical factor of causing viscosity increase.
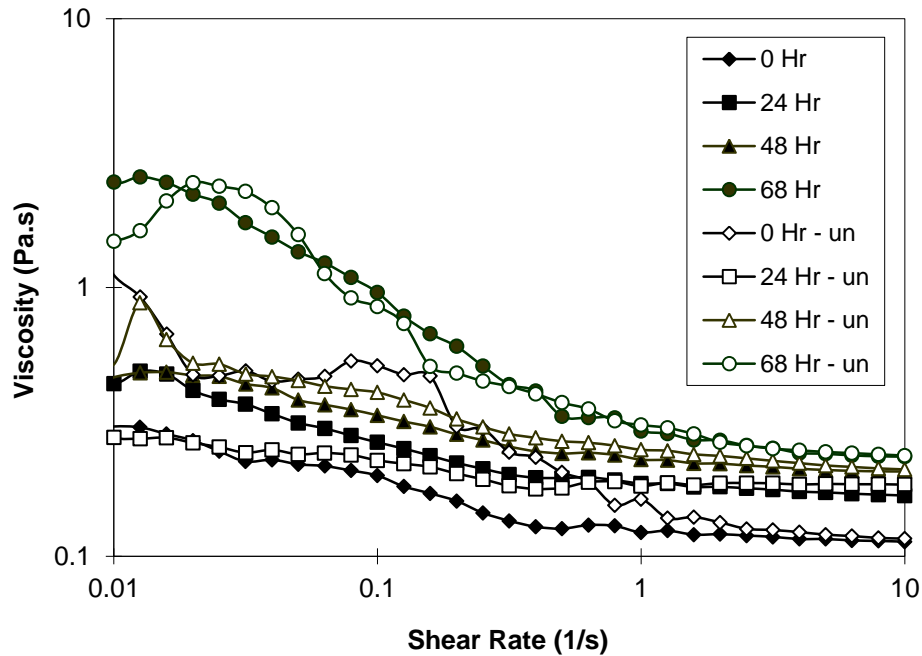
Figure 5.3 Comparison of viscosity behavior versus shear rate between untreated PWBO and filtered PWBO with 5 µm syringe filter. The solids are untreated PWBO, the opens are filtered PWBO. Samples were incubated at 90ºC, viscosity was measured at 40ºC.
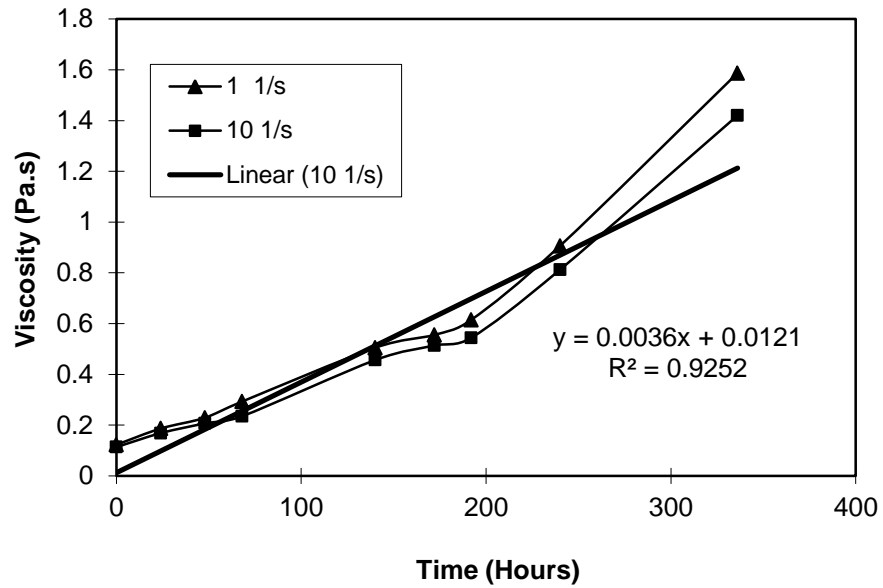
Figure 5.4 Viscosity of filtered PWBO versus incubation time at 90ºC. The lines are guides for eye. Samples were incubated at 90ºC, and viscosity was measured at 40ºC.
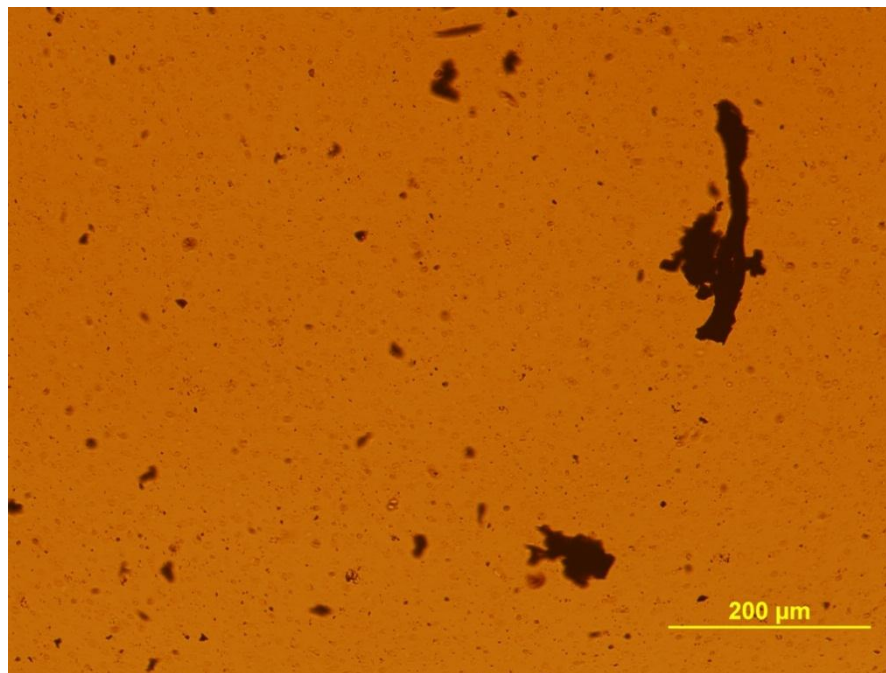
Figure 5.5 Micrograph of untreated PWBO before incubation. (20X) Large particles are observed.
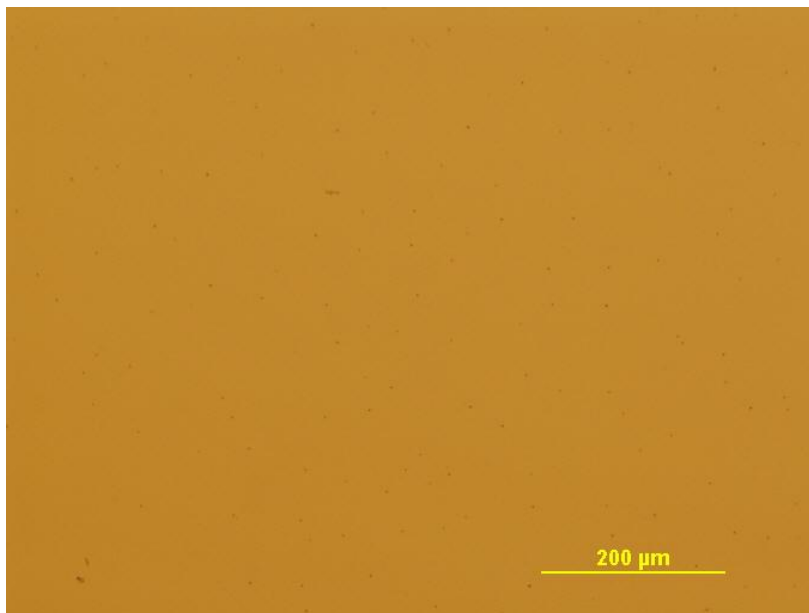
Figure 5.6 Micrograph of filtered PWBO with 5 μm syringe filter before incubation. (20X) Small dot particles are observed.

5.2.2 Effects of neutralization

Figure 5.7 shows the neutralized PWBO with Na_2CO_3 still has a increase rate of viscosity which is close to untreated PWBO. So the transition from acidic to basic didn't stop the instability. The polymerization reaction may not be catalyzed by acids, or may be able to continue in basic environment.
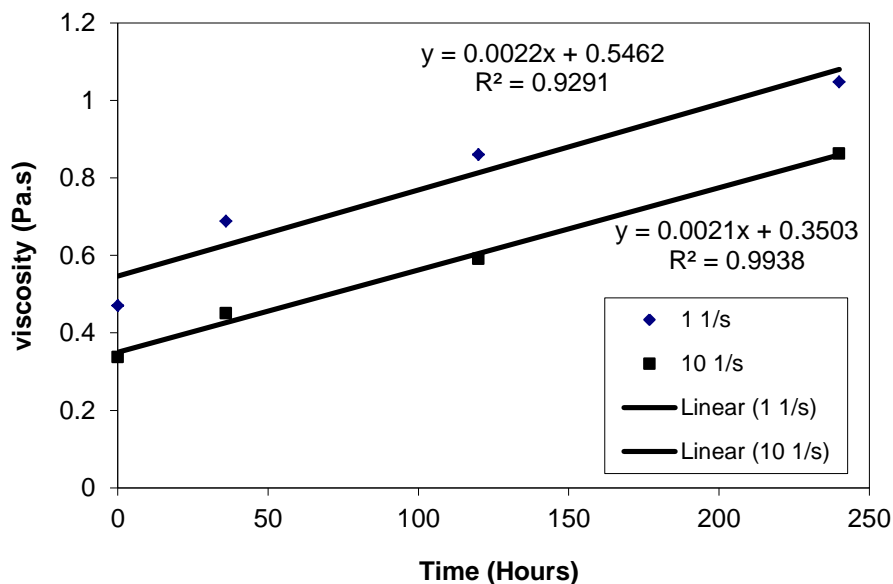
Figure 5.7 Viscosity of neutralized PWBO versus incubation time. Samples were incubated at 90ºC, viscosity was measured at 40ºC.

5.2.3 Effects of hydrogenation

Figure 5.8 shows the viscosity of unhydrogenated WSBO has an increase trend even after some

black viscous oil separated from the bulk solution (shown in Figure 5.10). Figure 5.9 shows a decrease trend of viscosity in hydrogenated WSBO, which only has a few black droplets separated from bulk solution after long time heating treatment (shown in Figure 5.11). The hydrogenated WSBO was filtered with 0.45 µm syringe filter. So we need to concern the effects of filtration together with the hydrogenation. A group of experiments without the factors of filtration will show us the influence of hydrogenation directly in the future work. Table 5.1 listed the chemicals already know in PWBO and their products of hydrogenation treatment.
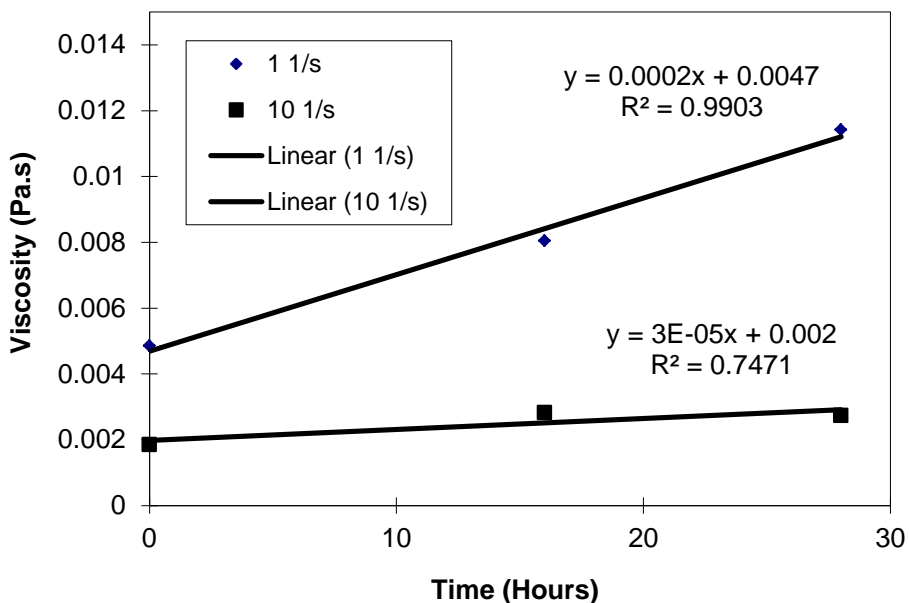
Figure 5.8 Viscosity of unhydrogenated 39.6wt% WSBO (unfiltered) as a function of incubation time. Samples were incubated at 90ºC, and viscosity was measured at 25ºC. The linear lines are trend lines of viscosity increase.
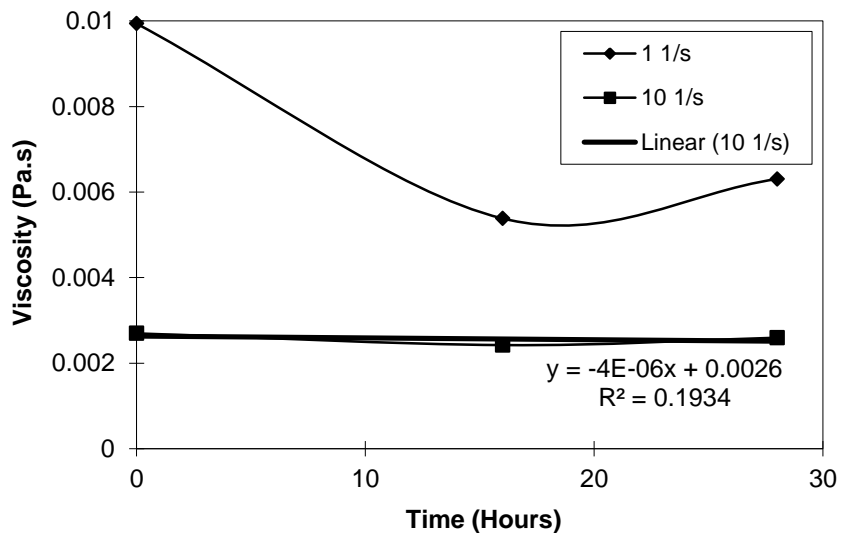
Figure 5.9 Viscosity of hydrogenated 39.6% WSBO (filtered with 0.45 □m syringe filter) versus incubation time. Samples were incubated at 90ºC, and viscosity was measured at 25ºC. Lines are guides for eye. Linear line is the trend line of viscosity at 10 1/s.
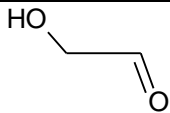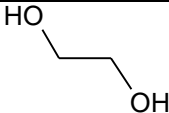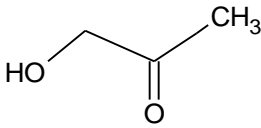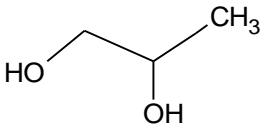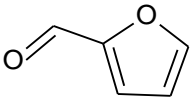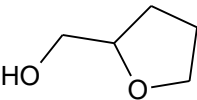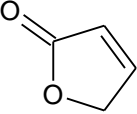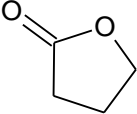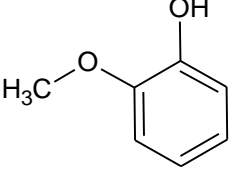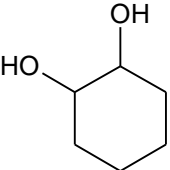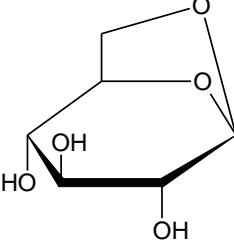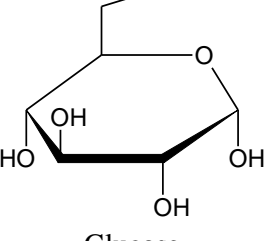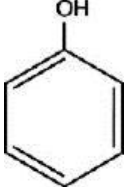
Figure 5.10 Unhydrogented WSBO at room temperature after heating treatment. Black viscous oils at the bottom and on the wall were created during heating treatment and separated from bulk solution.

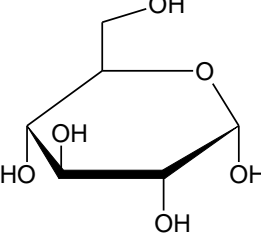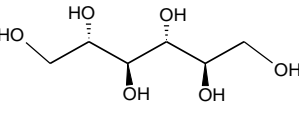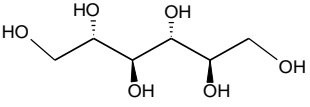**Figure 5.11** Hydgrogenated WSBO at room temperature after hearting treatment. Only a few of black oil droplets were created and separated from bulk solution.

Table 5.1 Some chemicals already known in PWBO and their products of hydrogenation treatment.

No.	Reactant	Product	Type of Reaction
1	Hydroxyacetaldehyde	Ethylene glycol	Hydrogenation
2	Hydroxyacetone	Propylene glycol	Hydrogenation
3	Furfural	Tetrahydrofurfuryl alcohol	Hydrogenation
4	2-Furanone	γ-Butyrolactone	Hydrogenation
5	Guaiacol	1,2-Cyclohexanediol	Hydrogenation
6	Levoglucosan	Glucose	Hydrolysis
7	Glucose	Sorbitol	Hydrogenation

8	 Sorbitol	Ethylene glycol, Propylene glycol & 1,4-Butanediol	Hydrogenolysis
9	CH$_3$-COOH Acetic acid		
10	 Phenol		

Some specific suggestions are to investigate the stability of model systems mixed by the chemicals in Table 5.1:

1) A model system with all the chemicals in the second column.
2) A model system with all the chemicals except acids in the second column.
3) An hydrogenated model system with all the chemicals in the second column.

A hydrogenated model system with all the chemicals except acids in the second column

5.3 Summary

This work investigated the stability of untreated pine wood bio-oil (PWBO) and PWBO treated with filtration, neutralization and hydrogenation in terms of viscosity increase over heating treatment time. Filtration and neutralization didn't inhibit the polymerization reactions in PWBO effectively. So acids and chars may not be the main factors of instability. Hydrogenation may be a promising solution technically although its cost is high. In future work, it is necessary to investigate the polymerization mechanisms and find efficient inhibition methods.

5.4 References

[1] M.E. Boucher; A. Chaala; H. Pakdel; C. Roy. *Biomass and Bioenergy* **2000**, 19, p351.

[2] R. K. Sharma; N. N. Bakhshi. *Canadian J. Chem. Eng.* **1991**, 69, p1071.

[3] B. Scholze; C. Hanser; D. Meier. *J. Analytical and Applied Pyrolysis* **2001**, 58–59, p387.

[4] J.D. Adjaye; N.N. Bakhshi. *Fuel Processing Technology* **1995**, 45, p185.

[5] S. T. Srinivas; A. K. Dalai; N. N. Bakhshi. *Canadian J. Chemical Engineering* **2000**, 78, p343.

Task 6.0 Commercialization Assessment

As part of this project Renewable Oil International LLC (ROI) was responsible for Task 6.0, "Commercialization Assessment." The planned activities for this task were as follows:

- **Milestone 9.** Complete designs for integrated bio-oil production systems incorporating the technologies developed through this project by UMass-Amherst.
- **Milestone 10**. Within budget capabilities and as warranted by UMass-Amherst laboratory success, incorporate the technologies developed into an existing ROI plant and assess the performance of the integrated system.
- **Milestone 11**. Conduct an economic analysis of the integrated system to determine business viability.

6.1 Milestone 9 comparison of actual accomplishments with goals and objectives of this project.

It is a common consensus that chars in the vapor acts as a vapor cracking catalyst and that chars in the bio-oil accelerate aging and exacerbate instability issues[1]. Therefore minimal vapor residence time in the reactor and minimal char particulate in the bio-oil is important[2]. Carbon generated from vapor cracking typically manifests itself in the form of a fine powder that coats internal surfaces in the bio-oil recovery system surfaces and can lead to slagging, fouling, and blockages in this system. If these internal surfaces are cool enough, some of the bio-oil constituents will condense out and form a sticky surface which further contributes to char buildup and accompanying slagging, fouling, and blockages. Thus any actions to decrease the residence of the bio-oil vapor before its recovery should contribute to lower concentrations of char particulate in the bio-oil.

Task 1 of this project was for UMASS to research the feasibility of removing char from the bio-oil using membrane microfiltration separation technology. "Char particles greater than 10μm are generally removed during pyrolysis by processes such as hot gas filtration and cyclone separation. Particulate solids less than 10 μm in size still remain in the bio-oil, and this can result in ash content being as high as 0.2 wt%[3]".

Cylindrical ceramic membranes of nominal pore sizes 0.5 and 0.8μm were used by UMASS to carry out bio-oil microfiltration. These cylindrical membranes were 250mm in length with an outer diameter of 10mm and an inner diameter of 7mm.

Using microfiltration UMASS researchers were able to reduce the ash content in the bio-oil by roughly 60%, to about 0.03% (wt). The results of this research were reported previously in this report. ROI worked with UMASS to scale up this technology by combining several of these cylindrical membranes into common top and bottom headers. One significant problem with the membrane separation system was what to do with the resulting retentate which was approximately 20% of the original unfiltered liquid which contained concentrated char particulate. One potential solution is to burn the retentate to provide heat for the process; however, burning could complicate environmental permitting. In addition to the retentate, solutions of methanol, sodium hydroxide, and acetic acid for cleaning the membranes were generated which would require disposal in a commercial installation. The necessity of cleaning chemicals coupled with disposal of the retentate would make it difficult to use this technology for distributed bio-oil production systems, but could lend itself to centralized upgrading

---

[1] Bridgewater, AV, 2011, Upgrading Fast Pyrolysis Liquids, in *Thermochemical Processing of Biomass: Conversion into Fuels, Chemicals, and Power*, ed Robert C. Brown, John Wiley & Sons, p166

[2] Basu, Prabir, 2010, *Biomass Gasification and Pyrolysis: Practical Design and Theory*, Academic Press, p76

[3] Javaid, Asad, etal., 2010, Removal of char particles from fast pyrolysis bio-oil by microfiltration, Journal of Membrane Science 363 (2010) 120–127

systems. Centralized processing would generate the bio-oil filtrate in a central location which may facilitate its marketing and beneficial use and ultimately increase its value.

One way to increase the UMASS membrane microfiltration efficiency was to reduce the char particulate loading in the gas/vapor from the reactor and hence in the bio-oil. Therefore ROI designed and retrofitted a cyclone into the transition ducting between the reactor and bio-oil recovery system. These cyclone systems were designed to fit inside the reactor with their drop tubes discharging into the moving reactor bed so that char removal from the cyclone was automatic (figures 6.1 and 6.2). Placing the cyclone inside the reactor kept the cyclone hot and allowed for recovery of the cyclone-captured char with the char from the reactor.   However, it also limited cyclone dimensions as the reactor was only approximately 25mm wide.

Figure 6.1 Single cyclone

Initially a single cyclone was tested in the reactor and it was determined that the velocity into the cyclone was not high enough to achieve desired particulate separation efficiency. This conclusion was partially based on observed char buildup at the entrance to the cyclone. Based on these observations, another cyclone was designed which was slightly smaller to increase efficiency, and a nitrogen sweep gas was added to the reactor to increase the gas velocity from the reactor and through the bio-oil recovery system. The increased gas velocity also significantly decreased the time for secondary reactions. A sweep gas rate of about 20% of the vapor generation rate was the goal.

The combination of the sweep gas and improved cyclone increased the plant run times by 5x before plant shut-down was required for cleanout of the tar trap and ducting. To attain greater efficiency, a third

cyclone system was designed which was composed of a single cyclone followed in series by two smaller cyclones located in parallel (multi-clone). The multi-cyclone design was not tested.

Figure 6.2 Two-stage cyclone consisting of a single cyclone followed by two smaller cyclones in parallel

Task 2 of this project was for UMASS to research the feasibility of acid removal by membrane separation technology. Bio-oil and its aqueous fraction contain large amounts of guaiacol and its derivatives. The UMASS research did not find a guaiacol resistant membrane hence membrane separation may not be feasible for the reduction of total acid number (TAN) in the bio-oil or its aqueous fraction. Therefore ROI could not integrate this technology into a bio-oil production system.

Task 3 of this project was for UMASS to research the feasibility of acid removal by catalytic processing. UMASS was able to catalytically process the bio-oil and upgrade the bio-oil using catalytic processing through catalytic hydrodeoxygenation of the entire bio-oil and aqueous fraction of the bio-oil. Catalytic processing involves high pressure processes, higher degrees of operator capability, and large plant capacities for economy of scale. Therefore catalytic processing would work best with distributed production of bio-oil using the modular ROI technology and centralized bio-oil upgrading facilities based on catalytic processing.

Task 4 of this project was for UMASS to research the feasibility of acid removal by using ion exchange resins. The UMASS research found that acid removal by ion-exchange resins was not feasible for the bio-oil because of the difficulties in the regeneration of the ion exchange resin. Therefore ROI could not integrate this technology into a bio-oil production system.

Task 5 of this project was for UMASS to characterize the upgraded bio-oils. This was an analytical task that did not provide fast pyrolysis system integration opportunities.

To address the issue of vapor residence time, ROI designed and retrofitted a direct condenser system onto the pilot plant at UMASS and replaced the 8-stage shell and tube fractional condenser system (figure 6.3). The direct condenser bio-oil recovery system consists of a tar trap (existing), two sequential direct contact condensers, and an ESP; with the previous shell and tube condensers used to cool the condensing fluid. Test runs with the direct contact condensing system were made using dodecane as a condensing fluid while processing mixed hardwoods. The dodecane was not completely insoluble in bio-oil leading to an unacceptable loss of the dodecane. Therefore tests were also run using bio-oil as a direct contact condensing fluid while processing mixed hardwoods. The maximum yields of bio-oil with either condensing fluid were in the range of 32%, based on dry weight of wood into the fast pyrolysis system.

Figure 6.3 Eight stage fractional condenser

The cause of the low bio-oil yield is thought to be inherent in the design of the direct contact condensers (DCC). The DCC were made from 8-inch long straight sections of 2-inch nominal diameter stainless steel pipe with a spray nozzle for the cooling fluid at top center and vapor flow concurrent. A chamber at the bottom of the pipe served as a settling/disengaging chamber. The DCC design was modeled after commercial designs used by Schutte & Koerting, a company that specializes in these types of systems.

It is felt that changing the condenser designs to countercurrent vapor flow and adding packing beneath the cone of spray would significantly increase the efficiency of the DCC system. Glass balls of

3/8-inch and ¼-inch diameter were obtained to serve as packing but were not received before the project funding ran out.

To address char carryover in the reactor vapor stream, ROI has developed a new reactor design that significantly increases the effectiveness of the reactor to keep char particulate out of the gas/vapor stream. A provisional US patent on this new design was filed on April 7, 2011. This design incorporates a moving bed filter into ROI's moving bed fast pyrolysis reactor to form a simple but highly efficient reactor that significantly reduces char carryover in the vapor stream. Moreover, unlike most fast pyrolysis systems, it allows for full recovery of the char as a co-product. This ability to recover char significantly enhances the cost effectiveness of the process and can provide a pathway for a carbon-negative process.

6.2 Milestone 10. Within budget capabilities and as warranted by UMass-Amherst laboratory success, incorporate the technologies developed into an existing ROI plant and assess the performance of the integrated system

Based on the ROI technology, ROI had previously designed and built a 15-ton per plant for DOD under a separate, independent project. Based on research results obtained from the UMASS bio-oil upgrading project, ROI designed and retrofitted into this DOD plant a two-stage cyclone gas/vapor cleanup system consisting of a single high-capacity, low-efficiency cyclone followed by two low-capacity, high-efficiency cyclones in parallel in the gas/vapor ducting out of the reactor. ROI also designed an automated system for recycling a portion of the syngas as a reactor sweep gas and incorporated this syngas recycling system into the plant. Any excess syngas is automatically shuttled to a burner by the system where it is consumed for process heat.

ROI has only preliminary results from the 15-ton per day plant as the project has been held up due to non-technical issues; however, the shakedown results have been very encouraging. The 15-ton per day is currently in the shakedown phase and the plant will be evaluated in detail by DOD when it is fully operational.

6.3 Milestone 11. Conduct an economic analysis of the integrated system to determine business viability

Since no results from the UMASS research were incorporated into the UMASS pilot plant, no detailed economic analysis was performed specifically as part of this project. However, the capital cost for adding cyclones and a sweep gas to reduce vapor residence time would be less than 2% of the total plant capital cost. Minimizing char in the vapor stream would significantly increase run times and reduce maintenance activities associated with removing slagging and fouling from the bio-oil recovery system. The cost of a direct contact condensing system would be comparable to a shell and tube indirect condensing system. Thus all plant improvements would have a significant positive impact on plant economics.

6.4 Conclusions

This research resulted in several improvements to ROI's fast pyrolysis system and reduced the amount of char in the bio-oil. All methods reduced char content of the bio-oil. The capital cost for hardware improvements would be less than 2% of the total plant capital cost and all plant improvements would have a significant positive impact on plant economics. To the extent possible improvements were made to the UMASS plant and retrofitted into the 15-dtpd plant that ROI has fabricated for the DOD.

Task 7.0 Project Management and Reporting

George Huber has provided overall leadership for this project with Ford, Badger, and Bhatia responsible for leading their respective elements. This team has been worked together on bio-oil stabilization technologies.

Reports regarding the progress of the project were provided in accordance with the Federal Assistance Reporting Checklist. These include quarterly reports spreadsheet format, yearly project management forms, and a final report.

Publications:

Asad Javaid, Tatiana Ryan, Gayla Berg, Xiaoming Pan, Tushar Vispute, Surita R. Bhatia, George W. Huber, David M. Ford, Removal of char particles from fast pyrolysis bio-oil by microfiltration, Journal of Membrane Science 363 (2010) 120–127

Achyuta Teella, George W. Huber, David M. Ford Separation of acetic acid from the aqueous fraction of fast pyrolysis bio-oils using nanofiltration and reverse osmosis membranes Journal of Membrane Science 378 (2011) 495– 502

Conference Papers/Proceedings:

G.W. Huber, Renewable Petrochemicals from Biomass by Catalytic Fast Pyrolysis, AICHE National Meeting, Salt Lake City, UT (November 2010) (Invited keynote lecture).

AICHE 2010
Renewable Petrocher

Xiaoming Pan, Tushar Vispute, Huber, G.W., Surita R. Bhatia, "Rheology and Stability Considerations in Processing of Bio-Oils" AIChE November 2009, Nashville, TN

AIChE-Bio-oil_tushar
.pdf

Vispute, Tushar P, Huber G. W., "Production of Hydrogen and alkanes by aqueous phase processing of aqueous fraction of bio-oil" 237th ACS National Meeting, Salt Lake City, UT, United States, March 22-26, 2009

ACS 2009-salt lake
city - Final.pptx

Huber, G.W., "The Potential of Cellulosic Biofuels" Congressional briefing: Biofuels-The next generation. June 18th, 2009, Washington DC. Sponsored by NSF, Discovery Channel.

Congressional
Briefing June 18 2009

Huber, G.W.; Breaking the Chemical and Engineering Barriers to Cellulosic Biofuels, The Business and Biology of Biofuels, University of San Diego, La Jolla, CA, January 2008.

Microsoft PowerPoint
97-2003 Presentation

Teella, A. and Ford, D.M., ³Removal of Organic Acids from the Aqueous Fraction of Fast Pyrolysis Bio-Oils using Nanofiltration and Reverse Osmosis Membranes,² American Institute of Chemical Engineers (AIChE) Annual Meeting, Minneapolis, MN, October 16-21, 2011

1FordMembrane.ppt

Javaid, A., Pan, X., Bhatia, S.R., Huber, G.W., and Ford, D.M., ³Removal of Char Particles from Bio-Oil by Liquid-Phase Microfiltration,² American Institute of Chemical Engineers (AIChE) Annual Meeting, Salt Lake City, UT, November 7-12, 2010

2FordMembrane.ppt

Ford, D.M., Javaid, A., Berg, G., Ryan, T., Teella, A., Huber, G.W., Vispute, T., Bhatia, S.R., and Pan, X., ³Membrane Processes for the Stabilization of Fast Pyrolysis Bio-Oil,² Symposium on Thermal and Catalytic Sciences for Biofuels and Biobased Products, Iowa State University, Ames, IA, September 21-23, 2010

3FordMembrane.pdf

Teella, A., Jeannotte, D., and Ford, D.M., ³Separation of Acids from Fast Pyrolysis Bio-Oils using Nanofiltration Membranes,² American Institute of Chemical Engineers (AIChE) Annual Meeting, Nashville, TN, November 8-13, 2009

AIChE_NF.pptx

Javaid, A., Ryan, T., and Ford, D.M., ³Removal of Char Particles by Microfiltration Process to Improve the Stability of Bio-Oils,² American Institute of Chemical Engineers (AIChE) Annual Meeting, Nashville, TN, November 8-13, 2009

5Removal of Char Particles by Microfiltra